ABSTRACT

Title of Document: Adaptive Gradient Assisted Robust Optimization with Applications to LNG Plant Enhancement

Amir Hossein Mortazavi, Doctor of Philosophy, 2012

Directed By: Shapour Azarm, Professor,
Department of Mechanical Engineering
Reinhard Radermacher, Professor,
Department of Mechanical Engineering
Steven A. Gabriel, Professor,
Department of Civil and Environmental Engineering

About 8% of the natural gas feed to a Liquefied Natural Gas (LNG) plant is consumed for liquefaction. A significant challenge in optimizing engineering systems, including LNG plants, is the issue of uncertainty. To exemplify, each natural gas field has a different gas composition, which imposes an important uncertainty in LNG plant design. One class of optimization techniques that can handle uncertainty is robust optimization. A robust optimum is one that is both optimum and relatively insensitive to the uncertainty. For instance, a mobile LNG plant should be both energy efficient and its performance be insensitive to the natural gas composition.

In this dissertation to enhance the energy efficiency of the LNG plants, first, several new options are investigated. These options involve both liquefaction cycle enhancements and driver cycle (i.e., power plant) enhancements. Two new liquefaction cycle enhancement options are proposed and studied. For enhancing the diver cycle performance, ten novel driver cycle configurations for propane pre-cooled mixed refrigerant cycles are proposed, explored and compared with five different conventional driver cycle options. Also, two novel robust optimization techniques applicable to black-box engineering problems are developed. The first method is called gradient assisted robust optimization (GARO) that has a built-in numerical verification scheme. The other method is called quasi-concave gradient assisted robust optimization (QC-GARO). QC-GARO has a built-in robustness verification that is tailored for problems with quasi-concave functions with respect to uncertain variables. The performance of GARO and QC-GARO methods is evaluated by using seventeen numerical and engineering test problems and comparing their results against three previous methods from the literature. Based on the results it was found that, compared to the previous considered methods, GARO was the only one that could solve all test problems but with a higher computational effort compared to QC-GARO. QC-GARO's computational cost was in the same order of magnitude as the fastest previous method from the literature though it was not able to solve all the test problems. Lastly the GARO robust optimization method is used to devise a refrigerant for LNG plants that is relatively insensitive to the uncertainty from natural gas mixture composition.

Adaptive Gradient Assisted Robust Optimization with Applications to LNG Plant Enhancement

By

Amir Hossein Mortazavi

Dissertation submitted to the Faculty of the Graduate School of the
University of Maryland, College Park, in partial fulfillment
of the requirements for the degree of
Doctor of Philosophy
2012

Advisory Committee:
Professor Shapour Azarm, Chair and Advisor
Professor Reinhard Radermacher, Co-Advisor
Professor Steven A. Gabriel, Co-Advisor
Professor Elise Miller-Hooks (Dean's Representative)
Professor Gregory Jackson

Dedication

To my beloved parents who have always supported me

To My Family, Friends and Colleagues

Acknowledgements

I would like to express my sincere gratitude first and foremost to my advising professors, Dr. Shapour Azarm and Dr. Reinhard Radermacher for their guidance, encouragement and generous support during my entire graduate study. I would also like to thank my co-advisor Dr. Steven Gabriel for his valuable comments and support. It was a great experience for me to work at Design Decision Support Laboratory (DDSL) and Center for Environmental and Energy Engineering (CEEE).

I would like to thank my committee members, Dr. Gregory Jackson and Dr. Ellise Miller-Hooks for their comments and recommendations. I would also like to thank Dr. Yunho Hwang for his guidance during my PhD program.

Furthermore, I would like to thank my current and former lab partners and friends at DDSL and CEEE, namely: Dr. Ali Alalili, Dr. Vikrant Aute, Dr. Tolga Aynur, Mr. John Bush, Dr. Weiwei Hu, Dr. Mian Li, Dr. Jiazhen Ling, Mr. Ethan Lust, Mr. Andrew Mueller, Dr. Sauleh Seddiqui and Dr. Zhichao Wang. I would like to specially thank Mr. Abdullah AlAbdulkarem, Dr. Kyle Gluesenkamp and Ms. Parastoo Delgoshaei for their helpful comments and suggestions.

The work presented in this thesis was supported in part by The Petroleum Institute (PI), Abu Dhabi, United Arab Emirates, as part of the Education and Energy Research Collaboration agreement between the PI and University of Maryland, College Park. The work was also supported in part by an ONR Grant N000140810384. Such support does not constitute an endorsement by the funding agency of the opinions expressed in the thesis.

Table of Contents

List of Tables

List of Figures

Nomenclature

Acronyms

APCI	Air Products and Chemicals Inc.
C	Constraint
COP	Coefficient of performance
Det	Deterministic
DSH	Degree of Super Heating
EIA	Energy information administration
FC	Function calls
FV	Function value
GA	Genetic algorithm
GARO	Gradient Assisted Robust Optimization
HP	High pressure
LNG	Liquefied natural gas
LP	Low pressure
MCR	Multi-component refrigerant
NG	Natural Gas
OT	Outlet Temperature
P	Parameter
PD	Pressure Drop
QC-GARO	Quasi-Concave Gradient Assisted Robust Optimization
RIP	Refrigerant Inlet Pressure
RIT	Refrigerant Inlet Temperature
RMFR	Refrigerant Mass Flow Rate
S.t.	Subject to
U	Uncertainty
V	Number of variables

English Symbols

CG	Number of function calls for global maximization of a constraint
CGB	Number of function calls for gradient based maximization of a constraint
DO	Deterministic optimization's number of function calls
dv	Vector of design variables
G	Gibbs free energy
$\mathbf{g}(\mathbf{z})$	Vector of constraint functions $\mathbf{g}=[g_1(\mathbf{z}),g_2(\mathbf{z}),g_3(\mathbf{z}),\ldots]$
h	Enthalpy
I	Number of constraints
k	Iteration counter
$\dot{m}$	Mass flow rate
n	Dimension of the **z** vector
N_i	Number of moles of component *i*
NU	Number of uncertain variables and parameters
p	Vector of design parameters $\mathbf{p}=[p_1, p_2, p_3,\ldots]$
P_{Boiler}	Pressure
P_{comp}	Compressor power consumption
P_{pump}	Pump power consumption
P_{turb}	Turbine power output
$Pw_{Compressor}$	Gas turbine compressor power
$Pw_{Liquefaction}$	Liquefaction cycle power demand
Pw_{Pump}	Pump power
$Pw_{Steam\ Turbine}$	Steam turbine power
$Pw_{Turbine}$	Gas turbine power
$\dot{Q}$	Heat exchanger heat duty
R_{mlp}	Ratio of low pressure water flow rate to total water flow rate
$T_{Exhaust}$	Exhaust temperature
$T_{Inlet,Turbine}$	Gas turbine turbine inlet temperature

$T_{\min,\ Exhaust}$	Minimum exhaust temperature
$T_{Super\ heater}$	Super heater outlet temperature
$\mathbf{x}$	Vector of design variables $\mathbf{x}=[x_1, x_2, x_3,\ldots]$
$x_{Outlet,Steam\ Turbin}$	Steam turbine outlet steam quality
$\mathbf{z}$	Vector of design variables and parameters, $\mathbf{z}=(\mathbf{x},\mathbf{p})$

Greek Symbols

$\boldsymbol{\alpha}$	Vector of Taylor series modifiers
$\boldsymbol{\alpha}_k$	Vector of Taylor series modifiers in iteration k
$\Delta\tilde{\mathbf{p}}$	Vector of design parameters' uncertainty range
$\Delta T_{p,Boiler}$	Boiler pinch temperature
$\Delta T_{p,Economizer}$	Economizer pinch temperature
$\Delta T_{p,Super\ heater}$	Super heater pinch temperature
$\Delta\tilde{\mathbf{x}}$	Vector of design variables' uncertainty range
$\Delta\tilde{\mathbf{z}}$	Vector of design variables and parameters uncertainty range
η	A positive user-defined parameter (used to check the accuracy of robustness estimation)
η_{comp}	Compressor isentropic efficiency
η_{pump}	Pump isentropic efficiency
η_{turb}	Turbine isentropic efficiency
ε	Solver threshold
λ	A positive user defined parameter (an initial guess for adjusting α_i)
μ_i	Chemical potential of component *i*
ω	Mass fraction

Chapter 1: Introduction

1.1 Motivation and Objective

Natural gas is the cleanest fossil fuel (Hubbard 2004). Fossil fuels are currently the main energy source for the human population. Based on the Energy Information Administration (EIA) data (EIA 2011) for the year 2008, 84.5% of the global energy demand was fulfilled by fossil fuels. Natural gas accounted for 22.6% (EIA 2011) of the total global energy consumption, and by the year 2035, its global demand is expected to increase by 52% from 2008 levels (EIA 2011). Natural gas is primarily transported either through the pipelines in a gaseous phase, or by Liquefied Natural Gas (LNG) tanker ships in a liquefied phase (Bumagin and Borodin 2007). LNG market share is approximately 7% (Cook 2005 and EIA 2010) of the global natural gas market, and liquefaction capacity is expected to increase more than 200% by 2035(EIA 2011).

Liquefaction of one kilogram of natural gas needs about 1,188 kJ of energy (Finn et al. 1999), depending on the liquefaction cycle and site conditions. This amount of energy leads to the consumption of about 8% of the feed gas for the liquefaction cycle (Patel 2005). Therefore, any enhancement to the energy efficiency of LNG plants will result in a significant reduction in the plant's gas consumption and consequently CO_2 emission. LNG plants can be conceptually divided into a liquefaction refrigeration cycle, and a power-producing "driver cycle". It follows that there are two ways to increase the energy efficiency of LNG plants: liquefaction cycle enhancement and driver cycle enhancement. In research task one of this dissertation, several

enhancement options for the propane pre-cooled mixed refrigerant liquefaction cycle, patented by Air Products and Chemicals Inc (APCI), and hereafter referred to as the APCI cycle, will be investigated. The APCI liquefaction cycle was selected for this dissertation due to the fact that a majority of LNG plants are using this liquefaction technology (Barclay 2005). The enhancement options encompass both liquefaction cycle enhancement and driver cycle enhancement and optimization. Here the enhancement refers to a design change by replacing components with new components or adding new components to the existing design. However, optimization refers to the selection of the components optimum specifications and operating conditions. The driver cycle enhancement is considered because a majority of the LNG plant energy consumption occurs at the compressor drivers (i.e., the power plants that maintain compressors power demand).

One of the barriers against the development of small remote gas fields is the transportation of natural gas from these reservoirs to the market, since it is not cost-effective to transport natural gas for long distances via pipeline (Foss 2007). On the other hand, it is not cost-effective to build a stationary LNG plant for a small natural gas reservoir due to the high current construction cost of LNG plant and relatively low natural gas price. One solution to this problem might be the development of mobile LNG plants (Tangen and Mønvik 2009). There are several uncertainties involved in the design of a mobile LNG plant including the natural gas composition and, ambient conditions such as sea water and air temperature. It should be noted that for a mobile LNG plant, the design should be insensitive to the natural gas composition of the gas field. Moreover, a mobile LNG plant should be energy

efficient. The enhancement options of the research task one could be implemented in the design of a mobile LNG plant that uses APCI liquefaction technology. However, one of the primary challenges is the development of a refrigerant mixture that is both efficient and insensitive to the natural gas composition. In this dissertation, an efficient refrigerant mixture refers to a refrigerant mixture composition that leads to minimum amount of energy consumed per unit mass of produced LNG. One method to develop this refrigerant mixture is by implementation of optimization techniques. However, conventional (deterministic) optimization techniques cannot handle problems which involve uncertainty. Robust optimization techniques would be the most suitable choice based on the design goal, which is the ability of a mobile LNG plant to process varying natural gas compositions. This due to the fact that robust optimization techniques will lead to a result that is feasible for all realization of uncertain variables. However, the current robust optimization techniques are either incapable of solving optimization problems that involve a full-scale simulation model of an LNG plant, or they are computationally expensive. This issue is addressed in the research task two, by developing a novel robust optimization technique. This robust optimization technique will be used in research task three to develop a robust optimum refrigerant mixture that is relatively insensitive to the uncertainty in the feed gas composition. The obtained robust optimum refrigerant mixture should be applicable for handling varying feed gas compositions in both stationary and mobile APCI LNG plants.

The overall objective of this dissertation is to study different enhancement options for propane pre-cooled LNG plants using both conventional and newly developed robust

optimization techniques.

The three research tasks are briefly introduced next in Sections 1.2.1 to 1.2.3 followed by a description of the organization of the dissertation in Section 1.3.

1.2 Research Tasks

In order to achieve the overall objective of this dissertation, three research tasks are considered. The first research task deals with the APCI liquefaction cycle enhancement and driver cycles enhancement and optimization. In the second research task, a robust optimization method capable of optimizing an APCI LNG plant refrigerant mixture is developed. The third research task deals with implementing the developed robust optimization method to design a refrigerant mixture that is insensitive to the uncertainty of the feed gas composition.

1.2.1 Research Task 1: LNG Plant Enhancement and Optimization (Chapter 2)

In this task, the APCI LNG plant liquefaction cycle and gas turbine driver cycles are modeled. These cycles are referred as the base liquefaction and driver cycles. To enhance the energy efficiency of the base liquefaction cycles, the effects of replacing expansion valves with expanders upon the performance of the base APCI liquefaction cycle are considered by modeling four different enhancement scenarios.

To enhance the base driver cycle, four different conventional LNG driver cycle enhancement configurations are considered. To achieve their optimum performance these four configurations were optimized using conventional optimization techniques. Based on the LNG plant conventional driver cycles optimization results ten new LNG

plant driver cycle configurations were developed. To fully explore the performance of the new driver cycle configurations in comparison to the conventional driver cycles, each of the new configurations is optimized using a conventional deterministic global optimization technique.

The objective of Research Task 1 is to investigate different enhancement options for APCI LNG plants by implementing a conventional deterministic global optimization technique.

1.2.2 Research Task 2: Developing Robust Optimization Algorithm (Chapter 3)

This task involves developing a new gradient-assisted robust optimization method. While the previous gradient-based robust optimization methods are computationally tractable, they could not handle general engineering problems that involve large uncertainty[1], while the proposed method can.

The objective of Research Task 2 is to develop a computationally more efficient gradient-assisted robust optimization algorithm compared to some related robust optimization methods from the literature that have applicability to general robust optimization problems with a large uncertainty range.

The computational efficiency of this algorithm is explored by solving 17 different test problems and the results are compared with the previous methods of Gunawan and

[1] In this dissertation, a large uncertainty corresponds to an interval uncertainty whose range is greater than 10% and less than 1000% of the absolute value of the corresponding uncertain variable or parameter at the robust optimum point

Azarm, (2004), Li et al., (2006), and Siddiqui et al., (2011). The test problems consist of 11 numerical problems, five engineering problems, and one black-box simulation problem.

1.2.3 Research Task 3: Developing a Robust Refrigerant Mixture for APCI LNG Plants (Chapter 4)

In this task, a robust optimization problem is formulated for developing a refrigerant mixture that is relatively insensitive to feed gas composition. A new liquefaction cycle model is developed in order to enhance the simulation speed while performing the optimization without losing any crucial liquefaction cycle detail. Research task two's robust optimization method is used to develop the refrigerant mixture.

The objective of Research Task 3 is to implement the robust optimization techniques to develop a refrigerant mixture applicable for use in both stationary and mobile APCI LNG plants that have varying feed gas compositions.

1.3 Organization of the Dissertation

The rest of the dissertation is organized as follows, Figure 1.1. By implementing only deterministic optimization, several methods of enhancing APCI LNG plants are explored in Chapter 2. In Chapter 3, two efficient robust optimization techniques are devised. The performance of these robust optimization techniques are analyzed using 17 different test problems, and the results are compared against three previous robust optimization methods from the literature. In Chapter 4, the robust optimization techniques developed in Chapter 3 are used to develop a robust mixture for APCI LNG plants. Chapter 5 concludes the dissertation and includes a discussion of the

contributions of the dissertation and potential future extensions.

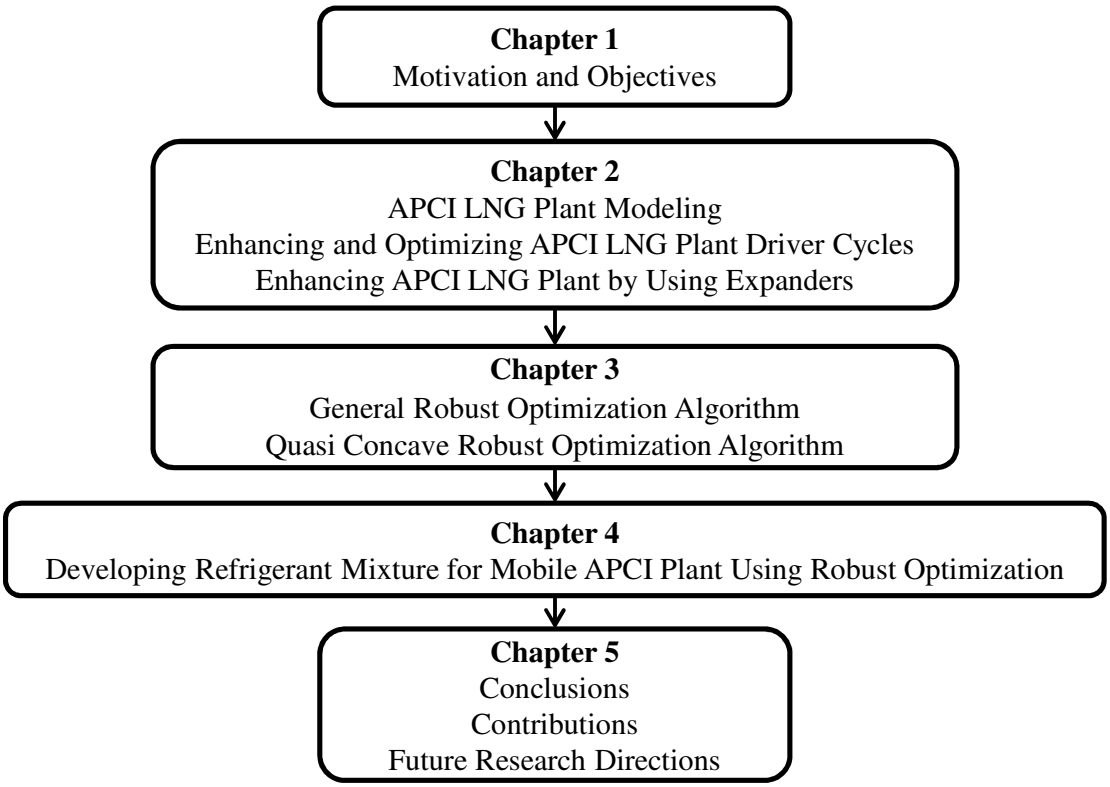

Figure 1.1: Dissertation organization and flow of information

Chapter 2: LNG Plant Enhancement and Optimization

2.1 Introduction:

In this chapter, Research Task 1 is discussed in detail. The material of this chapter was previously published by Mortazavi et al., (2010)[2] and Mortazavi et al., (2012)[3].

There are two ways to improve the energy efficiency of LNG plants: liquefaction cycle and driver cycle enhancements. Liquefaction cycle enhancements have been considered in several studies. Vaidyaraman et al., (2002), Lee et al., (2002), Paradowki et al., (2004), Del Nogal et al., (2008), Aspelund et al., (2010) and Alabdulkarem et al., (2011) improved the liquefaction energy efficiency by optimizing refrigerant composition, mass flow rate and pressure. Faruque Hasan et al., (2009) enhanced LNG plant energy consumption by optimizing the compressor networks. Kanoglu et al., (2001) examined the effect of replacing a Joule Thomson valve with a turbine expander for LNG expansion. Renaudin et al., (1995) studied the benefits of replacing LNG and mixed refrigerant expansion valves with liquid turbines. The main focus of the previous works was on enhancing the mixed refrigerant cycle and recovering energy from the LNG expansion process. However, the previous work did not consider the use of expanders for enhancing the propane cycle of APCI liquefaction cycle. Moreover, the previous literature did not consider the effect of these replacements on the performance of the entire APCI LNG plant.

---

[2] Mortazavi, A., Somers, C., Alabdulkarem, A., Hwang, Y. and Radermacher, R., 2010, "Enhancement of APCI Cycle Efficiency with Absorption Chillers", Energy, V. 35, No. 9, pp. 3877-3882.

[3] Mortazavi, A., Somers, C., Hwang, Y., Radermacher, R., Al-Hashimi, S. and Rodgers, P., 2012, Performance Enhancement of Propane Pre-cooled Mixed Refrigerant LNG Plant, Applied Energy, V. 93, pp. 125-131.

These two gaps are addressed by modeling several expansion loss reduction options. These options are modeled and compared with each other in order to investigate the potential of various solutions for improving liquefaction cycle efficiency.

In this dissertation, the driver cycle enhancements refer to any enhancement to LNG plant energy efficiency by considering the liquefaction cycle compressor drivers. Di Napoli, (1980) demonstrated that gas turbine and steam boiler combined cycle drivers are more energy efficient and more economical than steam boiler cycles driver for the LNG plants. Kalinowski et al., (2009) investigated the use of gas turbine waste heat to replace propane cycle of a LNG plant. Gas turbine waste heat refers to the gas turbine exhaust whose temperature is significantly higher than ambient temperature and its heat content is rejected to the ambient without any utilization. Rodgers et al., (2012) used APCI LNG plant gas turbine driver waste heat to reduce the propane cycle of an APCI LNG plant energy consumption.

Del Nogal et al., (2011a, 2011b) developed an optimization procedure to select the most economical set of drivers for the LNG plants. Although there are numerous studies regarding the enhancement of the power cycles, none of them except the mentioned studies are geared for the LNG plants. In this chapter fifteen different driver configurations are considered. Ten of the considered driver configurations are new and have not been proposed for the LNG plants. To examine the maximum performance of each driver cycle configuration, its design variables are optimized for the considered LNG plant.

The rest of this chapter is organized as follows. In Section 2.2 APCI liquefaction cycle is described. The thermodynamic equations used to model the main components

of the APCI liquefaction cycle, absorption chillers and the gas turbine combined cycles are explained in Section 2.3. In Sections 2.4, 2.5 and 2.6 the modeling of the APCI liquefaction cycle, enhancing the APCI liquefaction cycle and APCI driver cycle modeling are discussed respectively. APCI Driver cycle enhancement and optimization is discussed in Section 2.7 followed by the conclusions in Section 2.8.

2.2 APCI Natural Gas Liquefaction Process

Currently, about 77% of base-load natural gas liquefaction plants employ propane pre-cooled mixed refrigerant (APCI) cycle (Barclay 2005). In this process, as shown in Figure 2.1, the feed gas is sent to a gas sweetening unit for removal of H_2S, CO_2, H_2O and Hg. Subsequently, the feed gas temperature is reduced to approximately -30°C by passing through the pre-cooler and cold box. This process results in condensation of certain gas components which are be separated from the remaining gas in the separator. The condensate is sent to the fractionation unit, where it is separated into propane, butane, pentane, and heavier hydrocarbons. The remaining gas is sent to the cryogenic column where it is liquefied and cooled to below -160°C which is the natural gas boiling temperature at atmospheric pressure. After the cryogenic column, the LNG pressure is reduced to atmospheric pressure by passing it through the LNG expansion valve or expander. As shown in Figure 2.1, two refrigeration cycles are involved in the cooling and liquefaction of natural gas. These cycles are the propane cycle and the multi-component refrigerant (MCR) cycle. The propane cycle supplies the cooling demands of the pre-cooler, cold box and fractionation unit. The MCR cycle provides the cooling demand of the cryogenic column. Both the propane cycle and the MCR cycle condensers are typically cooled

by sea water. Throughout this dissertation it is assumed that the sea water temperature and the ambient air temperature are 35°C and 45°C respectively.

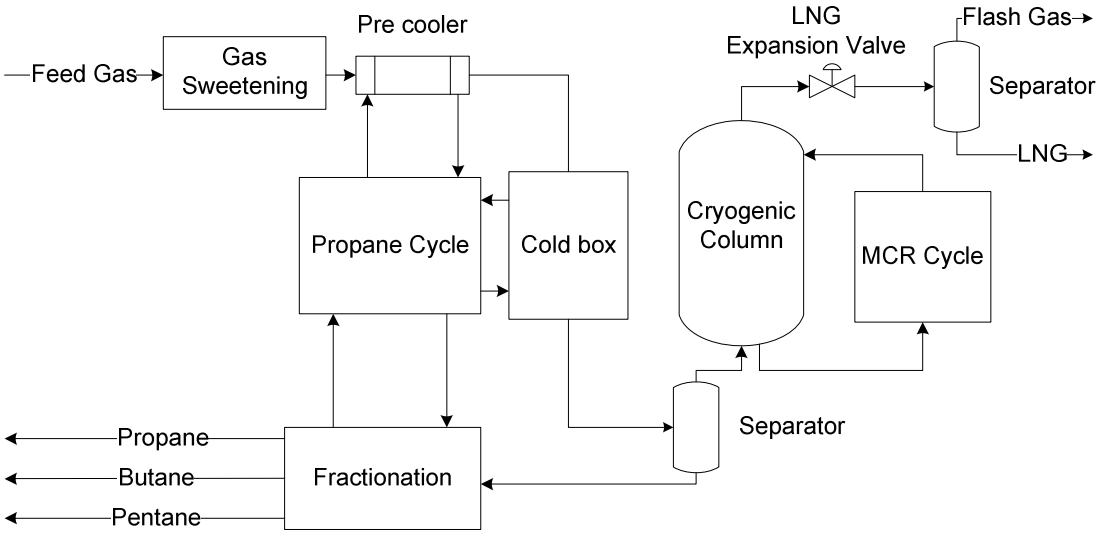

Figure 2.1: Schematic diagram of propane pre-cooled mixed refrigerant (APCI) cycle (Mortazavi et al., 2010).

2.3 Components Modeling

In this section the modeling details of the major components of the APCI liquefaction cycle, absorption chillers and gas turbine combined cycle are discussed. The main components are compressors, turbines, pumps, expansion valves and heat exchangers.

2.3.1 Compressor and Pump

The compressor (pump) power consumption, $P_{comp\ (pump)}$ is calculated by equation (2-1):

$$P_{comp(pump)} = \dot{m}(h_{outlet} - h_{inlet}) = \frac{\dot{m}(h_{ise,outlet} - h_{inlet})}{\eta_{comp(pump)}} \quad (2\text{-}1)$$

Where $\dot{m}$, h_{inlet}, $h_{ise,outlet}$, h_{outlet} and $\eta_{comp(pump)}$ are compressor (pump) mass flow rate, inlet enthalpy, isentropic outlet enthalpy, outlet enthalpy and compressor (pump) isentropic efficiency, respectively.

2.3.2 Turbine

The turbine power output, P_{turb}, is calculated by equation (2-2) :

$$P_{turb} = \dot{m}(h_{inlet} - h_{outlet}) = \dot{m}(h_{inlet} - h_{ise,outlet})\eta_{turb} \quad (2\text{-}2)$$

Where $\dot{m}$, h_{inlet}, $h_{ise,outlet}$, h_{outlet} and η_{turb} are turbine mass flow rate, inlet enthalpy, isentropic outlet enthalpy, outlet enthalpy and turbine isentropic efficiency, respectively.

2.3.3 Expansion Valve

The expansion process inside an expansion valve is assumed to be isenthalpic.

2.3.4 Heat Exchanger

In modeling the heat exchanger it is assumed that there is no heat leak in the heat exchanger. The heat exchanger duty ($\dot{Q}$) is calculated by equation (2-3):

$$\dot{Q} = \dot{m}(h_{outlet} - h_{inlet}) \quad (2\text{-}3)$$

2.3.5 Mixer and Separator

In modeling the mixers and the separators it is assumed that there is no heat leakage and no mechanical work is required for mixing or separation process.

2.3.6 Combustion Process

The combustion process is assumed to be isobaric and isenthalpic. It is modeled by minimizing the Gibbs free energy (G, see equation (2-4) (Olander 2008)) of the reactants and reaction products.

$$G = \sum_i N_i \mu_i \tag{2-4}$$

where μ_i and N_i are the chemical potential of component i and number of moles of component i, respectively.

2.3.7 Substance Property Modeling

In this dissertation, the Peng-Robinson-Boston-Mathias equation of state (Boston and Mathias 1980) is used for modeling the property of substances.

2.4 APCI Liquefaction Cycle Modeling:

ASPEN Plus (Aspen Plus 7.1), a steady-state process modeling software, was used for modeling the APCI Natural gas liquefaction. ASPEN Plus has a variety of databases that encompass thermodynamic and chemical properties for a range of chemical compounds and thermodynamic models for simulation of thermal systems. An ASPEN model consists of blocks corresponding to unit operations such as compressors, turbines, heat exchangers, and expansion valves and connecting streams such as material (fluid), work, and heat streams. To perform an ASPEN simulation the following parameters should be specified:

- Flow rates, compositions and operating conditions of the inlet streams.
- Operating conditions of the blocks used in the process, e.g., temperature

and pressure.

- Operating heat and/or work inputs into the process.

Flow rates, compositions, and state conditions of all outlet material streams as well as the heat and work output are computed based on the ASPEN model input data. The ASPEN model convergence tolerances for the relative residuals were set to be 1×10^{-4}. The natural gas sweetening process is not modeled for the sake of simplicity. Instead the gas composition after gas sweetening unit, as listed in Table 2.1, is used for modeling the liquefaction cycle. Due to the fact that heavier hydrocarbons do not affect the liquefaction cycle performance significantly, hexane plus hydrocarbons are approximated by n-hexane and iso-hexane with 0.16 and 0.24 for their mole fractions, respectively. The compressors of propane and MCR cycles are assumed to be centrifugal and axial types, respectively. All the condensers and inter-coolers are assumed to be cooled by sea water. The propane cycle is assumed to have five stages of cooling. The MCR cycle refrigerant consists of nitrogen, methane, ethane, and propane with mole fractions of 0.09, 0.36, 0.47 and 0.08, respectively. The fractionating columns of the fractionation unit are modeled by using "*radfrac"* component of the ASPEN plus software. All the expansion processes of the APCI liquefaction cycle were done by expansion valves, which is true for some of the APCI's LNG plants. In this dissertation this cycle option is referred as "*APCI base cycle"*. The flash gas recovery process after the expansion of LNG is not considered. Some of the other modeling assumptions used are listed in Table 2.2. The schematic of the *APCI base cycle* modeled in ASPEN is shown in Figure 2.2. In Figure 2.2, the propane and MCR cycle refrigerant streams are shown by the red and black streams

respectively. The natural gas streams undergoing liquefaction process are shown by the blue streams. The dark green streams from the separators are in liquid phase and are sent to the fractionation plant where they are separated into ethane (dark blue), propane (pink), butane (light green) and pentane-plus (purple). The ethane is sent to the cryogenic column for liquefaction. Ethane is then mixed with the liquefied natural gas before the expansion process. Further details of the ASPEN model components and streams are provided in the Appendix A.

Table 2.1. Gas composition after sweetening.

Component	Mole Fraction [%]
Nitrogen	0.1
Carbon Dioxide	0.005
Methane	85.995
Ethane	7.5
Propane	3.5
i-Butane	1
n- Butane	1
i-Pentane	0.3
n-Pentane	0.2
Hexane Plus	0.4
Total	100

Table 2.2. Modeling assumptions.

Axial compressor isentropic efficiency	0.86
Centrifugal compressor isentropic efficiency	0.83
Pinch temperature	3 K
Sea water temperature	35°C
Refrigerant temperature at condenser or super-heater exit	40°C
LNG temperature at the exit of cryogenic column	-160°C
Degree of superheating in propane cycle	10 K
LNG expander exit pressure	101.3 kPa

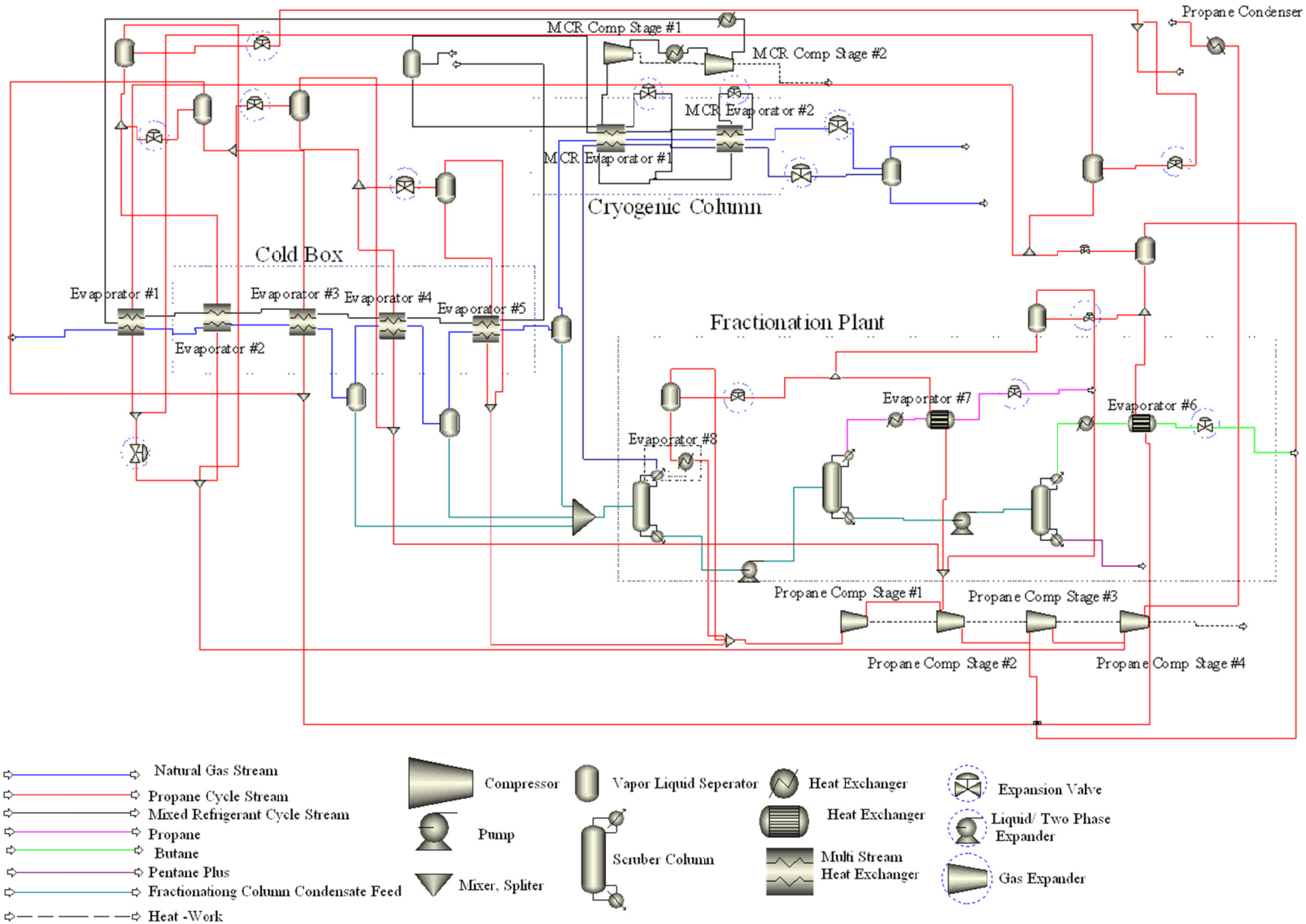

Figure 2.2: APCI base cycle modeled with ASPEN.

2.4.1 Results of APCI Base Cycle Model

The simulation results of the APCI base cycle are shown in Table 2.3. In this dissertation the results of APCI base cycle serves as a baseline for comparison of different enhancement options. In Table 2.3 COP refers to the coefficient of performance which is the ratio of the cooling capacity provided and the amount of power provided to the system.

Table 2.3. Modeling results for APCI base cycle.

Propane compressor power	43.7 MW
Mixed refrigerant compressor power	66.5 MW
Propane cycle cooling capacity	115.5 MW
Mixed refrigerant cycle cooling capacity	67.6 MW
Propane cycle COP	2.6
LNG vapor fraction after the expander	0.014 %
LNG production	98.83 kg/s
LPG (propane, butane, pentane and heavier hydrocarbons)	11 kg/s
Flash gas flow rate after LNG expander valve	1.28 kg/s

2.5 Enhancing APCI Natural Gas Liquefaction Cycle

Replacing the expansion valves of APCI base cycle with expanders will improve the liquefaction cycle energy efficiency. The points where there is a potential for recovering expansion losses are shown with the blue dashed circles in Figure 2.3. Liquid turbines or hydraulic turbines, a well established technology, are available with efficiencies over 90% (Gordon 2001) and can replace the MCR cycle and the LNG expansion process expansion valves. In order to apply liquid turbines to the

propane cycle, propane should be sub-cooled before being expanded in the turbine. Two-phase expanders are a developing technology with current efficiencies in the vicinity of 80% (Renaudin 1995, Kanoglu 2001). Two-phase expanders can replace expansion valves used in vapor compression cycles. Gas expanders could be used instead of expansion valves for expanding gases. Gas expanders or gas turbines are a well-developed technology and typically exist with efficiencies greater than 80% (Ordonez 2000).

The effect of replacing the expansion valves of the MCR and propane cycles and the LNG expansion process on the performance of the APCI base cycle is investigated in the current Section. Depending on the location, expansion valves could be replaced by liquid turbines, two-phase expanders and gas expanders. For replacing the expansion valves of the MCR cycle and the LNG expansion process, only two-phase expanders are considered. For the expansion valves of the propane cycle, both two-phase expanders and liquid turbines are considered. The gas expanders can only be used at the outlet of the propane cycle evaporator #1 which has the highest evaporating pressure. The isotropic efficiency of the two-phase expanders, liquid turbines and gas expander are assumed to be 0.85, 0.85 and 0.86, respectively. Four different enhancement options are considered, which are:

1. Replacing the LNG expansion valves by two-phase expanders. As shown in Figure 2.2, the LNG expansion valves are located after the cryogenic column.

2. Replacing the expansion valves of the evaporator # 1 and #2 of the MCR with two-phase expanders in addition to the enhancement of option 1.

3. Replacing all of the liquefaction cycle expansion valves with two-phase

expanders; except the expansion valve at the outlet of propane evaporator #1 which is replaced by a gas expander.

4. Replacing the propane cycle expansion valves (except the expansion valve at the outlet of propane cycle evaporator #1 which is replaced by a gas expander) with liquid turbines and MCR cycle and LNG expansion process expansion valves with two-phase expanders. It should be noted that for replacing the propane cycle expansion valves with liquid turbines the refrigerant (propane) is sub-cooled before the expansion process. Sub-cooling the propane before the expansion leads to a slight design change to the propane cycle as shown in Figure 2.3.

The enhancement results are shown in Table 2.4. Based on the Table 2.4 results, the APCI cycle enhanced with two-phase expanders for MCR cycle and LNG expansion process and liquid turbines for propane expansion process (Figure 2.3) is the most efficient cycle. In this cycle the total power consumption, flash gases after the LNG expander and energy consumed per unit mass of LNG are reduced by 2.43%, 96.09% and 3.68%, respectively in comparison to the APCI base cycle. In this enhanced APCI cycle about 3.47% of total consumed power is recovered by expanders. The LNG production is also increased by 1.24% in comparison to the APCI base cycle for the same amount of feed gas. If the recovered power is deducted from the liquefaction cycle total power consumption, the energy consumed per unit mass of LNG is reduced by 7.07%. The propane cycle COP enhancements are small and it is compatible with the analytical expectation. This is due to the fact that replacing expansion valves with expanders only utilizes the pressure exergy of the refrigerant which is not considerable. Although the enhancements are not significant

percentagewise, if these enhancement are considered from the amount of saved energy, it will lead to considerable saving and recovered power due to the scale of the plant. Due to the fact that MCR cycle receives cooling from the propane cycle, the conventional definition of COP, which is the ratio of the cooling capacity provided and the amount of power provided to the system, might not be suitable for describing its performance. Therefore the COP of the MCR cycle is not considered here.

Table 2.4. Modeling results for APCI enhanced cycles.

Cycle Option	Base APCI cycle	Enhanced with two-phase expanders for LNG expansion process	Enhanced with two-phase expanders for LNG and MCR expansion process	Enhanced with two-phase expanders for LNG, MCR, and propane expansion process	Enhanced with two-phase expanders and liquid turbines for LNG and propane expansion process
Propane cycle compressor power [MW]	43.7	43.7	43.0	42.8	42.1
MCR cycle compressor power [MW]	66.5	66.5	65.4	65.4	65.4
Propane cycle cooling capacity [MW]	115.5	115.5	113.9	113.9	114.0
MCR cycle cooling capacity [MW]	67.6	67.6	67.6	67.6	67.6
Propane cycle COP	2.6	2.6	2.7	2.7	2.7
LNG vapor fraction after the expander	0.0142	0.0006	0.0006	0.0006	0.0006
LNG production [kg/s]	98.83	100.06	100.06	100.06	100.06
LPG (propane, butane, pentane and heavier hydrocarbons) production [kg/s]	11	11	11	11	11
Flash gases after LNG expander [kg/s]	1.28	0.05	0.05	0.05	0.05
Recovered power from expanders [MW]	---	0.6	2.5	3.3	3.8
Total power consumption [MW]	110.2	110.2	108.3	108.1	107.5
Energy consumption per unit mass of LNG [MJ/kg]	1.11	1.10	1.08	1.08	1.07

Note: LPG = Liquefied Petroleum Gas. MCR = Multi-Component Refrigerant.

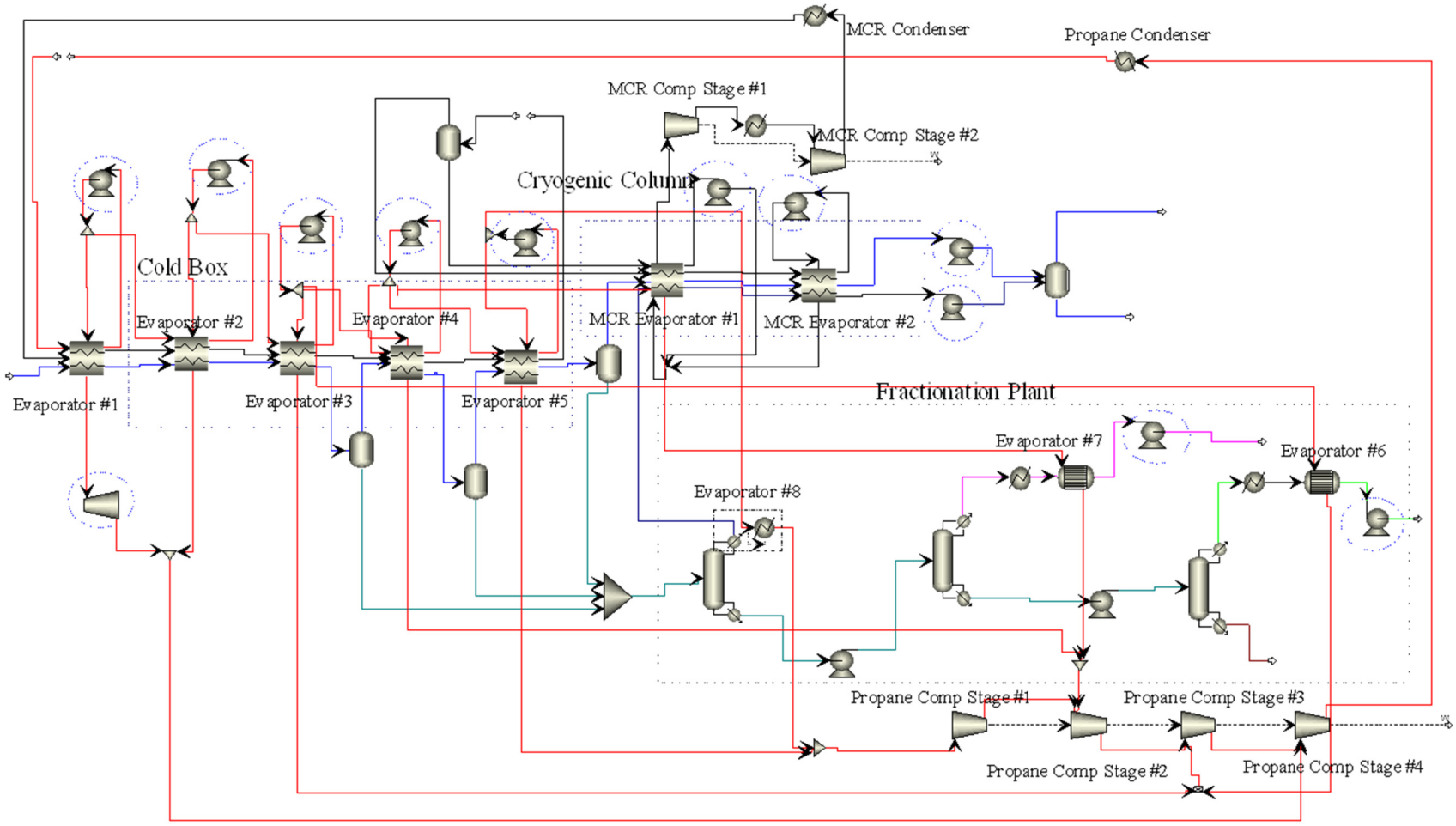

Figure 2.3. APCI cycle enhanced with two-phase expanders and liquid turbines for LNG and propane expansion processes.

2.6 APCI Driver Cycle Modeling

In this section first the modeling of different components of the gas turbine combined cycles are discussed. Then different gas turbine absorption chiller combined cycles and the corresponding design modification to the APCI liquefaction cycle are discussed. These design modifications will be used in the next section for introducing and optimizing different gas turbine combined cycles.

2.6.1 Absorption Cycle Modeling

Absorption chillers can provide refrigeration effect by getting heat from a heat source above the ambient temperature. Due to the availability of driver cycle waste heat such as gas turbine exhaust in the APCI LNG plant, absorption chillers are considered as a useful driver cycle efficiency improvement option. In this dissertation driver cycle efficiency (thermal efficiency) is defined as the ratio of the driver cycle output power to the rate of driver cycle energy consumption (i.e., fuel consumption).

In this section, double effect and single effect water/lithium-bromide absorption chillers are considered. These absorption chillers are assumed to be cooled by the sea water. The desorber outlet temperature for single effect and double effect absorption chillers are set to be 90°C and 180°C, respectively. The absorption chillers are modeled in ASPEN Plus. Comprehensive details of modeling both single effect and double effect absorption chillers can be found in Mortazavi et al., (2010), Somers, (2009) and Somers et al., (2012). The energy efficiency of an absorption chiller is represented by a coefficient of performance (COP) which is the ratio of the generated cooling to the heat input to the desorber of an absorption chiller. The calculated COP

of single effect and double effect absorption chillers for 7°C and 22°C evaporator temperatures are shown in Table 2.5. These two evaporating temperatures are the same as the two highest temperature stages of propane cycle. These COP values are used later to estimate the amount of waste heat that is required to generate the desired amount of cooling.

Table 2.5: COP of single-effect and double-effect absorption chillers for different evaporator temperatures.

	COP (9°C Evaporator)	COP (22°C Evaporator)
Single-effect absorption chiller	0.755	0.967
Double-effect absorption chiller	1.284	1.489

2.6.2 Gas Turbine Steam Combined Cycle Modeling

The driver cycles enhancements that are considered in this chapter are for gas turbine drivers. In this dissertation the liquefaction cycle with only gas turbines as the driver is considered as the base cycle for the comparison and the its drive cycle (i.e., gas turbine) is referred as "base driver cycle". In the base cycle, gas turbines are assumed to be the driver for the compressors of the propane and MCR cycles. In this dissertation the base driver cycle refers to the gas turbine driver cycle. To obtain an accurate estimate of gas turbine performance, a gas turbine having a rated capacity of 130 MW was modeled using the HYSYS software (HYSYS 7.1). The block diagram of the gas turbine cycle modeled with HYSYS is shown in Figure 2.4. It should be noted that although combustion chamber in Figure 2.4 has two outlets, the bottom outlet has a zero mass flow rate. This extra outlet is due to fact that in HYSYS the Gibbs minimizer reactor (HYSYS 7.1) always has two outlets, one for liquid phase and one for gaseous phase. Therefore since the combustion chamber outlet is in

gaseous phase the liquid outlet has a zero mass flow rate. The gas turbine fuel is assumed to be pure methane. To account for air leakages and blade cooling, a portion of the compressor discharge is diverted directly to the turbine instead of passing through the combustion chamber. To verify the gas turbine model, vender's data (GE Energy 2007) at ISO condition, which is 15°C and 1 atm inlet pressure, was used. The comparison of the gas turbine simulation results with the vender's data and the ASPEN model developed by Mortazavi et al., (2010) is shown in Table 2.6. As it is shown in Table 2.6, the maximum discrepancy of the HYSYS simulation results from the vender's data (GE Energy 2007) is about 0.35%, which is in an acceptable range.

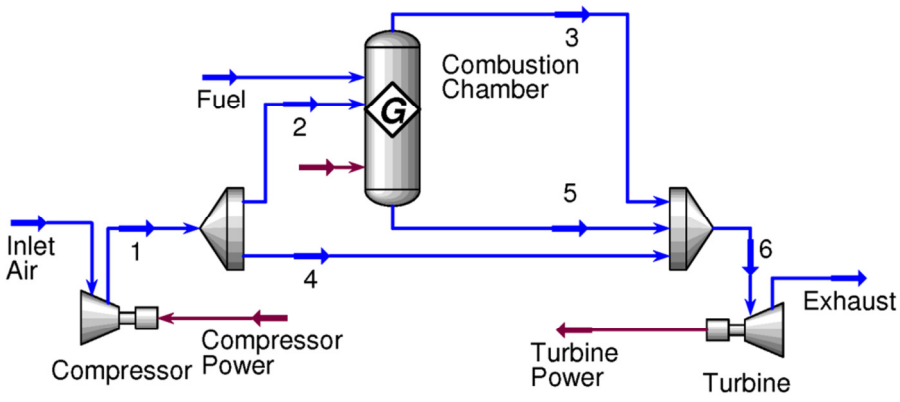

Figure 2.4: HYSYS block diagram of a gas turbine.

Table 2.6: Comparison of a gas turbine modeled in HYSYS with venders' data and Mortazavi et al., (2010) results.

	ISO rated power (MW)	Efficiency (%)	Exhaust temperature (°C)
Actual gas turbine*	130.100	34.6	540
ASPEN model**	130.103	35	540.4
HYSYS model	130.104	34.7	539.4
ASPEN discrepancy**	+0.003 (0.0%)	+0.4 (1.16%)	+0.4
HYSYS discrepancy	+0.004 (0.0%)	+0.1 (0.35%)	-0.6

*GE Energy (2007)
**Here the discrepancy is defined as the difference between the model result and the venders' data and the positive value is for the case where the model result is greater than venders' data value. The number in parenthesis represents the discrepancy as a percentage of the venders' data value.

The steam cycle of the combined cycle is also modeled in HYSYS software. It is assumed there is no pressure drop in the piping of the steam side of steam cycle. The air side pressure drop is defined for individual cycle in Section 2.7. The pumps isentropic efficiency in any combined cycle configuration is assumed to be 90%. Two isentropic steam turbine efficiencies with the value of 86% and 90% are considered for each combined cycle to examine the performance difference between conventional and more expensive high efficiency steam turbines. The water temperature at the outlet of the condenser temperature is assumed to be 45 °C. More details regarding each driver cycle's enhanced configuration are discussed in Section 2.7.

2.6.3 Gas Turbine Absorption Chiller Combined Cycle

To investigate the available amount of gas turbine waste heat for different gas turbine absorption chiller combined cycle options, the gas turbine ASPEN model was integrated to the APCI base cycle ASPEN model. The gas turbine ASPEN model was scaled to provide the plant demand at 45°C ambient temperature under its full load condition. Scaling gas turbine is not an unreasonable assumption due to the fact that

some gas turbine manufactures scale their gas turbine design to meet different power demands. Here scaling refers to increasing or decreasing the existing gas turbine design dimensions by multiplying them by a scaling factor. The scaling factor is equal to the ratio of the desired output power to existing gas turbine output power. To examine the gas turbine part load effects, two cases were considered for each enhancement option. In the first case, which is referred as an "unscaled-case", it is assumed that for each option the gas turbine will be the same as the base cycle gas turbine (i.e., same capacity). In the unscaled-case, there could be some part load degradation effects due to the fact that the liquefaction power demand is less than the base cycle power demand. In the second case, which is referred as a "scaled case", the assumption is that for each option a gas turbine is sized to deliver the maximum plant demand at its full load. The minimum exhaust temperature is set to be 180 °C, this is done to prevent condensing issues and excessive pressure drop at the gas turbine exhaust. It should be noted that the minimum exhaust temperature to run the absorption chiller desorber is assumed to be 200 °C. To calculate the gas turbine energy consumption, pure methane is assumed to be the gas turbine fuel with the low heating value of 50.1 MJ/kg. Double-effect water/lithium-bromide absorption chillers with 22°C and 9°C evaporating temperatures are used to utilize gas turbine waste heat.

Next, several gas turbine absorption chiller combined cycle options are described. The simulation results for these options are presented in Section 2.6.4.

Option 1_{abs}: Replacing 22°C propane cycle evaporators with absorption chillers

Option 1_{abs} enhancement is replacing the 22°C evaporators of the propane cycle with

a double effect absorption chiller powered by gas turbine waste heat.

Option 2 $_{abs}$: Replacing 22°C propane cycle evaporators and cooling the inlet of gas turbine with absorption chillers

In this option, the 22°C propane cycle evaporator is replaced with a 22°C absorption chiller evaporator. The gas turbine inlet is cooled to 30°C by the absorption chiller. The inlet cooler evaporator of the gas turbine is assumed to be at 22°C.

Option 3 $_{abs}$: Replacing 22°C and 9°C propane cycle evaporators with absorption chillers

In option 3_{abs}, the 22°C and 9°C propane cycle evaporators are replaced with absorption chillers evaporators with evaporating temperatures of 22°C and 9°C respectively. Propane is also subcooled to 25°C by a 22°C absorption chillers evaporator and to 12°C a 9°C absorption chillers evaporator.

Option 4 $_{abs}$: Replacing 22°C and 9°C propane cycle evaporators cooling the inlet of gas turbine with absorption chillers

In option 4_{abs}, the 22°C and 9°C propane cycle evaporators are replaced with absorption chillers evaporators with evaporating temperatures of 22°C and 9°C respectively. Propane is first subcooled to 25°C by a 22°C absorption chillers evaporator and then to 12°C by a 9°C absorption chiller evaporator. The gas turbine inlet is cooled down to 30°C and 17°C with the 22°C and 9°C evaporators of absorption chillers respectively.

Option 5 $_{abs}$: Replacing 22°C and 9°C evaporators and cooling the condenser of propane cycle at 27°C with absorption chillers

In this option, the 22°C and 9°C propane cycle evaporators are replaced with 22°C and 9°C evaporators of absorption chillers respectively. Propane is cooled and condensed at 27°C by a 22°C absorption chiller evaporator and subcooled to 12°C by a 9°C absorption chiller evaporator.

Option 6 $_{abs}$: Replacing 22°C and 9°C evaporators and cooling the condenser of propane at 27°C cycle and turbine inlet with absorption chillers

In option 6_{abs}, the 22°C and 9°C propane cycle evaporators are replaced with absorption chillers evaporator with evaporating temperatures of 22°C and 9°C respectively. Propane is condensed at 27°C and subcooled to 12°C with the 22°C and 9°C evaporators of absorption chillers respectively. The gas turbine inlet was first cooled to 30°C then cooled down to 17°C by 22°C and 9°C absorption chillers evaporators respectively.

Option 7 $_{abs}$: Replacing 22°C and 9°C evaporators and cooling the condenser of propane cycle at 14°C with absorption chillers

In this option, the 22°C and 9°C propane cycle evaporators are replaced with 22°C and 9°C absorption chillers evaporators respectively. Propane is condensed at 14°C and subcooled to 12°C by a 9°C absorption chillers evaporator.

Option 8 $_{abs}$: Replacing 22°C and 9°C evaporators and cooling the condenser of propane at 14°C cycle and inter cooling the compressor of mixed refrigerant cycle with absorption chillers

For the last option, the 22°C and 9°C propane cycle evaporators are replaced with 22°C and 9°C absorption chillers evaporators respectively. Propane is condensed at

14°C and subcooled to 12°C by a 9°C absorption chillers evaporator. MCR cycle refrigerant is intercooled to 40°C and then to 14°C by sea water and a 9°C absorption chiller evaporator respectively. This option is shown in Figure 2.5.

2.6.4 Gas Turbine Absorption Chiller Combined Cycle Simulation Results

The simulation results of eight gas turbine absorption chiller combined cycle enhancement options are summarized in Table 2.7. In Table 2.7 for each option the gas turbine fuel consumption, the power reduction, and the required amount of waste heat to operate the absorption chiller are listed. In Table 2.7 the numbers in the parenthesis represents the percentile saving with respect to the base cycle. In Table 2.7 the options are ranked based on their fuel consumption where the option 1_{abs} has the highest amount of fuel consumption. Fuel consumption is directly related to the energy efficiency of the plant due to the fact that the LNG production capacity of the plant is held constant for all the gas turbine absorption chiller combined cycle options. The fuel consumption could be reduced by either increasing the gas turbine power generation efficiency and/or reducing the compressor power demand. The gas turbine efficiency could be increased by cooling the inlet air of the gas turbine. The compressor power consumption will be reduced by replacing the propane evaporators by waste heat run absorption chillers evaporators, lowering the propane cycle condenser temperature by cooling it using absorption chillers and/or inter-cooling the compressor of the MCR cycle using absorption chillers. Based on the results of Table 2.7, by implementing option 8_{abs} the compressor power consumption could be reduced by 21.3%. By using a scaled gas turbine option 8_{abs} also leads to reduction of gas turbine fuel consumption by 21.3%. In each option the fuel consumption of the

unscaled gas turbine case is higher than that of the scaled gas turbine case. This fact means that the efficiency of the unscaled-case is lower than the scaled case for the same option. The source of the gas turbine efficiency difference is that in the scaled case the gas turbine is operated at the full load running condition while in the unscaled-case the gas turbine is operated at part load running condition. At the part load running condition the gas turbine firing temperature is lower than the full load running condition. Lowering the gas turbine firing temperature leads to reduction in gas turbine efficiency. Furthermore due to higher gas turbine air mass flow rate of the unscaled-case, it requires both more amount of waste heat and higher percent of available waste heat than the scaled case for the same option. Considering the results of Table 2.7, the better the option the more amount of waste heat is required. For the same options the scaled gas turbines have smaller power capacity in comparison to the baseline plant gas turbine (i.e., unscaled-case). This difference in size means the scaled gas turbines will result in lower capital cost for the gas turbine driver in comparison to the base.

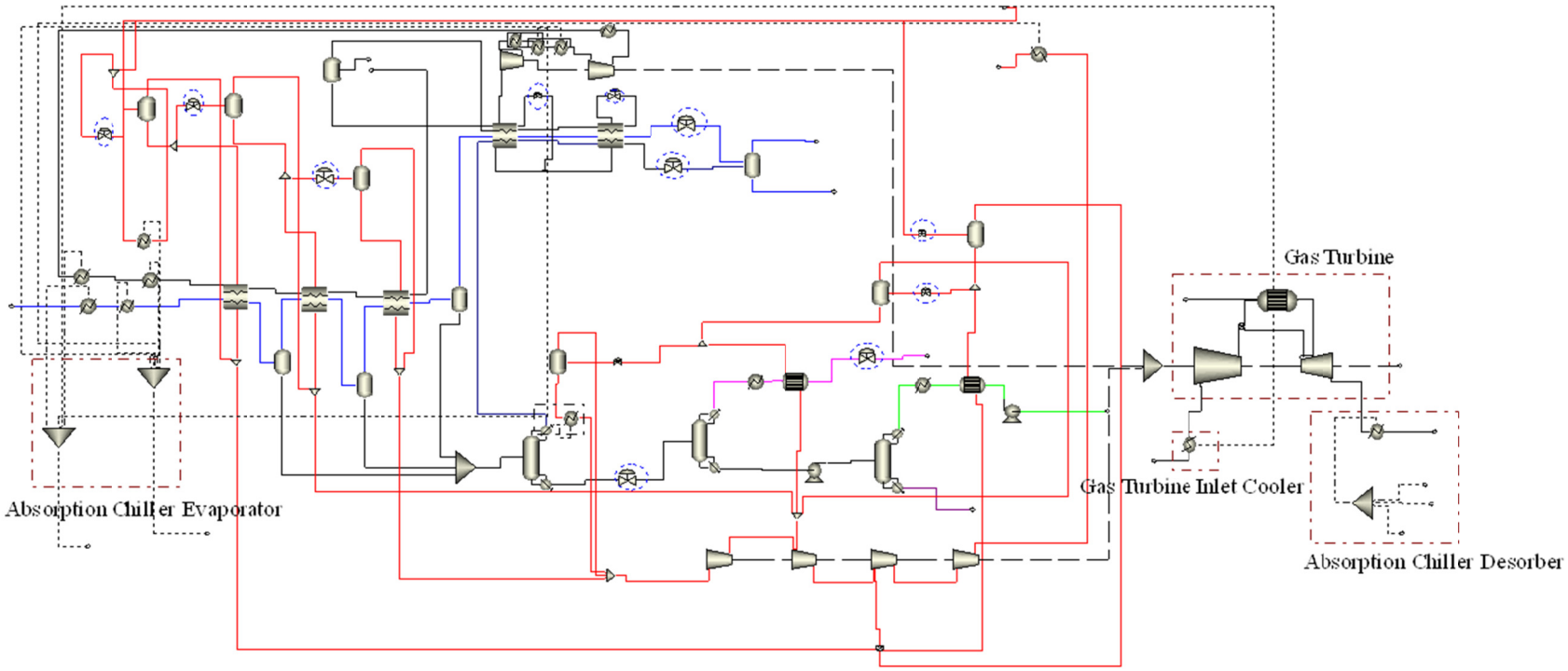

Figure 2.5 APCI driver cycle enhanced with option abs8

Table 2.7: Enhancement results of different waste heat utilization options

Gas Turbine Sizing						Scaled turbine size case		Unscaled turbine size case
Option	Compressor Power [MW]	Power Reduction [MW] (% saving)	Required Amount of Waste Heat [MW]	Fraction of Available Amount of Waste Heat [%]	Fuel Consumption [MW] (% saving)	Required Amount of Waste Heat [MW]	Fraction of Available Amount of Waste Heat [%]	Fuel Consumption [MW] (% saving)
APCI base cycle	110.2	-----	-----	-----	329.4	-----	-----	329.4
1_{abs}	107.5	2.7 (2.4)	8.9	5.9	321.4 (2.4)	8.9	6.0	322.8 (2.0)
2_{abs}	107.5	2.7 (2.4)	12.6	9.0	314.0 (4.7)	12.9	9.3	318.8 (3.4)
3_{abs}	100.3	9.9 (8.9)	35.0	25.2	300.0 (8.9)	35.0	25.3	304.9 (7.5)
4_{abs}	100.3	9.9 (8.9)	41.6	33.5	287.6 (12.7)	43.1	36.3	296.5 (10.0)
5_{abs}	94.0	16.1 (14.6)	98.3	75.4	281.2 (14.6)	98.3	76.1	289.5 (12.2)
6_{abs}	94.0	16.1 (14.6)	104.5	89.9	269.6 (18.2)	106.4	97.0	281.0 (14.7)
7_{abs}	88.4	21.8 (19.7)	105.6	86.1	264.4 (19.7)	105.6	87.2	275.3 (16.4)
8_{abs}	86.7	23.5 (21.3)	116.4	96.8	259.2 (21.3)	116.4	98.2	271.1 (17.7)

2.7 APCI Driver Cycle Enhancement and Optimization

In this section, first, different driver cycle enhancement configurations are introduced. Then, the optimization method used for optimizing these configurations is discussed followed by the optimization results.

2.7.1 Driver Cycle Enhancement Configurations

Two types of driver cycle enhancement are considered. The first type, called conventional enhancements, refers to LNG plant driver cycle enhancement configurations that have been previously proposed in the literature (Di Napoli 1980, Mortazavi et al., 2010). The second type, called proposed triple combined cycle enhancements, are new LNG plant driver cycle configurations that have not been proposed before for an LNG plant. The details of the conventional driver cycle configurations and the proposed triple combined cycle configurations are discussed in Section 2.7.1.1 and 2.7.1.2 respectively with their related optimization objective, design constraints and design variables.

2.7.1.1 Conventional Enhancements

The following driver cycle enhancements are considered as the conventional enhancements. The schematics of options 2-4 and their optimization formulations are shown in Figure 2.6 and Table 2.8, respectively.

Option 1: Combined gas turbine and double-effect absorption chiller

In this option the gas turbine exhaust is used to run double-effect absorption chillers. The absorption chiller evaporators replace the 22°C and 9°C evaporators of the propane cycle. The double-effect absorption chiller also cools the propane cycle

condenser, gas turbine inlet-air and the intercooler of the MCR cycle with its 22°C and 9°C evaporators. The results of this option are taken from Mortazavi et al., (2010).

Option 2: Combined gas turbine and single pressure steam cycle

In this option a single pressure gas turbine cycle combined cycle is used as the driver cycle. Here the single pressure refers to the steam cycle of the combined cycle. The schematic of this option is shown in Figure 2.6(a).

Option 3: Combined gas turbine and double pressure steam cycle without reheat

In this option a two pressure gas turbine combined cycle is selected as the driver cycle. As shown in Figure 2.6(b), the outlet steam of the high pressure (HP) turbine is not reheated before expansion in the low pressure (LP) steam turbine.

Option 4: Combined gas turbine and double pressure steam cycle with reheat

In this option, a two pressure gas turbine combined cycle with reheat is selected as the driver cycle. As shown in Figure 2.6(c), the outlet steam of high pressure turbine is reheated before expansion in the low pressure steam turbine.

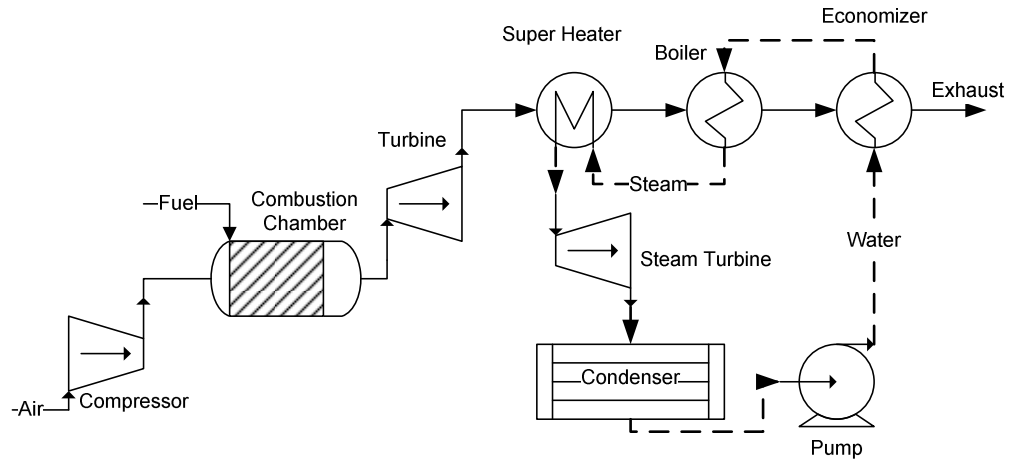
Economizer
Super Heater
Boiler
Exhaust
Turbine
Steam
Fuel
Combustion
Chamber
Steam Turbine
Water
Condenser
-Air
Compressor
Pump

(a)

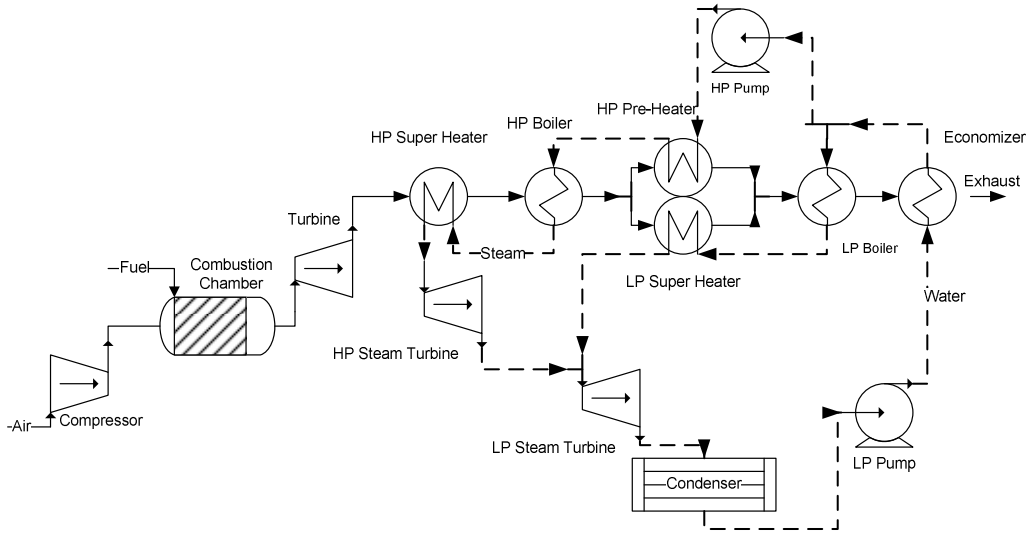
HP Pump
HP Pre-Heater
HP Boiler
HP Super Heater
Economizer
Exhaust
Turbine
Steam
LP Boiler
Fuel
Combustion
Chamber
LP Super Heater
Water
HP Steam Turbine
-Air
Compressor
LP Steam Turbine
LP Pump
Condenser

(b)

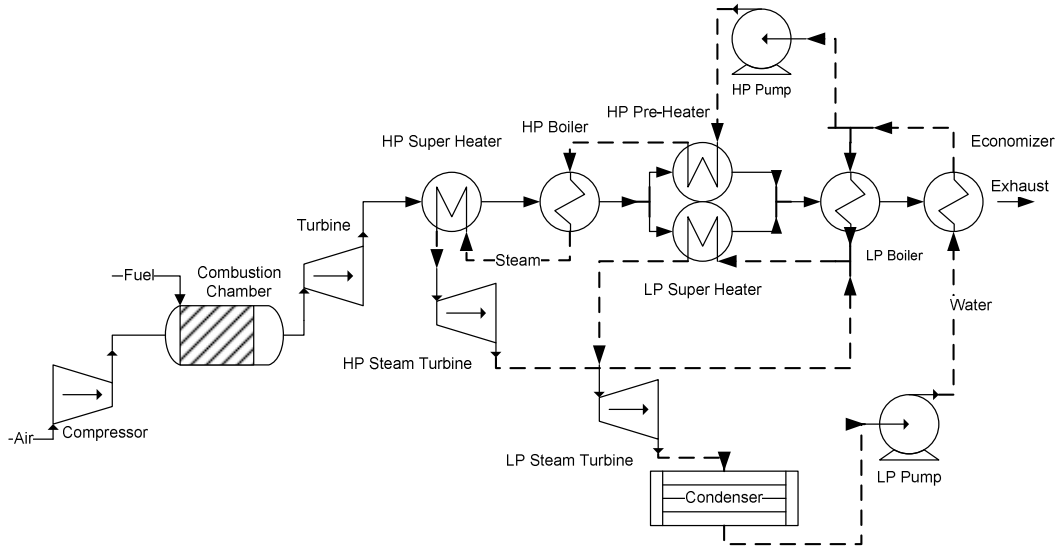

(c)

Figure 2.6: Schematic diagram of (a) option 2, (b) option 3, and (c) option 4.

Table 2.8: The optimization formulation of conventional options.

Option	Formulation
2	$\min_{\mathbf{dv}} \dot{m}_{Fuel}$
	$S.t.$
	$\Delta T_{p,Super\ heater} \geq 10\ ^{\circ}\mathrm{C}$
	$\Delta T_{p,Boiler} \geq 10\ ^{\circ}\mathrm{C}$
	$\Delta T_{p,Economizer} \geq 10\ ^{\circ}\mathrm{C}$
	$T_{\min,\ Exhaust} \leq T_{Exhaust}$
	$T_{Inlet,Turbine} \leq 1124\ ^{\circ}\mathrm{C}$
	$0.9 \leq x_{Outlet,Steam\ Turbine}$
	$Pw_{Turbine} + Pw_{Steam\ Turbine} - Pw_{Compressor} - Pw_{Pump} - Pw_{Liquefaction} \geq 0$
	$\mathbf{dv} = [\dot{m}_{Water}, P_{Boiler}, T_{Super\ heater}, \dot{m}_{Air}, \dot{m}_{Fuel}]$
	$[1,1000,350,200,4] \leq \mathbf{dv} \leq [90,20000,560,415,7.5]$

3

$$\min_{\mathbf{dv}} \ \dot{m}_{Fuel}$$

$$S.t.$$

$$\Delta T_{p,HP\ Super\ heater} \geq 10\ ^{\circ}\mathrm{C}$$

$$\Delta T_{p,HP\ Boiler} \geq 10\ ^{\circ}\mathrm{C}$$

$$\Delta T_{p,HP\ Pre\ heater} \geq 10\ ^{\circ}\mathrm{C}$$

$$\Delta T_{p,LP\ Super\ heater} \geq 10\ ^{\circ}\mathrm{C}$$

$$\Delta T_{p,LP\ Boiler} \geq 10\ ^{\circ}\mathrm{C}$$

$$\Delta T_{p,Economizer} \geq 10\ ^{\circ}\mathrm{C}$$

$$T_{\min,\ Exhaust} \leq T_{Exhaust}$$

$$T_{Inlet,Turbine} \leq 1124\ ^{\circ}\mathrm{C}$$

$$0.9 \leq x_{Outlet,HP\ Steam\ Turbine}$$

$$0.9 \leq x_{Outlet,LP\ Steam\ Turbine}$$

$$T_{LP\ Super\ heater} \leq T_{HP\ Super\ heater}$$

$$P_{LP,\ Boiler} \leq P_{HP,\ Boiler}$$

$$Pw_{Turbine} + Pw_{HP,\ Steam\ Turbine} + Pw_{LP,\ Steam\ Turbine} - Pw_{Compressor}$$

$$-Pw_{HP,\ Pump} - Pw_{LP,\ Pump} - Pw_{Liquefaction} \geq 0$$

$$\mathbf{dv} = [\dot{m}_{Water}, R_{mlp}, P_{LP,\ Boiler}, T_{LP,\ Super\ heater}, P_{HP,\ Boiler}, T_{HP,\ Super\ heater}, \dot{m}_{Air}, \dot{m}_{Fuel}]$$

$$[1,0.0001,1000,350,1000,400,200,4] \leq \mathbf{dv}$$

$$\mathbf{dv} \leq [60,0.9999,20000,560,20000,565,415,7.5]$$

4

$$\min_{\mathbf{dv}} \ \dot{m}_{Fuel}$$

$$S.t.$$

$$\Delta T_{p,HP\ Super\ heater} \geq 10\ ^{\circ}\mathrm{C}$$

$$\Delta T_{p,HP\ Boiler} \geq 10\ ^{\circ}\mathrm{C}$$

$$\Delta T_{p,HP\ \mathrm{Pre}\ heater} \geq 10\ ^{\circ}\mathrm{C}$$

$$\Delta T_{p,LP\ Super\ heater} \geq 10\ ^{\circ}\mathrm{C}$$

$$\Delta T_{p,LP\ Boiler} \geq 10\ ^{\circ}\mathrm{C}$$

$$\Delta T_{p,Economizer} \geq 10\ ^{\circ}\mathrm{C}$$

$$T_{\min,\ Exhaust} \leq T_{Exhaust}$$

$$T_{Inlet,Turbine} \leq 1124\ ^{\circ}\mathrm{C}$$

$$0.9 \leq x_{Outlet,HP\ Steam\ Turbine}$$

$$0.9 \leq x_{Outlet,LP\ Steam\ Turbine}$$

$$T_{LP\ Super\ heater} \leq T_{HP\ Super\ heater}$$

$$P_{LP,\ Boiler} \leq P_{HP,\ Boiler}$$

$$Pw_{Turbine} + Pw_{HP,\ Steam\ Turbine} + Pw_{LP,\ Steam\ Turbine} - Pw_{Compressor}$$

$$-Pw_{HP,\ Pump} - Pw_{LP,\ Pump} - Pw_{Liquefaction} \geq 0$$

$$\mathbf{dv} = [\dot{m}_{Water}, R_{mlp}, P_{LP,\ Boiler}, T_{LP,\ Super\ heater}, P_{HP,\ Boiler}, T_{HP,\ Super\ heater}, \dot{m}_{Air}, \dot{m}_{Fuel}]$$

$$[1,0.0001,1000,350,1000,400,200,4] \leq \mathbf{dv}$$

$$\mathbf{dv} \leq [60,0.9999,20000,560,20000,565,415,7.5]$$

2.7.1.2 Proposed Triple Combined Cycle Enhancements

The following driver cycle enhancements are considered as the proposed enhancements. These cycles have not been proposed as the driver of natural gas liquefaction cycles. In this dissertation, the triple combined cycle refers to a cycle that consists of a gas turbine cycle, a steam cycle and an absorption cooling cycle. The schematics of these cycles and their optimization formulations are shown in Figure 2.7 and Table 2.9, respectively.

Option 5: Triple gas turbine combined cycle with a single pressure steam cycle and a double-effect absorption chiller

In this option, a triple gas turbine combined cycle with a single pressure steam cycle and a double effect absorption chiller is used as the driver cycle. As shown in Figure 2.7(a), the single pressure steam cycle utilizes the gas turbine exhaust to generate superheated steam and run the steam turbine. The steam cycle condenser outlet temperature is set to be 185 °C. The absorption chiller generator is heated by the steam cycle condenser. The double-effect absorption chiller evaporators replace the 22°C and 9°C evaporators of the propane cycle. The absorption chiller also cools the gas turbine inlet-air and the MCR cycle intercooler.

Option 6: Triple gas turbine combined cycle with a single pressure steam cycle and a single-effect absorption chiller

In this option, a triple gas turbine combined cycle with a single pressure steam cycle and a single effect absorption chiller is used as the driver cycle. As shown in Figure 2.7(a), the single pressure steam cycle utilizes the gas turbine exhaust to generate superheated steam and run the steam turbine. The steam cycle condenser outlet temperature is set to be 95°C. The absorption chiller generator is heated by the steam cycle condenser. The single-effect absorption chiller evaporators replace the 22°C and 9°C evaporators of the propane cycle. The absorption chiller also cools the gas turbine inlet-air and the MCR cycle intercooler.

Option 7: Split design triple gas turbine combined cycle with a single pressure steam cycle and a double-effect absorption chiller

In this option, a triple gas turbine combined cycle with a single pressure steam cycle and a double effect absorption chiller is used as the driver cycle. As shown in Figure 2.7(b), the single pressure steam cycle utilizes the gas turbine exhaust to generate superheated steam. The superheated steam is sent to the high pressure steam turbine where it is expanded. Then a portion of the high pressure steam turbine outlet is used to heat the generator of the double-effect absorption chiller. The remaining portion of the steam is expanded in the low pressure steam turbine and then it is condensed at 45°C in the condenser. The double-effect absorption chiller evaporators replace the 22°C and 9°C evaporators of the propane cycle. The absorption chiller also cools the gas turbine inlet-air and the MCR cycle intercooler.

Option 8: Split design triple gas turbine combined cycle with a single pressure steam cycle and a single-effect absorption chiller

In this option, a triple gas turbine combined cycle with a single pressure steam cycle and a single-effect absorption chiller is used as the driver cycle. As shown in Figure 2.7(b), the single pressure steam cycle utilizes the gas turbine exhaust to generate superheated steam. The superheated steam is sent to the high pressure steam turbine where it is expanded. Then a portion of the high pressure steam turbine outlet is used to heat the generator of the single effect absorption chiller. The remaining portion of the steam is expanded in the low pressure steam turbine and then it is condensed at 45°C in the condenser. The single-effect absorption chiller evaporators replace the 22°C and 9°C evaporators of the propane cycle. The absorption chiller also cools the gas turbine inlet-air and the MCR cycle intercooler.

Option 9: Triple gas turbine combined cycle with a single pressure steam cycle and a double-effect absorption chiller with an auxiliary burner

In this option, a triple gas turbine with an auxiliary burner combined cycle with a single pressure steam cycle and a double-effect absorption chiller is used as the driver cycle. As shown in Figure 2.7(c), the auxiliary burner is located at the exhaust of the gas turbine. The function of the auxiliary burner is to increase the temperature of the gas turbine exhaust. The single pressure steam cycle utilizes the gas turbine exhaust to generate superheated steam and run the steam turbine. The steam cycle condenser outlet temperature is set to be 185°C. The absorption chiller generator is heated by the steam cycle condenser. The double-effect absorption chiller evaporators replace the 22°C and 9°C evaporators of the propane cycle. The absorption chiller also cools the gas turbine inlet-air and the MCR cycle intercooler.

Option 10: Triple gas turbine combined cycle with a single pressure steam cycle and a single effect absorption chiller with an auxiliary burner

In this option a triple gas turbine with an auxiliary burner combined cycle with a single pressure steam cycle and a single effect absorption chiller is used as the driver cycle. As shown in Figure 2.7(c), the auxiliary burner is located at the exhaust of the gas turbine. The function of the auxiliary burner is to increase the temperature of the gas turbine exhaust. The single pressure steam cycle utilizes the gas turbine exhaust to generate superheated steam and run the steam turbine. The steam cycle condenser outlet temperature is set to be 95°C. The absorption chiller generator is heated by the steam cycle condenser. The single-effect absorption chiller evaporators replace the 22°C and 9°C evaporators of the propane cycle. The absorption chiller also cools the

gas turbine inlet-air and the MCR cycle intercooler.

Option 11: Triple gas turbine combined cycle with a double pressure steam cycle with reheat and a double-effect absorption chiller

In this option, a triple gas turbine combined cycle with a double pressure steam cycle with reheat and a double-effect absorption chiller is used as the driver cycle. As shown in Figure 2.7(d), the double pressure steam cycle utilizes the gas turbine exhaust to generate high pressure superheated steam. The high pressure superheated steam is expanded in the high pressure steam turbine. Then the outlet steam of the high pressure steam turbine is reheated before expansion in the low pressure steam turbine. The steam cycle condenser outlet temperature is set to be 185°C. The absorption chiller generator is heated by the steam cycle condenser. The double-effect absorption chiller evaporators replace the 22°C and 9°C evaporators of the propane cycle. The absorption chiller also cools the gas turbine inlet-air and the MCR cycle intercooler.

Option 12: Triple gas turbine combined cycle with a double pressure steam cycle with reheat and a single-effect absorption chiller

In this option, a triple gas turbine combined cycle with a single pressure steam cycle with reheat and a double effect absorption chiller is used as the driver cycle. As shown in Figure 2.7(d), the double pressure steam cycle utilizes the gas turbine exhaust to generate high pressure superheated steam. The high pressure superheated steam is expanded in the high pressure steam turbine. Then the outlet steam of the high pressure steam turbine is reheated before expansion in the low pressure steam turbine. The steam cycle condenser outlet temperature is set to be 95°C. The

absorption chiller generator is heated by the steam cycle condenser. The single-effect absorption chiller evaporators replace the 22°C and 9°C evaporators of the propane cycle. The absorption chiller also cools the gas turbine inlet-air and the MCR cycle intercooler.

Option 13: Split design triple gas turbine combined cycle with a double pressure steam cycle with reheat and a double-effect absorption chiller

In this option, a triple gas turbine combined cycle with a double pressure steam cycle with reheat and a double effect absorption chiller is used as the driver cycle. As shown in Figure 2.7(e), the double pressure steam cycle utilizes the gas turbine exhaust to generate high pressure superheated steam. The high pressure superheated steam is expanded in the high pressure steam turbine. Then a portion of the high pressure steam turbine outlet is used to heat the generator of the double-effect absorption chiller. The remaining portion of the steam is then reheated before expansion in the low pressure steam turbine. The outlet of the low pressure steam turbine is condensed at 45°C in the condenser. The double effect absorption chiller evaporators replace the 22°C and 9°C evaporators of the propane cycle. The absorption chiller also cools the gas turbine inlet-air and the MCR cycle intercooler.

Option 14: Split design triple gas turbine combined cycle with a double pressure steam cycle with reheat and a single-effect absorption chiller

In this option, a triple gas turbine combined cycle with a double pressure steam cycle with reheat and a single-effect absorption chiller is used as the driver cycle. As shown in Figure 2.7(e), the double pressure steam cycle utilizes the gas turbine exhaust to generate high pressure superheated steam. The high pressure superheated steam is

expanded in the high pressure steam turbine. Then a portion of the high pressure steam turbine outlet is used to heat the generator of the single effect absorption chiller. The remaining portion of the steam is then reheated before expansion in the low pressure steam turbine. The outlet of the low pressure steam turbine is condensed at 45°C in the condenser. The single-effect absorption chiller evaporators replace the 22°C and 9°C evaporators of the propane cycle. The absorption chiller also cools the gas turbine inlet-air and the MCR cycle intercooler.

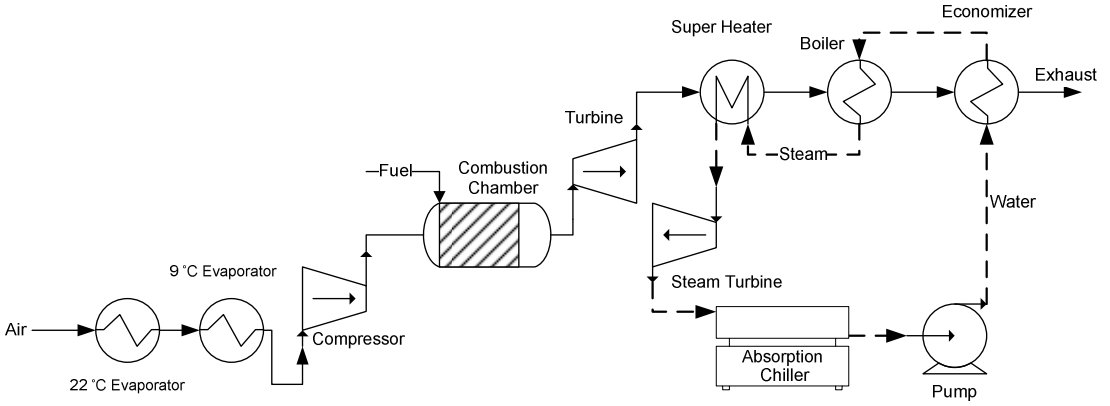

(a)

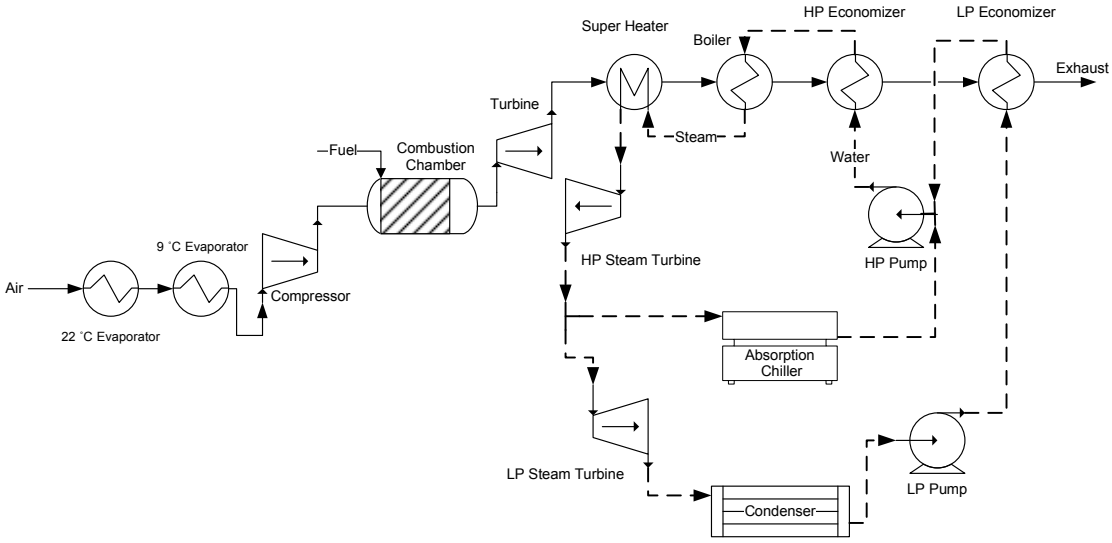

(b)

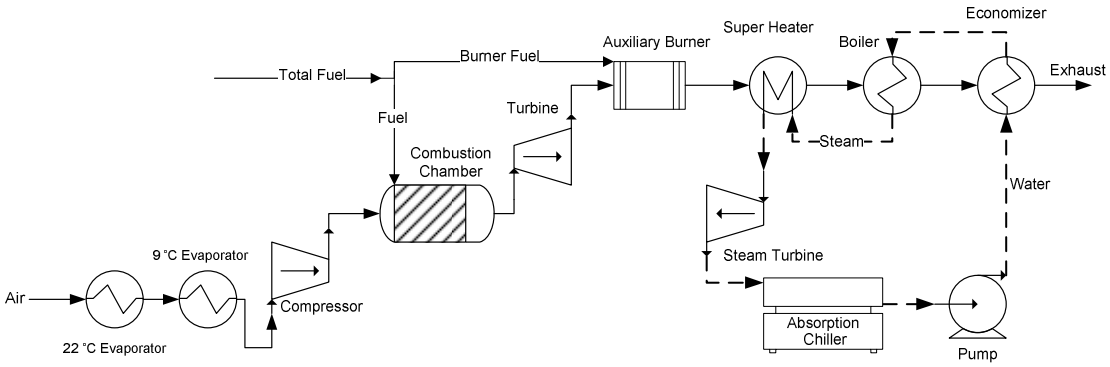
Total Fuel
Burner Fuel
Auxiliary Burner
Super Heater
Boiler
Economizer
Exhaust
Fuel
Turbine
Steam
Combustion Chamber
Water
9 °C Evaporator
Steam Turbine
Air
Compressor
Absorption Chiller
22 °C Evaporator
Pump

(c)

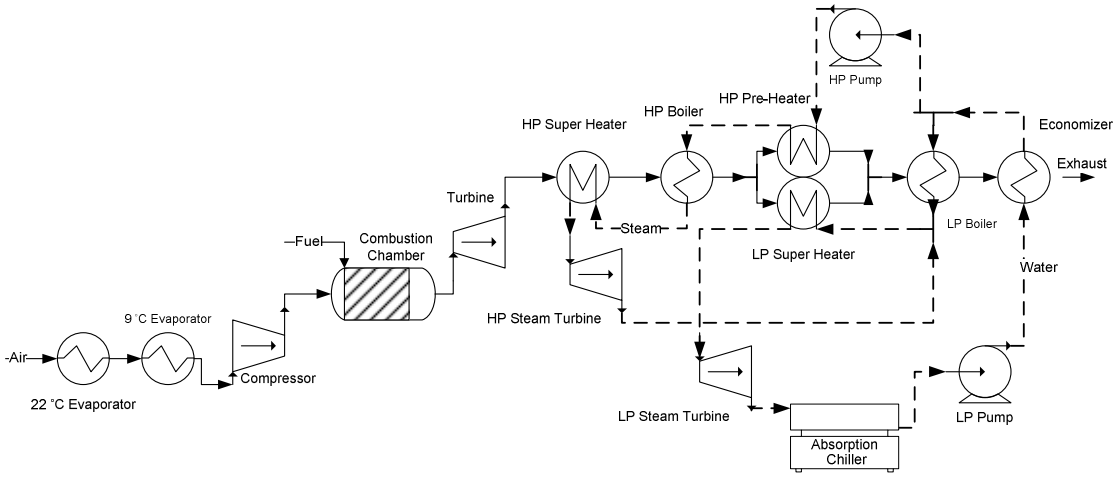
HP Pump
HP Pre-Heater
HP Super Heater
HP Boiler
Economizer
Exhaust
Turbine
Steam
LP Boiler
Fuel
Combustion Chamber
LP Super Heater
Water
9 °C Evaporator
HP Steam Turbine
Air
Compressor
22 °C Evaporator
LP Steam Turbine
Absorption Chiller
LP Pump

(d)

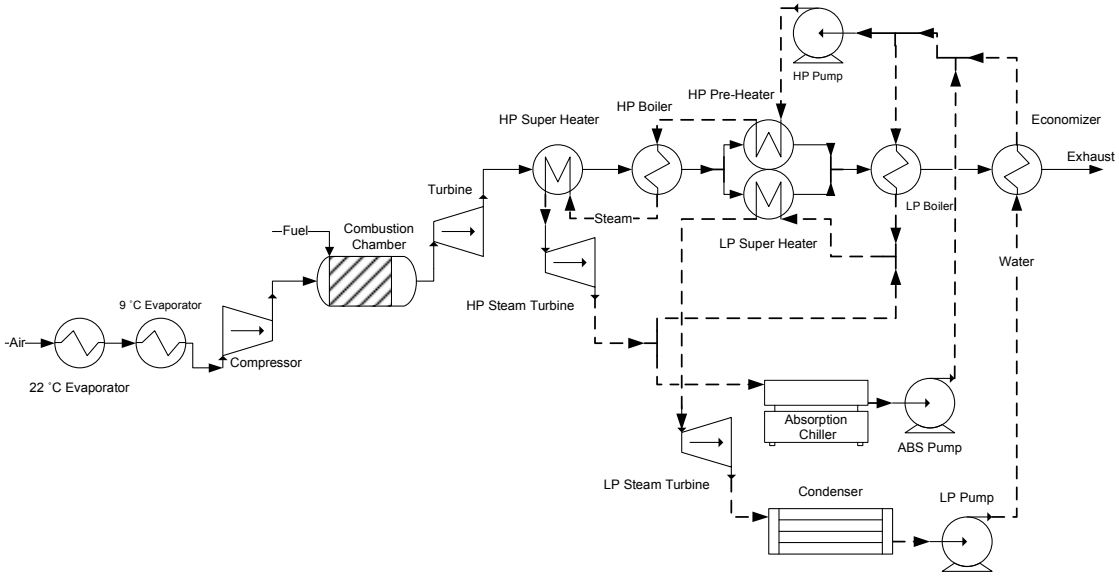
HP Pump
HP Pre-Heater
HP Boiler
HP Super Heater
Economizer
Exhaust
Turbine
Steam
LP Boiler
Fuel
Combustion Chamber
LP Super Heater
Water
9 °C Evaporator
HP Steam Turbine
Air
Compressor
22 °C Evaporator
Absorption Chiller
ABS Pump
LP Steam Turbine
Condenser
LP Pump

(e)

Figure 2.7: Schematic diagram of (a) option 5 and 6, (b) option 7 and 8, (c) option 9 and 10, (d) option 11 and 12, (e) option 13 and 14.

Table 2.9: The optimization formulation of proposed triple combined cycle options.

Option	Optimization formulation
5 and 6	$\min_{\mathbf{dv}} \dot{m}_{Fuel}$
	$S.t.$
	$\Delta T_{p,Super\ heater} \geq 10\ ^{\circ}\mathrm{C}$
	$\Delta T_{p,Boiler} \geq 10\ ^{\circ}\mathrm{C}$
	$\Delta T_{p,Economizer} \geq 10\ ^{\circ}\mathrm{C}$
	$T_{\min,\ Exhaust} \leq T_{Exhaust}$
	$T_{Inlet,Turbine} \leq 1124\ ^{\circ}\mathrm{C}$
	$0.9 \leq x_{Outlet,Steam\ Turbine}$
	$Pw_{Turbine} + Pw_{Steam\ Turbine} - Pw_{Compressor} - Pw_{Pump} - Pw_{Liquefaction} \geq 0$
	$\frac{Q_{\text{Abs, Eva,9°C}}}{COP_{\text{Abs, Eva,9°C}}} + \frac{Q_{\text{Abs, Eva,22°C}}}{COP_{\text{Abs, Eva,22°C}}} - Q_{\text{Steam Cycle, Cond}} \leq 0$
	$\mathbf{dv} = [\dot{m}_{Water}, P_{Boiler}, T_{Super\ heater}, \dot{m}_{Air}, \dot{m}_{Fuel}]$
	$[1,1000,350,200,4] \leq \mathbf{dv} \leq [90,20000,560,415,7.5]$

7 and 8

$$\min_{\mathbf{dv}} \ \dot{m}_{Fuel}$$

$$S.t.$$

$$\Delta T_{p,Super\ heater} \geq 10\ ^{\circ}\mathrm{C}$$

$$\Delta T_{p,Boiler} \geq 10\ ^{\circ}\mathrm{C}$$

$$\Delta T_{p,HP\ Economizer} \geq 10\ ^{\circ}\mathrm{C}$$

$$\Delta T_{p,LP\ Economizer} \geq 10\ ^{\circ}\mathrm{C}$$

$$T_{\min,\ Exhaust} \leq T_{Exhaust}$$

$$T_{Inlet,Turbine} \leq 1124\ ^{\circ}\mathrm{C}$$

$$0.9 \leq x_{Outlet,HP\ Steam\ Turbine}$$

$$0.9 \leq x_{Outlet,LP\ Steam\ Turbine}$$

$$Pw_{Turbine} + Pw_{HP,\ Steam\ Turbine} + Pw_{LP,\ Steam\ Turbine}$$

$$-Pw_{Compressor} - Pw_{HP,\ Pump} - Pw_{LP,\ Pump} - Pw_{Liquefaction} \geq 0$$

$$\frac{Q_{\text{Abs, Eva,9°C}}}{COP_{\text{Abs, Eva,9°C}}} + \frac{Q_{\text{Abs, Eva,22°C}}}{COP_{\text{Abs, Eva,22°C}}} - Q_{\text{Steam Cycle to Abs}} \leq 0$$

$$\dot{m}_{LP\ Water} \leq \dot{m}_{Total\ Water}$$

$$\mathbf{dv} = [\dot{m}_{LP\ Water}, \dot{m}_{Total\ Water}, P_{Boiler}, T_{Super\ heater}, \dot{m}_{Air}, \dot{m}_{Fuel}]$$

$$[1,1,1000,350,200,4] \leq \mathbf{dv} \leq [90,90,20000,560,415,7.5]$$

9 and 10

$$\min_{\mathbf{dv}} \ \dot{m}_{Total\ Fuel}$$

$$S.t.$$

$$\Delta T_{p,Super\ heater} \geq 10\ ^{\circ}\mathrm{C}$$

$$\Delta T_{p,Boiler} \geq 10\ ^{\circ}\mathrm{C}$$

$$\Delta T_{p,Economizer} \geq 10\ ^{\circ}\mathrm{C}$$

$$T_{\min,\ Exhaust} \leq T_{Exhaust}$$

$$T_{Inlet,Turbine} \leq 1124\ ^{\circ}\mathrm{C}$$

$$0.9 \leq x_{Outlet,Steam\ Turbine}$$

$$Pw_{Turbine} + Pw_{Steam\ Turbine} - Pw_{Compressor} - Pw_{Pump} - Pw_{Liquefaction} \geq 0$$

$$\frac{Q_{\text{Abs, Eva,9°C}}}{COP_{\text{Abs, Eva,9°C}}} + \frac{Q_{\text{Abs, Eva,22°C}}}{COP_{\text{Abs, Eva,22°C}}} - Q_{\text{Steam Cycle, Cond}} \leq 0$$

$$\dot{m}_{Fuel} \leq \dot{m}_{Total\ Fuel}$$

$$\mathbf{dv} = [\dot{m}_{Water}, P_{Boiler}, T_{Super\ heater}, \dot{m}_{Air}, \dot{m}_{Fuel}, \dot{m}_{Total\ Fuel}]$$

$$[1,1000,350,200,4,4] \leq \mathbf{dv} \leq [90,20000,560,415,7.5,7.5]$$

11and12

$$\min_{\mathbf{dv}} \ \dot{m}_{Fuel}$$

$$S.t.$$

$$\Delta T_{p,HP\ Super\ heater} \geq 10\ ^{\circ}\mathrm{C}$$

$$\Delta T_{p,HP\ Boiler} \geq 10\ ^{\circ}\mathrm{C}$$

$$\Delta T_{p,HP\ \mathrm{Pre}\ heater} \geq 10\ ^{\circ}\mathrm{C}$$

$$\Delta T_{p,LP\ Super\ heater} \geq 10\ ^{\circ}\mathrm{C}$$

$$\Delta T_{p,LP\ Boiler} \geq 10\ ^{\circ}\mathrm{C}$$

$$\Delta T_{p,Economizer} \geq 10\ ^{\circ}\mathrm{C}$$

$$T_{\min,\ Exhaust} \leq T_{Exhaust}$$

$$T_{Inlet,Turbine} \leq 1124\ ^{\circ}\mathrm{C}$$

$$0.9 \leq x_{Outlet,HP\ Steam\ Turbine}$$

$$0.9 \leq x_{Outlet,LP\ Steam\ Turbine}$$

$$T_{LP\ Super\ heater} \leq T_{HP\ Super\ heater}$$

$$P_{LP,\ Boiler} \leq P_{HP,\ Boiler}$$

$$Pw_{Turbine} + Pw_{HP,\ Steam\ Turbine} + Pw_{LP,\ Steam\ Turbine}$$

$$-Pw_{Compressor} - Pw_{HP,\ Pump} - Pw_{LP,\ Pump} - Pw_{Liquefaction} \geq 0$$

$$\frac{Q_{\mathrm{Abs,\ Eva,9°C}}}{COP_{\mathrm{Abs,\ Eva,9°C}}} + \frac{Q_{\mathrm{Abs,\ Eva,22°C}}}{COP_{\mathrm{Abs,\ Eva,22°C}}} - Q_{\mathrm{Steam\ Cycle,\ Cond}} \leq 0$$

$$\mathbf{dv} = [\dot{m}_{Water}, R_{mlp}, P_{LP,\ Boiler}, T_{LP,\ Super\ heater}, P_{HP,\ Boiler}, T_{HP,\ Super\ heater}, \dot{m}_{Air}, \dot{m}_{Fuel}]$$

$$[1,0.0001,1000,350,1000,400,200,4] \leq \mathbf{dv}$$

$$\mathbf{dv} \leq [60,0.9999,20000,560,20000,565,415,7.5]$$

13and14

$$\min_{\mathbf{dv}} \ \dot{m}_{Fuel}$$

$$S.t.$$

$$\Delta T_{p,HP\ Super\ heater} \geq 10\ ^{\circ}\mathrm{C}$$

$$\Delta T_{p,HP\ Boiler} \geq 10\ ^{\circ}\mathrm{C}$$

$$\Delta T_{p,HP\ \mathrm{Pre}\ heater} \geq 10\ ^{\circ}\mathrm{C}$$

$$\Delta T_{p,LP\ Super\ heater} \geq 10\ ^{\circ}\mathrm{C}$$

$$\Delta T_{p,LP\ Boiler} \geq 10\ ^{\circ}\mathrm{C}$$

$$\Delta T_{p,Economizer} \geq 10\ ^{\circ}\mathrm{C}$$

$$T_{\min,\ Exhaust} \leq T_{Exhaust}$$

$$T_{Inlet,Turbine} \leq 1124\ ^{\circ}\mathrm{C}$$

$$0.9 \leq x_{Outlet,HP\ Steam\ Turbine}$$

$$0.9 \leq x_{Outlet,LP\ Steam\ Turbine}$$

$$T_{LP\ Super\ heater} \leq T_{HP\ Super\ heater}$$

$$Pw_{Turbine} + Pw_{HP,\ Steam\ Turbine} + Pw_{LP,\ Steam\ Turbine} - Pw_{Compressor}$$

$$-Pw_{HP,\ Pump} - Pw_{LP,\ Pump} - Pw_{ABS,\ Pump} - Pw_{Liquefaction} \geq 0$$

$$\frac{Q_{\mathrm{Abs,\ Eva,9°C}}}{COP_{\mathrm{Abs,\ Eva,9°C}}} + \frac{Q_{\mathrm{Abs,\ Eva,22°C}}}{COP_{\mathrm{Abs,\ Eva,22°C}}} - Q_{\mathrm{Steam\ Cycle\ to\ Abs}} \leq 0$$

$$\mathbf{dv} = [\dot{m}_{HP}, R_{HP,ABS}, \dot{m}_{LP}, T_{LP,\ Super\ heater}, P_{HP,\ Boiler}, T_{HP,\ Super\ heater}, \dot{m}_{Air}, \dot{m}_{Fuel}]$$

$$[1,0.0001,0.0001,185,1000,400,200,4] \leq \mathbf{dv}$$

$$\mathbf{dv} \leq [60,0.9999,15,560,20000,565,415,7.5]$$

2.7.2 Optimization Methodology

The objective in the optimization of each cycle enhancement configuration is to minimize its fuel consumption. The constraint functions for each cycle configuration are discussed in Section 2.7.1. To perform the optimization, a hybrid genetic algorithm (Matlab 2010a), which is a global optimization method, is used. A hybrid genetic algorithm first performs a global optimization by a genetic algorithm. After the convergence of the genetic algorithm to a solution, a local search optimization algorithm such as sequential quadratic programing (Arora 2004) is followed by using the solution of the genetic algorithm as the staring point of the local search. It should

be noted that for each cycle configuration, the optimization is performed 20 times to capture the stochasticity of the hybrid genetic algorithm.

The settings of the hybrid genetic algorithm are as follows. The population size of twenty five individuals per design variable is used. The tournament selection is chosen as the selection function. *Fmincon* (Matlab 2010a) is selected as the hybrid function in the genetic algorithm tool box of Matlab 2010a. The rest of the settings are selected as the default values of the genetic algorithm solver of Matlab 2010a (Matlab 2010a).

2.7.3 Optimization Results

The optimization results for different driver cycle options are shown in Table 2.10 for different minimum exhaust temperatures and steam cycle efficiencies. As it is shown in Table 2.10, the proposed options with double-effect absorption chillers have lower efficiency than the ones with single-effect absorption chillers. This is due to the fact that the COP of the double-effect absorption cycles will not increase by increasing their generator temperatures above 140°C (90°C for single-effect absorption chillers). However, steam cycle efficiency will increase by increasing maximum steam temperature (i.e., super heater temperature). Therefore, it will be more beneficial to further expand the steam in the steam turbine than using it for heating the desorber of double-effect absorption chiller. Figure 2.8 shows the main design variables and constraints that are affecting the efficiency of the Rankine cycle (Olander 2008) (steam cycle). In Figure 2.8 the direction of efficiency increase with respect to design variables is shown by a green vector. As it is shown in Figure 2.8 increasing maximum steam temperature and/or steam mass flow rate will increase the efficiency

of the steam cycle. However, as it is shown in Figure 2.8 this efficiency increase is bounded by the second law of thermodynamics (i.e., the heat cannot be transferred from one object to another that has a higher temperature (Olander 2008)). As it is shown in Figure 2.8, increasing the maximum steam pressure will increase the steam cycle efficiency while keeping the other parameters fixed. However, increasing the maximum steam pressure at a given temperature will reduce the steam quality at the outlet of the steam turbines. The steam quality at outlet of a steam turbine can be increased by increasing the steam turbine inlet temperature or increasing the steam turbine outlet pressure. Steam turbine inlet temperature can be increased by increasing the steam maximum temperature or using reheat. Increasing the turbine outlet pressure will reduce the turbine output power and consequently steam cycle efficiency. This effect can be mitigated by using triple combined cycle in which the steam turbine outlet steam is used to run absorption chillers. This is due to the fact that the minimum steam temperature to run an absorption chiller should be at least 95 °C. This means that the steam turbine outlet pressure should be higher than the case with condenser temperature of 45 °C. By using triple combined cycles the maximum steam cycle pressure can be increased without violating the steam turbine outlet steam quality constraint. In Table 2.10, all the options with minimum efficiency of 49% are utilizing either reheat or triple cycle configuration which means they have higher maximum steam pressure. As it can be seen in Table 2.10, there is no difference between the efficiency of option 2 and option 3. This due to the fact that the limiting constraint in these two options is steam quality at the outlet of the steam turbine and both of these cycles have the same maximum steam pressure at their optimal points.

Based on the Table 2.10, results option 12 has the highest efficiency and lowest fuel consumption for different minimum exhaust temperatures and steam cycle efficiencies.

Option 4 is the most efficient conventional driver cycle which is at least 32.5% more efficient than the base driver cycle. In case of the proposed driver cycles, option 12 is the most efficient option with maximum enhancement of 38% over the base driver cycle. It should be noted that option 12 is at least 2% more efficient than the option 4. This difference is due to the fact that in option 12 the inlet-air to gas turbine is cooled by the absorption chiller; however, there is not inlet-air cooling in option 4. Cooler inlet-air means higher gas turbine efficiency since the compressor work per unit mass of air will be reduced by reducing the inlet air temperature while the gas turbine power remains constant which means higher gas turbine output per unit mass of air.

It should be noted that the 180°C minimum exhaust temperature is a better representation of the existing practice at LNG plants. This is due to the fact that reducing the exhaust temperature below 180°C will increase the corrosion due to condensation of acid gases. If only the 180°C minimum exhaust temperature is considered then 4 of the proposed options will have higher thermal efficiencies than option 4 (i.e., the best conventional option). Moreover for this exhaust temperature the efficiency of the option 12 will be 5% higher than option 4. It should be noted that the gap between the efficiency of the single pressure options and dual pressure options is smaller for 180°C exhaust temperature in comparison to 110°C one.

Table 2.10: Optimization results of different driver cycle options.

Steam Turbine Efficiency (%)	86	90	90	86	90	90	86	90	90
Exhaust Temperature (°C)	180	180	110	180	180	110	180	180	110
Cycle	Fuel Consumption (kg/s)			Efficiency (%)			Efficiency Enhancement (%)		
Base Driver Cycle	6.575	6.575	6.575	33.52	33.52	33.52	---	---	---
Option 1 *	5.174	5.174	5.174	42.59	42.59	42.59	21.31	21.31	21.31
Option 2	4.571	4.541	4.407	48.21	48.53	50.00	30.48	30.93	32.98
Option 3	4.571	4.541	4.407	48.21	48.53	50.00	30.48	30.93	32.98
Option 4	4.438	4.367	4.140	49.65	50.46	53.22	32.5	33.58	37.03
Option 5	4.704	4.641	4.641	46.85	47.48	47.48	28.46	29.41	29.41
Option 6	4.251	4.235	4.219	51.84	52.03	52.23	35.35	35.59	35.84
Option 7	4.581	4.556	4.556	48.10	48.37	48.37	30.33	30.71	30.71
Option 8	4.594	4.585	4.556	47.97	48.06	48.37	30.13	30.27	30.71
Option 9	4.704	4.641	4.641	46.85	47.48	47.48	28.46	29.41	29.41
Option 10	4.251	4.235	4.219	51.84	52.03	52.23	35.35	35.59	35.84
Option 11	4.791	4.707	4.707	46	46.82	46.82	27.13	28.41	28.41
Option 12	4.241	4.195	4.066	51.96	52.53	54.20	35.50	36.20	38.16
Option 13	4.395	4.347	4.325	50.14	50.59	50.95	33.16	33.89	34.22
Option 14	4.269	4.236	4.152	51.62	52.02	53.07	35.07	35.57	36.85

*Mortazavi et al., 2010

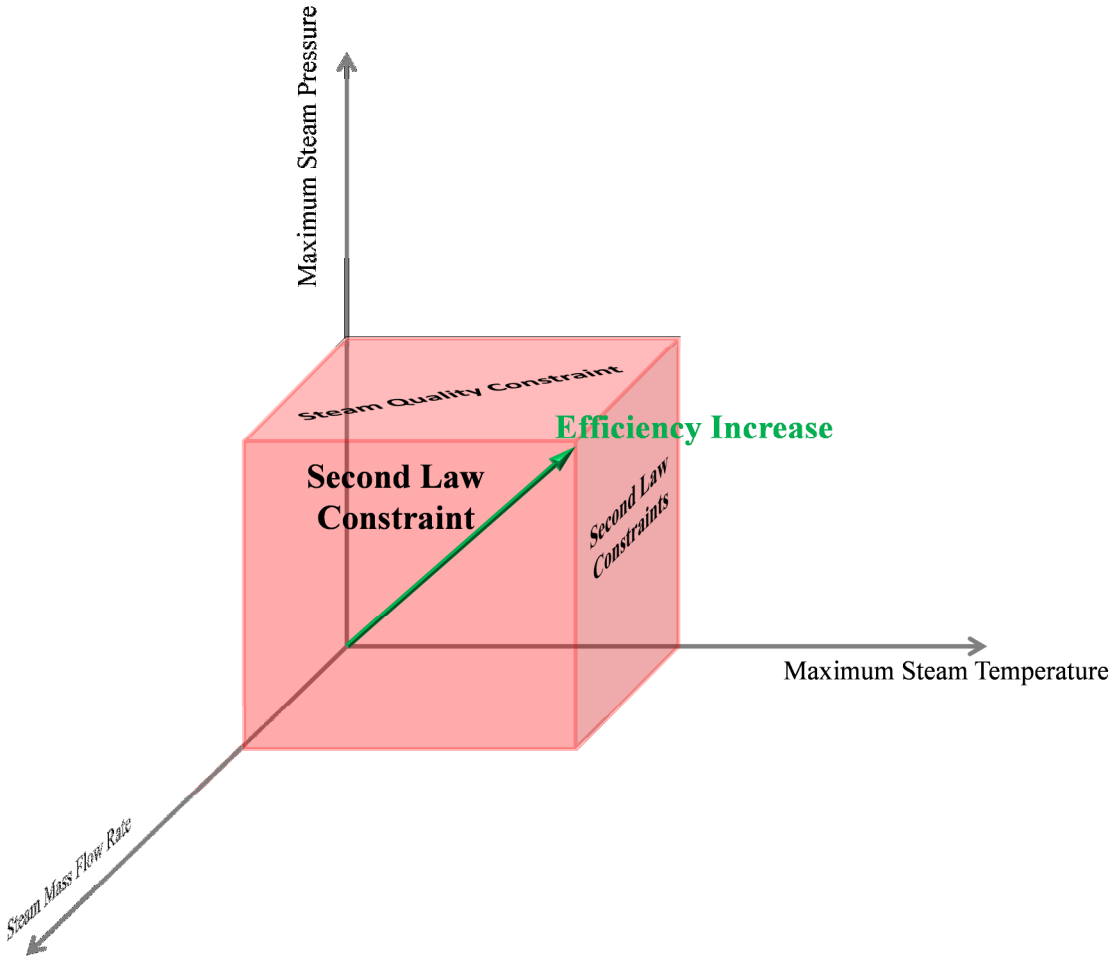

Figure 2.8: Steam cycle main design variables and constraints

2.8 Conclusions

In this chapter, several APCI liquefaction cycle and driver cycle enhancement options are considered. It is shown that the best liquefaction cycle enhancement option devised could improve the liquefaction cycle energy efficiency and production capacity by 7.07% and 1.24% respectively. The best liquefaction cycle enhancement option recovers all the expansion losses by replacing the expansion valves with the expanders.

Different triple gas turbine steam cycle and absorption chiller combined cycles which have not been considered for LNG plants along with conventional driver cycles are investigated. The design variables of each driver cycle are optimized to ensure a fair performance comparison. The driver design variable optimizations are performed for different minimum exhaust temperatures, corresponding to different material technologies for handling different levels of condensation of acidic exhaust moisture. It is shown that the best driver cycle is triple gas turbine combined cycle with a double pressure steam cycle with reheat and a single effect absorption chiller. The thermal efficiency of this cycle is 54%. This triple combined cycle improves the thermal efficiency of the base driver cycle and the best considered conventional driver cycle by 38% and 5% respectively. The most efficient options are either proposed triple combined cycles or gas turbine steam combined cycles with reheat. These options have the highest steam pressure which contributes in maximizing the steam cycle efficiency. Based on the simulation results the gap between the efficiency of the single pressure options and dual pressure options is smaller for 180°C exhaust temperature in comparison to 110°C one.

In the next chapter two new and novel robust optimization techniques will be devised. One of these robust optimization techniques will be used in Chapter 4 for developing a refrigerant mixture for APCI LNG plants that is relatively insensitive to the feed gas mixture composition.

Chapter 3: Gradient-Assisted Robust Optimization with Interval Uncertainty

In this chapter, for Research Task 2, two robust optimization methods are devised. One of these robust optimization methods are used in Chapter 4 to develop a refrigerant mixture that is optimized and is relatively insensitive to the feed gas mixture. The material of this chapter is borrowed from the Mortazavi et al., (2012)[4] paper.

There are two classes of optimization problems, namely, deterministic and stochastic. In the deterministic problems, there is no uncertainty in the inputs to an optimization problem. A deterministic optimum solution might be too sensitive to the input uncertainty to the extent that an optimum solution might become inferior, or even infeasible, by a slight change in the inputs. Conversely, methods developed for stochastic optimization problems account for uncertainty in the inputs while obtaining an optimum solution.

The uncertainty considered in this chapter is of an interval type that exists in many engineering design problems. Examples of this type of uncertainty occur when specifying tolerances in part dimensions, material properties and operating and environmental conditions. One class of stochastic optimization techniques is referred to as robust optimization. The goal in robust optimization is to obtain a solution that

---

[4] Mortazavi, A., Azarm, S., Gabriel, S., 2012, *Adaptive Gradient Assisted Robust DESIGN Optimization under Interval Uncertainty*, Engineering optimization, In Press.

is both relatively insensitive to input uncertainty and also optimal. Such a solution is called a "robust optimum" solution. Most of the current methods in robust optimization, especially those that handle interval uncertainty, are either computationally too expensive or not sufficiently general for solving nonlinear engineering optimization problems. This chapter presents methods that address these shortcomings.

First, in Section 3.1, the main definitions and terminologies are provided. Next, an overview of the previous literature is presented in Section 3.2. Subsequently, two new robust optimization methods are presented. The first method, called "Gradient-Assisted Robust Optimization" (GARO), is discussed in Section 3.3. The second method, which is a faster version of GARO but with more limited capabilities, called "Quasi-Concave Gradient-Assisted Robust Optimization" (QC-GARO), is discussed in Section 3.4. In Section 3.5, GARO and QC-GARO are applied to a variety of numerical and engineering test problems that include objective and/or constraint functions that range from closed-form quasi-convex to "black-box" simulation forms. A black-box problem refers to problems for which there is little or no information in closed-form about the characteristics of its objective and constraint functions. The results obtained from the GARO and QC-GARO methods are compared with three previous approaches. Section 3.6 concludes the chapter.

3.1 Definitions and Terminologies

In this section the main definitions and terminologies are presented. Note that vectors are represented by a bold letter and are in a row form.

3.1.1 Deterministic Optimization

Definition 1- *Deterministic Optimization*: A deterministic optimization problem is formulated as follows (Bazaraa et al., 1993):

$$\min_{\mathbf{x}} f(\mathbf{x},\mathbf{p}) \tag{3.1}$$

Subject to:

$$g_i(\mathbf{x},\mathbf{p}) \le 0 \quad i=1,\ldots,\mathrm{I}\,\mathbf{x} \in \Re^n, \mathbf{p} \in \Re^m$$

where f and g_i each represents a scalar objective and inequality constraint function, respectively. The quantity **x** is the vector of (design or decision) variables, and **p** is the vector of parameters. In equation (3.1), the optimizer changes the values of variables, while keeping parameters fixed, to obtain an optimum solution point.

3.1.2 Robust Design

A robust design is one whose performance (objective and/or feasibility) is relatively insensitive to input uncertainty from the variables and/or parameters. As reported in the literature, there are two types of robustness, objective robustness and feasibility robustness (Parkinson et al., 1993; Li et al., 2006 and Beyer and Sendhoff, 2007), as they are defined next.

Definition 2- *Objective Robustness*: A design **x** is objectively robust if the relative objective function variation remains in a pre-specified range Δf^* for all realizations of uncertain variables and parameters $(\hat{\mathbf{x}},\hat{\mathbf{p}})$ that are also within an uncertainty range pre-specified around a (nominal) point (**x**,**p**). Mathematically, objective robustness

can be stated as:

$$\forall(\hat{\mathbf{x}},\hat{\mathbf{p}})\in\{(\hat{\mathbf{x}},\hat{\mathbf{p}})\,|\,\mathbf{x}-\Delta\tilde{\mathbf{x}}\le\hat{\mathbf{x}}\le\mathbf{x}+\Delta\tilde{\mathbf{x}},\,\mathbf{p}-\Delta\tilde{\mathbf{p}}\le\hat{\mathbf{p}}\le\mathbf{p}+\Delta\tilde{\mathbf{p}}\},\left|f(\hat{\mathbf{x}},\hat{\mathbf{p}})-f(\mathbf{x},\mathbf{p})\right|\le\Delta f^{*} \qquad (3.2a)$$

Where $\Delta\tilde{\mathbf{x}}$ and $\Delta\tilde{\mathbf{p}}$ represent a pre-specified maximum uncertainty for variables and parameters, respectively, from the nominal point. The type of uncertainty that is used in equation (3.2a) is interval-based and symmetric with respect to the nominal point (**x,p**). This fact means that the nominal point has an equal distance from the lower and upper bounds of the uncertainty range, i.e., $\mathbf{x}-\Delta\tilde{\mathbf{x}}$, $\mathbf{p}-\Delta\tilde{\mathbf{p}}$ and $\mathbf{x}+\Delta\tilde{\mathbf{x}}$, $\mathbf{p}+\Delta\tilde{\mathbf{p}}$.

When the objective robustness is based only on the degradation of the objective function, (not considering the absolute value of the degradation) equation (3.2a) becomes:

$$\forall(\hat{\mathbf{x}},\hat{\mathbf{p}})\in\{(\hat{\mathbf{x}},\hat{\mathbf{p}})\,|\,\mathbf{x}-\Delta\tilde{\mathbf{x}}\le\hat{\mathbf{x}}\le\mathbf{x}+\Delta\tilde{\mathbf{x}},\,\mathbf{p}-\Delta\tilde{\mathbf{p}}\le\hat{\mathbf{p}}\le\mathbf{p}+\Delta\tilde{\mathbf{p}}\},\, f(\hat{\mathbf{x}},\hat{\mathbf{p}})-f(\mathbf{x},\mathbf{p})\le\Delta f^{*} \qquad (3.2b)$$

If the normalized variation of an objective function is of interest, equations (3.2a) and (3.2b) can be stated as:

$$\forall(\hat{\mathbf{x}},\hat{\mathbf{p}})\in\{(\hat{\mathbf{x}},\hat{\mathbf{p}})\,|\,\mathbf{x}-\Delta\tilde{\mathbf{x}}\le\hat{\mathbf{x}}\le\mathbf{x}+\Delta\tilde{\mathbf{x}},\,\mathbf{p}-\Delta\tilde{\mathbf{p}}\le\hat{\mathbf{p}}\le\mathbf{p}+\Delta\tilde{\mathbf{p}}\},\,\frac{\left|f(\hat{\mathbf{x}},\hat{\mathbf{p}})-f(\mathbf{x},\mathbf{p})\right|}{\left|f(\mathbf{x},\mathbf{p})\right|}\le\Delta f^{*} \qquad (3.3a)$$

$$\forall(\hat{\mathbf{x}},\hat{\mathbf{p}})\in\{(\hat{\mathbf{x}},\hat{\mathbf{p}})\,|\,\mathbf{x}-\Delta\tilde{\mathbf{x}}\le\hat{\mathbf{x}}\le\mathbf{x}+\Delta\tilde{\mathbf{x}},\,\mathbf{p}-\Delta\tilde{\mathbf{p}}\le\hat{\mathbf{p}}\le\mathbf{p}+\Delta\tilde{\mathbf{p}}\},\,\frac{f(\hat{\mathbf{x}},\hat{\mathbf{p}})-f(\mathbf{x},\mathbf{p})}{\left|f(\mathbf{x},\mathbf{p})\right|}\le\Delta f^{*} \qquad (3.3b)$$

It should be noted that in equation (3.3a) and (3.3b) the value of Δf^{*} is normalized.

The concepts of an uncertainty range around a nominal point and objective robustness of equations (3.2a) and (3.2b) are shown in Figure 3.1. In this figure the uncertainty

regions around nominal points x, x' and x'' are shown. Based on the objective robustness of equation (3.2a), only x' is objectively robust since the objective function value does not vary significantly in the uncertainty region around point x'. However, based on the objective robustness of equation (3.2b) both x and x' are robust. This condition is due to the fact that the equation (3.2b) allows variations that enhance the value of objective function (in Figure 3.1 the goal is minimization).

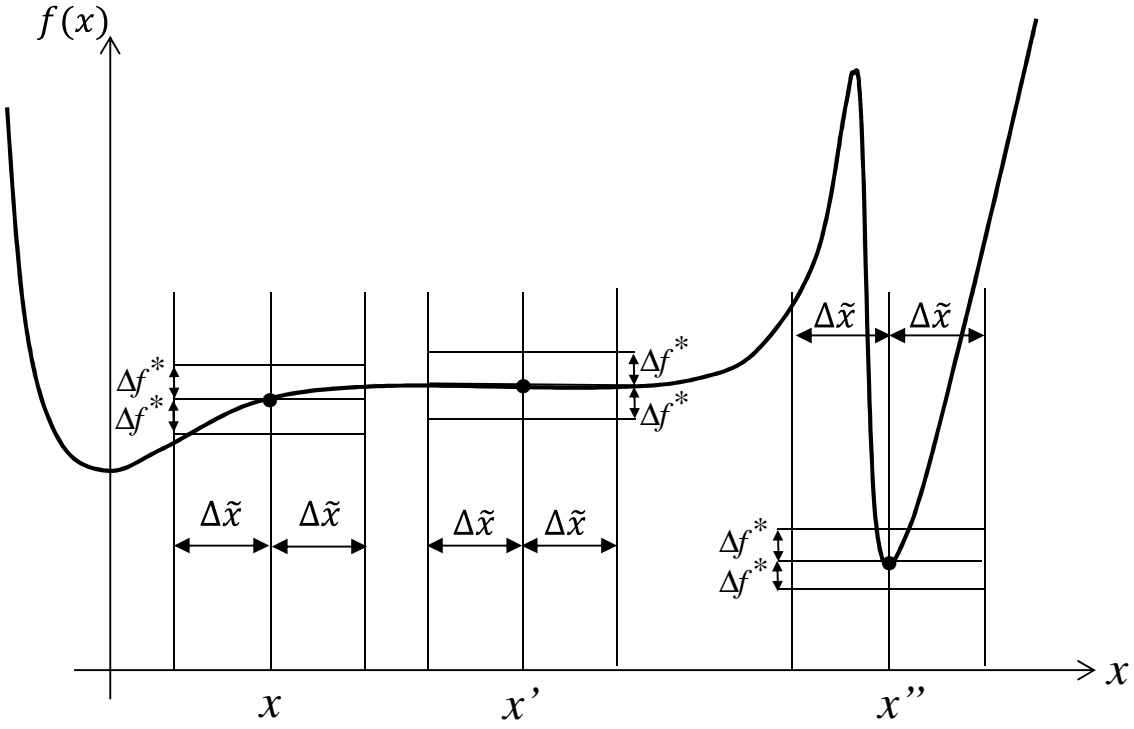

Figure 3.1: Uncertainty region around points *x*, *x'* and *x''*

Definition 3- *Feasibility Robustness*: A design **x** is feasibly robust if it stays feasible for all realizations of the variables and parameters $(\hat{\mathbf{x}},\hat{\mathbf{p}})$ in their uncertainty range around a nominal point $(\mathbf{x},\mathbf{p})$. Here this concept can be written mathematically as follows:

$$\forall(\hat{\mathbf{x}},\hat{\mathbf{p}})\in\{(\hat{\mathbf{x}},\hat{\mathbf{p}})\,|\,\mathbf{x}-\Delta\tilde{\mathbf{x}}\le\hat{\mathbf{x}}\le\mathbf{x}+\Delta\tilde{\mathbf{x}}\,,\,\mathbf{p}-\Delta\tilde{\mathbf{p}}\le\hat{\mathbf{p}}\le\mathbf{p}+\Delta\tilde{\mathbf{p}}\},\ g_i(\hat{\mathbf{x}},\hat{\mathbf{p}})\le 0\quad i=1,...,I \tag{3.4}$$

Let $\hat{\mathbf{x}}=\mathbf{x}+\Delta\mathbf{x}$ and $\hat{\mathbf{p}}=\mathbf{p}+\Delta\mathbf{p}$ then equation (3.4) can be re-written as:

$$\max_{\Delta\mathbf{x},\Delta\mathbf{p}} g_i(\mathbf{x}+\Delta\mathbf{x},\mathbf{p}+\Delta\mathbf{p})\le 0\quad i=1,...,I \tag{3.5}$$
$$\forall\Delta\mathbf{x}\in[-\Delta\tilde{\mathbf{x}},\Delta\tilde{\mathbf{x}}]$$
$$\forall\Delta\mathbf{p}\in[-\Delta\tilde{\mathbf{p}},\Delta\tilde{\mathbf{p}}]$$

Considering equation (3.2a) for objective robustness, by moving Δf^* to the left side of the first inequality from the right, the formulation becomes similar to that of an inequality constraint. This fact means that objective robustness can be treated as feasibility robustness. Therefore, in the rest of the dissertation, the robust optimization formulation is developed based on feasibility robustness. For the remainder of this dissertation the terms "robustness" and "robust" will refer to feasibility robustness and feasibly robust, respectively. The concept of feasibility robustness is shown in Figure 3.2. As shown in this figure, the point *x*' is not robust since part of its uncertainty region lies in the infeasible region. However, the point *x* is robust since all the points in its uncertainty region are feasible.

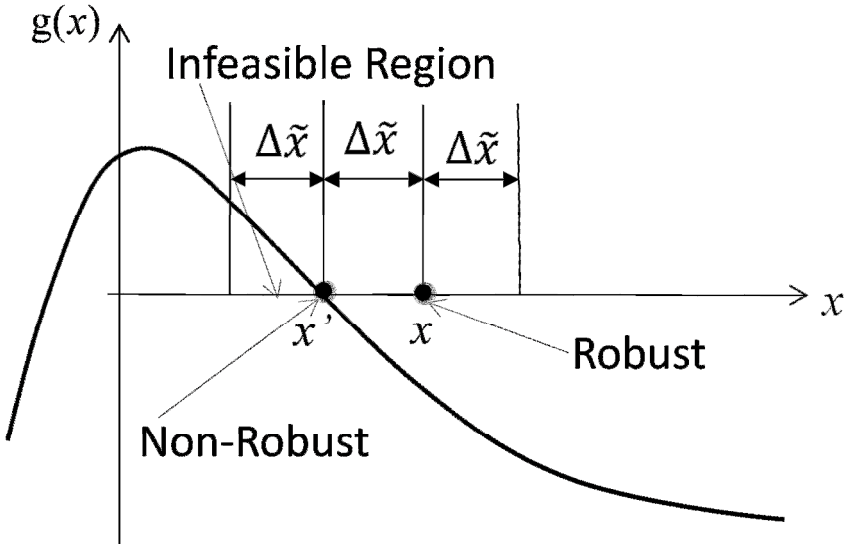

Figure 3.2: Feasibility robustness

3.1.3 Robust Optimization

Mathematically, a general robust optimization problem is stated as:

$$\min_{\mathbf{x}} f(\mathbf{x},\mathbf{p}) \tag{3.6}$$

Subject to:

$$\mathbf{x} \in S_r(\mathbf{x}, \Delta\tilde{\mathbf{x}}, \Delta\tilde{\mathbf{p}})$$

$$S_r(\mathbf{x}, \Delta\tilde{\mathbf{x}}, \Delta\tilde{\mathbf{p}}) = \{\mathbf{x} \mid \max_{\Delta\mathbf{x},\Delta\mathbf{p}} g_i(\mathbf{x}+\Delta\mathbf{x}, \mathbf{p}+\Delta\mathbf{p}) \le 0 \quad i=1,...,I, \forall\Delta\mathbf{x} \in [-\Delta\tilde{\mathbf{x}}, \Delta\tilde{\mathbf{x}}], \forall\Delta\mathbf{p} \in [-\Delta\tilde{\mathbf{p}}, \Delta\tilde{\mathbf{p}}]\}$$

Equation (3.6) represents a general robust optimization problem since no assumption is made regarding the characteristics of the objective and constraint functions. The set S_r is called "robust feasible set".

Definition 4- *Robust Optimum*: A solution to equation (3.6) is a robust optimum solution.

3.1.4 Concave, Quasi-Concave, Convex and Quasi-Convex Functions

Next, for a constraint function of the form ($g_i(\mathbf{x},\mathbf{p}) \le 0$), the notions of convexity and concavity and quasi-convexity and quasi-concavity are defined.

Definition 5- Concave Function: A function f defined on a convex set D is said to be concave if (Bazaraa et al., 1993):

$$f: D \subseteq \Re^n \to \Re,\ \forall \mathbf{x},\mathbf{y} \in D,\ f(\lambda\mathbf{x}+(1-\lambda)\mathbf{y}) \ge \lambda f(\mathbf{x})+(1-\lambda) f(\mathbf{y})\ \forall \lambda \in [0,1] \tag{3.7}$$

Definition 6- Quasi-Concave Function: A function f on a convex set D is said to be quasi-concave if (Bazaraa et al., 1993):

$$f: D \subseteq \Re^n \to \Re,\ \forall \mathbf{x},\mathbf{y} \in D,\ f(\lambda\mathbf{x}+(1-\lambda)\mathbf{y}) \ge \min\{f(\mathbf{x}), f(\mathbf{y})\}\ \forall \lambda \in [0,1] \tag{3.8}$$

Definition 7- Convex Function: A function f on a convex set D is said to be convex if (Bazaraa et al., 1993):

$$f: D \subseteq \Re^n \to \Re, \forall \mathbf{x},\mathbf{y} \in D,\ f(\lambda\mathbf{x}+(1-\lambda)\mathbf{y}) \le \lambda f(\mathbf{x})+(1-\lambda) f(\mathbf{y})\ \forall \lambda \in [0,1] \tag{3.9}$$

Definition 8- Quasi-Convex Function: A function f on a convex set D is said to be quasi-convex if (Bazaraa et al., 1993):

$$f: D \subseteq \Re^n \to \Re, \forall \mathbf{x},\mathbf{y} \in D,\ f(\lambda\mathbf{x}+(1-\lambda)\mathbf{y}) \le \max\{f(\mathbf{x}), f(\mathbf{y})\}\ \forall \lambda \in [0,1] \tag{3.10}$$

3.2 Overview of Previous Work

There are two classes of robust optimization methods in the literature: probabilistic and deterministic (e.g., Yang et al., 2007 and Bertsimas et al., 2010). In probabilistic methods, to evaluate robustness, statistical measures such as mean, variance, semi-variance and mean loss are used, e.g., Parkinson et al., (1993); Yu and Ishii, (1998); Chen et al., (1999); Tu et al., (1999); Du and Chen, (2000); Choi et al., (2001); Jung

and Lee, (2002); Ray (2002); Youn et al., (2003) Shen and Zhang, (2008) and Gancarova and Todd, (2011). In deterministic methods, to calculate robustness, non-statistical measures such as a gradient or the worst-case value of the objective and/or constraint functions with respect to uncertainty are utilized, see e.g., Taguchi, (1987); Balling et al., (1986); Sundaresan et al., (1992 and 1993); Su and Renaud, (1997); Zhu and Ting, (2001); Lee and Park, (2001); Messac and Yahaya, (2002) and Kim et al., (2010), for gradient-based robustness measures, and see e.g., Gunawan, (2004); Gunawan and Azarm, (2004a); Gunawan and Azarm, (2005a); Gunawan and Azarm, (2005b); Li et al., (2006); Teo, (2007); Bertsimas et al., (2010); Bertsimas and Nohadani, (2010); Siddiqui et al., (2011) and Hu et al., (2011); for worst-case robustness measures. However, to the best of our knowledge, there is no robust optimization method that employs a gradient-based feasibility robustness approach that is applicable to nonlinear problems with large uncertainty[5] in parameters and/or variables. However, there are robust optimization methods, such as Li et al., (2006) or Bertsimas et al., (2010) that are applicable to general robust optimization problems with large uncertainty. But these methods are not computationally tractable (scalable) due to their optimization structure, as will be further discussed in the next paragraph.

Essentially two types of methods are used for solving a general robust optimization problem (recall equation (3.6)). The type-one methods have (as part of the robust optimization method) a built-in scheme that numerically verifies the robustness of an obtained candidate solution, as in equation (3.5). The type-two methods do not have

---

[1] Here, a large uncertainty refers to an uncertain interval for variables (and parameters) which is beyond the linear range of objective (and constraint) functions when measured from a nominal point.

such a scheme. Previous methods such as Parkinson et al., (1993), Gunawan and Azarm, (2004b), Gunawan, (2004), Gunawan and Azarm, (2005b), Li et al., (2006), Teo, (2007), Bertsimas et al., (2010) and Bertsimas and Nohadani, (2010) are of the type-one methods. However, these methods are not computationally tractable for large-scale problems due to employing an outer-inner optimization structure through which the inner loop checks the robustness of candidate points obtained from the outer loop. These methods are referred to as two-level methods. Methods like Hu et al., (2011) are type-one methods and have a semi-single level (or sequential) structure. In semi-single level methods the robust optimization problem is converted to a deterministic optimization problem (deterministic version) by approximating the robustness constraints. After solving the deterministic version the accuracy of robustness approximation is evaluated. If the approximation accuracy is satisfactory a robust optimum point is achieved; otherwise the robustness approximation is modified and deterministic version is solved again. This process is continued until the robustness approximation accuracy criteria are met. The method of Hu et al., (2011) is for multi-objective robust optimization problems. This method employs online approximation and constraint cuts to approximate the robustness. Although this method is computationally efficient, based on their reported results, this method may eliminate some of the feasible points and thus robust solutions.

The type-two methods do not have a built-in numerical robustness verification scheme and may not be suitable for general problems with large uncertainty. The type-two methods have a one-level optimization structure. These type-two methods (e.g., Lee and Park, 2001, Kim et al., 2010 and Siddiqui et al., 2011) are

computationally tractable in comparison to the type-one methods. A number of type-two methods will lead to a guaranteed robust solution for a special class of problems. To exemplify, there are methods for problems with linear (e.g., Soyster, 1973; Balling et al., 1986; Ben-Tal and Nemirovski, 2002 and Bertsimas and Sim, 2006) and quadratic (e.g., Li et al., 2011) objective and constraint functions. However, these methods cannot necessarily be applied to more general problems due to their specific formulation. There is no reported method with a general formulation that is computationally tractable and leads to a robust answer for problems with quasi-concave constraints.

In some previous gradient-based methods such as Lee and Park, (2001) and Kim et al., (2010), adjusting constants (implemented to tailor the algorithm for a specific problem) are used to achieve a robust solution. However, those methods require the user to set the adjusting constants. The role of such constants is to adjust the linear or quadratic terms in the Taylor series near a candidate point to check its robustness. On the other hand, the computational effort in finding an optimal value of these constants is similar in complexity to finding a robust optimal point.

In this dissertation, a novel robust optimization method with a built-in robustness-checking mechanism for robust optimization problems is developed. In this method, instead of using an inner loop, the robustness is estimated based on the gradient information. The proposed method has a semi-single level (or sequential) structure in which first a single-level approximated robust optimization is solved. Then the robustness approximation is verified. If the approximation accuracy is satisfactory a robust optimum solution is found; otherwise the robustness approximation is

modified. After modifying the robustness approximation the single-level approximated robust optimization should be solved again. This procedure of solving a single-level approximated robust optimization, robustness approximation verification and robustness approximation modification continues until an acceptable robustness approximation is developed. This method is called the "Gradient Assisted Robust Optimization" (GARO).

As previously mentioned there is no known method leading to a robust solution for problems with quasi-concave functions. This gap will be addressed by the Quasi-Concave Gradient Assisted Robust Optimization (QC-GARO) algorithm. QC-GARO is a faster version of GARO that if it numerically converges to a solution, the solution will be a robust solution for problems with quasi-concave constraint functions. This method can be applied to general robust optimization problems (with non-quasi-concave constraint functions). However, there is no guarantee for the robustness of the solution obtained using QC-GARO for a general robust optimization problem.

The GARO and QC-GARO methods will be discussed in more details in Section 3.3 and Section 3.4, respectively.

3.3 Gradient-Assisted Robust Optimization (GARO) Algorithm

To simplify the exposition, initially, the robust optimization formulation is developed for a single variable case (that has uncertainty) and with a single constraint as in equation (3.11). Subsequently, starting with equation (3.16), this formulation is generalized for multiple variables, parameters and constraints.

Consider the following robust optimization problem, the single variable case:

$$\min_{x} f(x) \tag{3.11}$$

Subject to:

$$\max_{\Delta x} g(x+\Delta x) \le 0$$
$$\forall \Delta x \in [-\Delta\tilde{x}, \Delta\tilde{x}]$$
$$f : \Re \to \Re$$
$$g : \Re \to \Re$$

For now assume g(x+Δx) is a first-order differentiable function; this assumption will be relaxed later in Section 3.3.2. In equation (3.11) by employing a Taylor series expansion for $g(x+\Delta x)$ in the uncertainty region around a (nominal) point x, the constraint $\max_{\Delta x} g(x+\Delta x)$ can be re-written as:

$$\max_{\Delta x} g(x+\Delta x) = \max_{\Delta x} (g(x) + \frac{dg(x)}{dx}\Delta x + \theta) \tag{3.12}$$

where θ is the error caused by using just the linear terms of the Taylor series. The maximum of $\frac{dg(x)}{dx}\Delta x$ occurs when both $\frac{dg(x)}{dx}$ and Δx have the same sign and Δx has the maximum value, i.e., $\Delta\tilde{x}$. Therefore equation(3.12) can be re-written as:

$$\max_{\Delta x} g(x+\Delta x) = g(x) + \left|\frac{dg(x)}{dx}\right| \Delta\tilde{x} + \theta \tag{3.13}$$

As long as $\left|\frac{dg(x)}{dx}\right| \Delta\tilde{x} \neq 0$ (which will be relaxed in Section 3.3.2) equation (3.13) can be written as:

$$\max_{\Delta x} g(x+\Delta x) = g(x) + \left|\frac{dg(x)}{dx}\right| \Delta\tilde{x} \left(1 + \frac{\theta}{\left|\frac{dg(x)}{dx}\right| \Delta\tilde{x}}\right) \tag{3.14}$$

Suppose: $(1+\frac{\theta}{\left|\frac{dg(x)}{dx}\right|\Delta\tilde{x}}) = \alpha$, then equation (3.14) becomes:

$$\max_{\Delta x} g(x+\Delta x) = g(x)+\alpha\left|\frac{dg(x)}{dx}\right|\Delta\tilde{x} \tag{3.15}$$

Equation (3.15) is called a "modified Taylor series approximation" of the maximum of the constraint (or simply approximated maximum of the constraint). Consequently the robust optimization formulation of equation (3.11), can be re-written as:

$$\min_{x} f(x) \tag{3.16}$$

Subject to:

$$g(x)+\alpha\left|\frac{dg(x)}{dx}\right|\Delta\tilde{x} \le 0$$

Equation (3.16) serves as a deterministic version of the robust optimization problem of equation (3.11). It is called a "deterministic version" due to the fact that α is constant while performing the optimization. In other words, calculation of the constraint function does not require solving another optimization problem (i.e., maximization of the constraint over the uncertainty range). In short, the two-level problem is collapsed to a one-level problem as long as the correct value for α is known.

We now extend the equation (3.16) to a more general case. A deterministic formulation for a general robust optimization problem (recall equation (3.6)) where both variables and parameters have interval uncertainty and there are multiple variables, parameters and constraints expressed as follows:

$$\min_{\mathbf{x}} f(\mathbf{x},\mathbf{p}) \tag{3.17}$$

Subject to:

$$g_i(\mathbf{z})+\alpha_i \sum_{j=1}^{n} \left|\frac{\partial g_i(\mathbf{z})}{\partial z_j}\right| \Delta\tilde{z}_j \le 0 \quad i=1,...,I$$

$\mathbf{z}=[\mathbf{x},\mathbf{p}]$

$\Delta\tilde{\mathbf{z}}=[\Delta\tilde{\mathbf{x}},\Delta\tilde{\mathbf{p}}]$

$f: \Re^n \to \Re$

$g_i : \Re^n \to \Re \quad i=1,...,I$

where $\Delta\tilde{\mathbf{x}}$ and $\Delta\tilde{\mathbf{p}}$ are non-negative vectors. The set of all feasible solutions of the optimization problem in equation (3.17) is called the "approximated robust feasible set". The main challenge here is to determine the setting for $\boldsymbol{\alpha}=[\alpha_1,...,\alpha_i,...,\alpha_I]$. It should be noted that the exact value of $\boldsymbol{\alpha}$ is needed at a robust optimum point especially for active constraints of equation (3.17). This is due to the fact that for an active constraint a larger (than the exact) value of α leads to a conservative (overly) robust optimal solution while a smaller value leads to a non-robust solution. The initial step in solving the robust optimization problem equation (3.17), is to set an initial value for the $\boldsymbol{\alpha}$ vector. For this initial step, all elements of the $\boldsymbol{\alpha}$ vector are set equal to one (i.e., based on a first-order (linear) Taylor series expansion, recall equation (3.14)). Call this step "Step 0". Up to now, the original robust optimization problem (see Definition 4) is converted to a deterministic optimization in which the robustness is approximated by the first order Taylor series expansion.

The next step is to solve the optimization problem of equation (3.17). Call this "Step 1". After accomplishing Step 1, a solution is obtained. However, the robustness of

Step 1 solution and also the robustness approximation accuracy have not been verified. Therefore in the following steps, the robustness of Step 1 solution and the accuracy of the robustness approximation should be assessed. Step 2 evaluates the robustness of the solution obtained from Step 1. Step 3 evaluates the accuracy of the robustness approximation used in Step 1.

A solution obtained in Step 1 is a robust optimum solution if it satisfies two conditions. The first condition is robustness of the solution, which is calculated in Step 2. The second condition is the accuracy of the robustness approximation used in Step 1. The second condition is evaluated in Step 3. The first condition was elaborated in Definition 3 and by equation (3.5). Regarding the second condition, it can be satisfied if one of the following two sub-conditions is met. The first sub-condition is met if the approximated maximum value of a constraint is less than the maximum value of the constraint in the uncertainty range around the solution obtained from Step 1. This fact means that the robust feasible set is a subset of the approximated robust feasible set. Therefore the solution of the robust optimization problem (i.e., Definition 4) cannot be superior to Step 1's solution. The second sub-condition is met if the difference between the approximated maximum value of a constraint and the maximum value of the constraint in the uncertainty range around the solution to Step 1 is less than a positive user-defined tolerance. Call this tolerance η and this step "Step 3". If both conditions are satisfied an optimal solution is obtained; otherwise, the $\boldsymbol{\alpha}$ vector elements should be updated in the next step: "Step 4".

Step 4 updates the value of the $\boldsymbol{\alpha}$ vector elements. Adjustment of an $\boldsymbol{\alpha}$ vector

element is determined based on the difference between the approximated maximum value and the actual maximum value of the corresponding constraint. That is, an $\boldsymbol{\alpha}$ vector element will be decreased (or increased) if the approximation maximum value is greater (or less) than the actual maximum value in the uncertainty range around Step 1's solution. The main challenge here is to determine by how much each element of $\boldsymbol{\alpha}$ vector should be decreased (or increased). One approach would be to decrease (or increase) the $\boldsymbol{\alpha}$ element by a fixed amount or by a constant factor. However, such an approach may not be computationally efficient. One method was found to be efficient. In this method the value of element α_i is changed based on the variation of the maximum value of g_i (i.e., Step 2 result) over the variation of α_i in two consecutive iterations. This method can be stated mathematically as:

$$\frac{\alpha_{i,k+1}-\alpha_{i,k}}{g_i^M(\mathbf{x}_k^*)-(g_i(\mathbf{x}_k^*,\mathbf{p})+\alpha_{i,k}\sum_{j=1}^{n}\left|\frac{\partial g_i(\mathbf{x}_k^*,\mathbf{p})}{\partial z_j}\right|\Delta\tilde{z}_j)}=\left|\frac{\alpha_{i,k}-\alpha_{i,k-1}}{g_i^M(\mathbf{x}_k^*)-g_i^M(\mathbf{x}_{k-1}^*)}\right| \tag{3.18}$$

where $\mathbf{x}_k^*$ is the solution to Step 1 in iteration *k* and $g_i^M(\mathbf{x}_k^*)$ is the maximum of the constraint g_i in the uncertainty range around point $\mathbf{x}_k^*$. The unknown in equation (3.18) is the value of $\alpha_{i,k+1}$. The other parameters of equation (3.18) have been calculated in the current (*k*) and previous (*k-1*) iterations. It should be noted that in the first iteration, equation (3.18) cannot be used for the modification of $\boldsymbol{\alpha}$ vector elements since there is no previous iteration. Therefore for the first iteration the $\boldsymbol{\alpha}$ vector elements are adjusted by changing them using a user-defined parameter λ (discussed in more detail in Sections 3.3.1 and 3.3.2). After adjusting $\boldsymbol{\alpha}$ vector elements in Step 4, proceed to Step 1. In this way, one iteration of the algorithm is

completed. The modification of $\boldsymbol{\alpha}$ vector elements continues until Step 3 conditions are satisfied and a robust optimum solution is achieved.

3.3.1. Steps in GARO Algorithm

The steps in GARO algorithm are as follows (further details will be provided in Section 3.3.2):

Step 0: Initialize by setting $\boldsymbol{\alpha}_1 = [1,1,\ldots,1]$ (with the number of elements in $\boldsymbol{\alpha}_1$ being the same as the number of constraints I) and, set the iteration counter k=1, λ, ε (solver threshold) and η.

Step 1: Solve the optimization problem in equation (3.19) (deterministic version):

$$\min_{\mathbf{x}} f(\mathbf{x},\mathbf{p}) \tag{3.19}$$

Subject to:

$$g_i(\mathbf{z}) + \alpha_i \sum_{j=1}^{n} \max\left(\left|\frac{\partial g_i(\mathbf{z})}{\partial z_j}\right|, \varepsilon\right)\Delta\tilde{z}_j \le 0 \quad i=1,\ldots,I$$

$\mathbf{z}=[\mathbf{x},\mathbf{p}]$

$\Delta\tilde{\mathbf{z}}=[\Delta\tilde{\mathbf{x}},\Delta\tilde{\mathbf{p}}]$

$f:\Re^n \to \Re$

$g_i:\Re^n \to \Re \quad i=1,\ldots,I$

Denote a solution to (3.19) as $\mathbf{x}_k^*$.

Step 2: Maximize the constraints within the uncertainty range around $\mathbf{x}_k^*$ (keeping $\mathbf{x}_k^*$ fixed). Mathematically, this is:

For i=1,...,I (3.20)

$$g_i^M(\mathbf{x}_k^*) = \max_{\Delta\mathbf{x},\Delta\mathbf{p}} g_i(\mathbf{x}_k^* + \Delta\mathbf{x}, \mathbf{p} + \Delta\mathbf{p})$$

$$\forall \Delta\mathbf{x} \in [-\Delta\tilde{\mathbf{x}}, \Delta\tilde{\mathbf{x}}]$$

$$\forall \Delta\mathbf{p} \in [-\Delta\tilde{\mathbf{p}}, \Delta\tilde{\mathbf{p}}]$$

Step 3: Check the convergence criteria (robustness of the solution and accuracy of the robustness approximation). Mathematically:

if (3.21)

$$g_i^M(\mathbf{x}_k^*) \leq 0 \text{ and } g_i^M(\mathbf{x}_k^*) - (g_i(\mathbf{x}_k^*, \mathbf{p}) + \alpha_{i,k} \sum_{j=1}^{n} \left| \frac{\partial g_i(\mathbf{x}_k^*, \mathbf{p})}{\partial z_j} \right| \Delta\tilde{z}_j) \geq -\eta$$

$$\Delta\tilde{\mathbf{z}} = [\Delta\tilde{\mathbf{x}}, \Delta\tilde{\mathbf{p}}]$$

for i=1,...,I

$\eta > 0$

then, the algorithm has found a robust optimum. If successful, stop; otherwise, proceed to Step 4.

Step 4: Adjust the $\boldsymbol{\alpha}_k$ parameter vector. Mathematically:

For i=1,...,I

$$\text{If } g_i^M(\mathbf{x}_k^*) \geq 0 \text{ and } g_i^M(\mathbf{x}_k^*) \geq (g_i(\mathbf{x}_k^*, \mathbf{p}) + \alpha_{i,k} \sum_{j=1}^{n} \left| \frac{\partial g_i(\mathbf{x}_k^*, \mathbf{p})}{\partial z_j} \right| \Delta\tilde{z}_j) \quad (3.22)$$

then:

If k=1 then $\alpha_{i,2} = \alpha_{i,1} + \lambda$.

If k>1 then

$$\alpha_{i,k+1} = \alpha_{i,k} + \left(g_i^M(\mathbf{x}_k^*) - (g_i(\mathbf{x}_k^*, \mathbf{p}) + \alpha_{i,k} \sum_{j=1}^{n} \left| \frac{\partial g_i(\mathbf{x}_k^*, \mathbf{p})}{\partial z_j} \right| \Delta\tilde{z}_j \right) \max\left(\left| \frac{\alpha_{i,k} - \alpha_{i,k-1}}{g_i^M(\mathbf{x}_k^*) - g_i^M(\mathbf{x}_{k-1}^*)} \right|, \varepsilon \right) \quad (3.23)$$

If $g_i^M(\mathbf{x}_k^*) \le 0$ and $g_i^M(\mathbf{x}_k^*) \le (g_i(\mathbf{x}_k^*,\mathbf{p}) + \alpha_{i,k}\sum_{j=1}^{n}\left|\frac{\partial g_i(\mathbf{x}_k^*,\mathbf{p})}{\partial z_j}\right|\Delta\tilde{z}_j)$ (3.24)

then:

If k=1 then $\alpha_{i,2} = \alpha_{i,1} - \lambda$,

If k>1 then

$$\alpha_{i,k+1} = \alpha_{i,k} + (g_i^M(\mathbf{x}_k^*) - (g_i(\mathbf{x}_k^*,\mathbf{p}) + \alpha_{i,k}\sum_{j=1}^{n}\left|\frac{\partial g_i(\mathbf{x}_k^*,\mathbf{p})}{\partial z_j}\right|\Delta\tilde{z}_j))\ \max\left(\left|\frac{\alpha_{i,k} - \alpha_{i,k-1}}{g_i^M(\mathbf{x}_k^*) - g_i^M(\mathbf{x}_{k-1}^*)}\right|, \varepsilon\right) \quad (3.23)$$

set k=k+1 and return to Step 1.

3.3.2. GARO Algorithm: Discussion

In this section more details about the different steps in GARO algorithm will be discussed.

3.3.2.1. Step 0:

In Step 0 since η is a desired approximation tolerance, it should be set by the user. Regarding setting the λ value, refer to the discussion in Section 3.3.2.5. The parameter ε, should be set to the solver threshold (Matlab, 2010a).

3.3.2.2. Step 1:

In Step 1 there is no restriction for choosing the type of deterministic optimization method. Therefore, both local and global optimization methods can be used.

To ensure the adjustability of the robustness approximation, the term $\max\left(\left|\frac{\partial g_i(\mathbf{z})}{\partial z_j}\right|, \varepsilon\right)$ is

used to prevent the case in which $\left|\frac{\partial g_i(\mathbf{z})}{\partial z_j}\right| = 0$. Therefore, the condition $\left|\frac{dg(x)}{dx}\right|\Delta\tilde{x} \neq 0$ is not necessary and can be relaxed. Since ε is too small, it does not affect the optimization process.

In Step 1, the modified Taylor series approximation generates a cushion (gap) and keeps the constraint function from being close to the deterministic feasible region boundary. It should be mentioned that the robust feasible region (set) is a subset (and inside) of the deterministic feasible region (set). The generated cushion is approximating the robust feasible region based on the deterministic feasible region and the gradient of the constraint functions with respect to uncertain inputs. The thickness of the cushion is increased or decreased by increasing or decreasing the absolute value of the gradient with respect to uncertain inputs. The cushion size also can be increased (or decreased) by increasing (or decreasing) $\boldsymbol{\alpha}_k$ elements. This concept is illustrated in Figure 3.3. In this figure the deterministic feasible region boundary, approximated robust feasible region boundary and robust feasible region boundary in the variable domain (x_1, x_2) are depicted by solid, dotted and dashed lines respectively. In Figure 3.3 the cushion area is shaded.

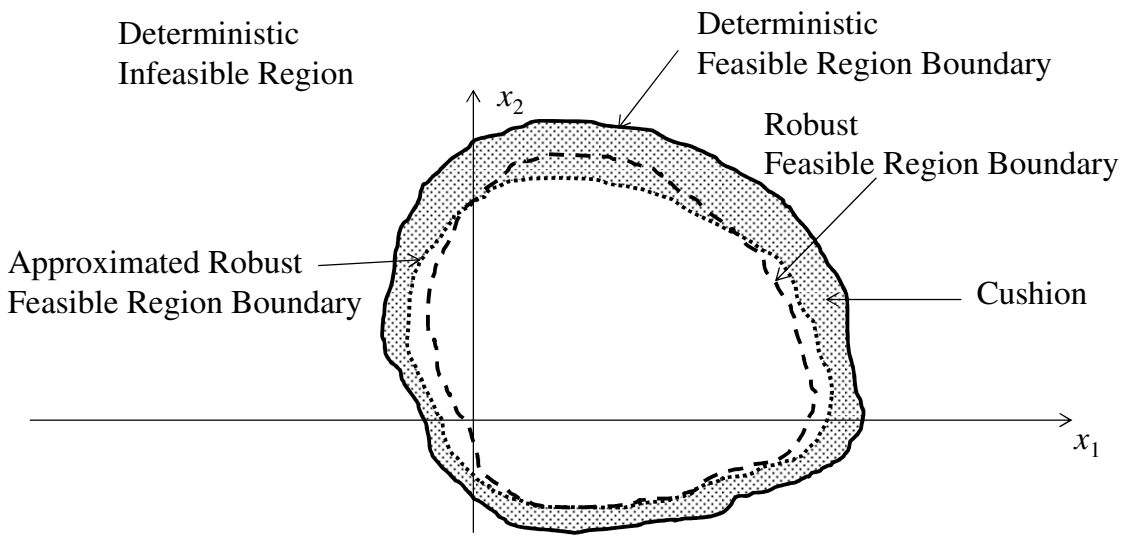

Figure 3.3: The cushion generated by the modified Taylor series approximation

If the optimization in Step 1 does not converge, the initial values of the $\boldsymbol{\alpha}_l$ vector elements should be reduced by half. Non-convergence occurs especially in the cases in which the constraint functions are quasi-concave and the robust feasible region is small. Since the robust feasible region is small, the cushion may occupy the whole robust feasible region. Consequently, there will be no approximated robust feasible region and obviously no solution for Step 1. Therefore reducing $\boldsymbol{\alpha}_l$ reduces the cushion thickness which helps Step 1 to converge to a solution.

3.3.2.3. Step 2:

In Step 2, the maximization is performed to check whether the constraints are still feasible in the uncertainty range, i.e., if the solution $\mathbf{x}_k^*$ from Step 1 is feasibly robust.

In Step 2, a global optimization method such as branch and bound or hybrid genetic algorithm should be used. In this dissertation, a hybrid genetic algorithm (a heuristic

global optimization method) (Matlab 2010a) is used for solving the test problems. The hybrid genetic algorithm first executes a genetic algorithm optimization then the result of the genetic algorithm optimization will be used as an initial point of a gradient-based optimization.

3.3.2.4. Step 3:

In Step 3, the first condition ($g_i^M(\mathbf{x}_k^*) \le 0$) examines the robustness of the candidate solution $\mathbf{x}_k^*$. The second condition is $(g_i^M(\mathbf{x}_k^*) - (g_i(\mathbf{x}_k^*, \mathbf{p}) + \alpha_{i,k} \sum_{j=1}^{n} \left| \frac{\partial g_i(\mathbf{x}_k^*, \mathbf{p})}{\partial z_j} \right| \Delta \tilde{z}_j) \ge -\eta)$.

The second condition checks whether the approximated maximum is close to the maximum value of the constraint in the uncertainty region around a candidate solution $\mathbf{x}_n^*$. The term $-\eta$ is applied to allow convergence under the condition where the approximated maximum is slightly larger (η) than the maximum value of the constraint in the uncertainty region around a candidate solution $\mathbf{x}_n^*$. Meanwhile, the second condition will be satisfied if the maximum value of the constraint in the uncertainty region around a candidate solution $\mathbf{x}_n^*$ is greater than the approximated maximum. If the maximum value approximation of each constraint is not sufficiently close to the constraint maximum value, the corresponding $\alpha_{i,k}$ value will be updated in Step 4.

3.3.2.5. Step 4:

In Step 4 the condition (3.22) occurs when a candidate point is not robust with respect to a specific constraint, i.e., $g_i^M(\mathbf{x}_k^*) \ge 0$. This condition is due to the fact that the

approximated maximum is less than the actual value of the maximum of the constraint function i within the uncertainty region around the candidate point ($g_i^M(\mathbf{x}_k^*) \geq (g_i(\mathbf{x}_k^*, \mathbf{p}) + \alpha_{i,k} \sum_{j=1}^{n} \left| \frac{\partial g_i(\mathbf{x}_k^*, \mathbf{p})}{\partial z_j} \right| \Delta \tilde{z}_j)$ part). As mentioned before, since there is no history for the $\boldsymbol{\alpha}$ vector in the first iteration, i.e., k=1, $\alpha_{i,2}$ is calculated either by increasing or decreasing $\alpha_{i,1}$ by a user-defined value λ; λ should have a small positive value such as 0.1. λ is introduced to test how $g_i^M(\mathbf{x}^*)$ approximation value changes by changing α_i.

In equation (3.23) the $\alpha_{i,k}$ value is adjusted based on the simple proportion of equation (3.18). The proportion is the ratio of the variation of α_i value over the variation of $g_i^M(\mathbf{x}^*)$ in successive iterations. This proportion is multiplied by the difference between the maximum value of the constraint and its modified Taylor series approximation to calculate the adjustment value. The inverse of $\left| \frac{\alpha_{i,k} - \alpha_{i,k-1}}{g_i^M(\mathbf{x}_k^*) - g_i^M(\mathbf{x}_{k-1}^*)} \right|$ is a rough estimate of how the $g_i^M(\mathbf{x}^*)$ approximation value varies by changing α_i. To ensure the adjustability of α_i, the term $\max\left(\left| \frac{\alpha_{i,k} - \alpha_{i,k-1}}{g_i^M(\mathbf{x}_k^*) - g_i^M(\mathbf{x}_{k-1}^*)} \right|, \varepsilon \right)$ is used to prevent the case where $\alpha_{i,k} - \alpha_{i,k-1} = 0$.

Equation (3.24) holds when two conditions are satisfied at a candidate point. The first condition is satisfied when a candidate point is robust with respect to a specific constraint ($g_i^M(\mathbf{x}_k^*) \leq 0$ part). The second condition is satisfied when the approximated maximum is greater than the value of the maximum within the uncertainty region

around the candidate point ($g_i^M(\mathbf{x}_k^*) \le (g_i(\mathbf{x}_k^*,\mathbf{p}) + \alpha_{i,k} \sum_{j=1}^{n} \left| \frac{\partial g_i(\mathbf{x}_k^*,\mathbf{p})}{\partial z_j} \right| \Delta\tilde{z}_j$) part).

Figure 3.4 shows the GARO algorithm flowchart.

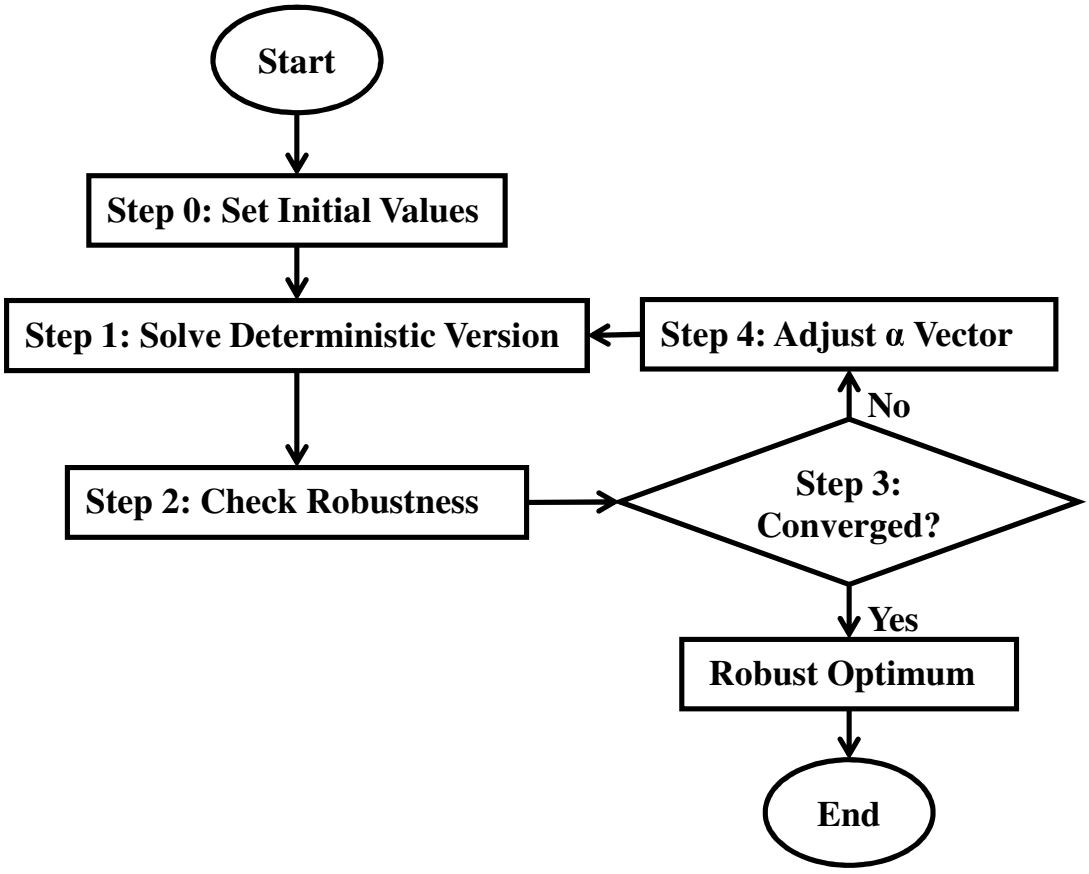

Figure 3.4: General robust optimization (GARO) flow chart

It should be noted that although the modified Taylor series is used to approximate robustness, neither the differentiability nor the continuity of the constraint function is necessary. There are two reasons for this fact. First, the gradient is calculated numerically (by finite difference). Second, the robustness approximation can be adjusted by adjusting the corresponding $\boldsymbol{\alpha}$ vector element in case the discontinuity or non-differentiability affects the robustness approximation.

3.3.3. GARO Algorithm: Simple Numerical Example

In this section, the GARO algorithm is demonstrated by a simple numerical example and also illustrated graphically. Consider the robust optimization problem of equation (3.25)

$$\begin{aligned} &\min_{x} f(x) = x \\ &\text{subject to} \\ &g(x+\Delta x) \le 0 \\ &\forall \Delta x \in [-\Delta\tilde{x}, \Delta\tilde{x}] = [-1,1] \\ &g(x) = 1 - x^2 \end{aligned} \tag{3.25}$$

The robust optimization problem of equation (3.25) can also be written as:

$$\begin{aligned} &\min_{x} f(x) = x \\ &\text{subject to} \\ &\max_{\Delta x} g(x+\Delta x) \le 0 \\ &\Delta x \in [-\Delta\tilde{x}, \Delta\tilde{x}] = [-1,1] \\ &g(x) = 1 - x^2 \end{aligned} \tag{3.26}$$

Now the GARO steps are implemented:

Step 0: Set α_1=1, k=1, λ=0.1, $\varepsilon=10^{-16}$ and η=0.001.

Step 1: Solve the deterministic version by solving the optimization problem of equation (3.27)

$$\begin{aligned} &\min_{x} f(x) = x \\ &\text{subject to} \\ &1 - x^2 + \alpha_1 |2x| \le 0 \end{aligned} \tag{3.27}$$

After solving the problem the following solution was obtained x_1^*=2.41.

Step 2: Check the robustness of x_1^* by solving optimization problem of equation (3.28)

$$g^M(x_1^*) = \max_{\Delta x}(1-(x_1^* + \Delta x)) \quad (3.28)$$

subject to:

$\Delta x \in [-1,1]$

After solving equation (3.28) the following solution was obtained $g^M(x_1^*) = -1$

Step 3: Check the convergence criteria of equation (3.21).

The $g^M(x_k^*) - (g(x_k^*) + \alpha_k \left|\frac{\partial g(x_k^*)}{\partial x}\right| \Delta\tilde{x}) \geq -\eta$ condition of equation (3.21) is not satisfied.

Proceed to Step 4

Step 4: Adjust α: $\alpha_2 = \alpha_1 - \lambda$

Proceed to Step 1.

The algorithm iterations are summarized in Table 3.1 with a graphical representation as shown in Figure 3.5. In Figure 3.5 the dashed line represents the modified Taylor series approximation of the maximum of the constraint in the uncertainty range around point x_k^*. Only in the first iteration in which $\alpha_k = 1$, the dashed line is tangent to g(x) at the point x_k^*. In both Table 3.1 and Figure 3.5, θ represents the difference between the actual value of the maximum and the approximated value of the maximum in the uncertainty region around point x_k^*. As it is shown in Table 3.1 and Figure 3.5, the absolute value of θ decreases as the algorithm proceeds. It should be noted that in this example due to the shape of g(x) the maximum occurred at the end point of the uncertainty interval. Generally the maximum of g(x) can occur at any

point in the uncertainty range around point x_k^*.

Table 3.1: Iteration results for the simple numerical example

k	α_k	x_k^*	g^M	$\theta = g^M(x_k^*) - (g(x_k^*) + \alpha_k \left\lvert \frac{\partial g(x_k^*)}{\partial x} \right\rvert \Delta\tilde{x})$	Converged?
1	1	2.414	-1.000	-1.000	No
2	0.900	2.245	-0.551	-0.551	No
3	0.777	2.044	-0.090	-0.090	No
4	0.753	2.006	-0.011	-0.011	No
5	0.750	2.000	-0.000	-0.000	Yes

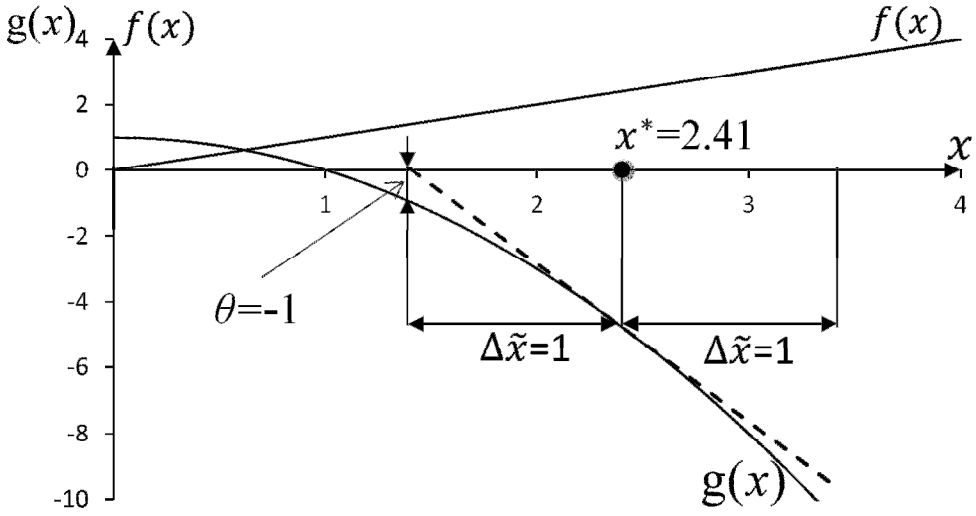

(a)

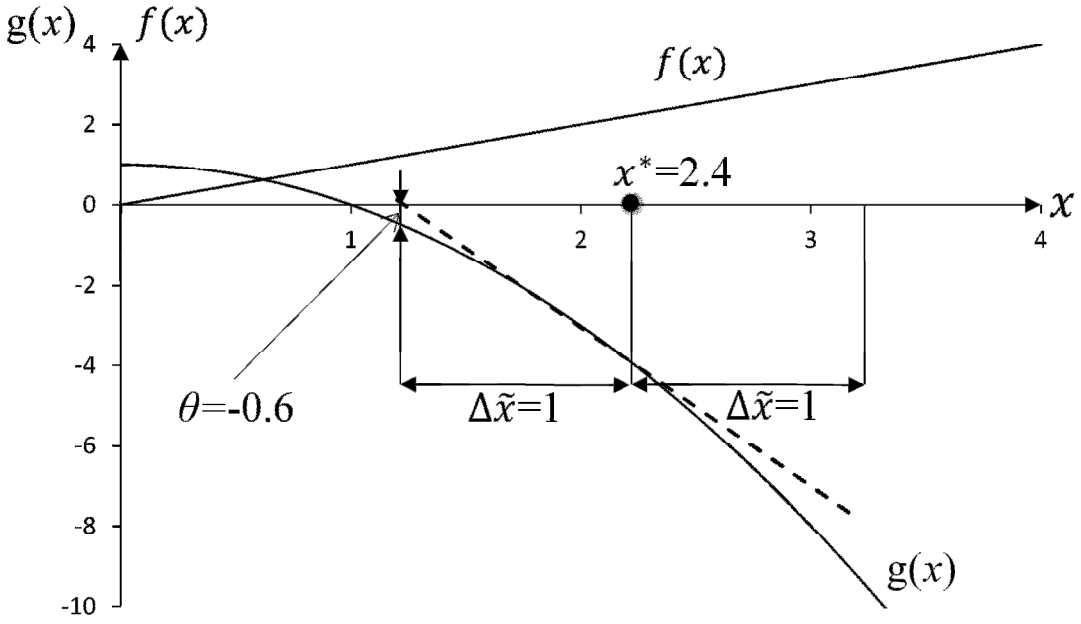

(b)

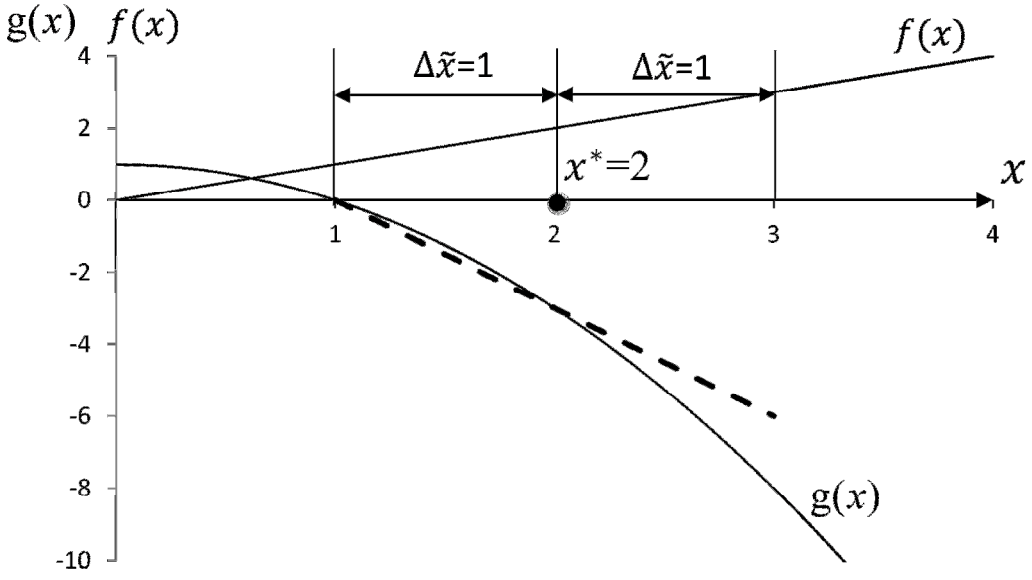

(c)

Figure 3.5: Graphical representation of GARO algorithm applied to a simple problem: (a) k=1 (b) k=2 (c) k=3

3.3.4. GARO Algorithm: Computational Effort

The computational effort of the GARO algorithm is estimated as:

$$number\ of\ \ function\ calls = \left(2 \times DO \times NU + \sum_{1}^{NC} CG_i\right) \times k \tag{3.29}$$

Here a function call refers to each time that the objective or constraint function is calculated. "DO" refers to the average number of function calls required to solve a similar deterministic optimization problem (i.e., Optimization problem without uncertainty). "NU" refers to the total number of uncertain variables and parameters. "CG_i" refers to the average number of function calls required to perform global maximization of constraint i in the uncertainty region around a candidate point. The computational cost of Step 1 and 2 are estimated by $2 \times NU \times DO$ and $\sum_{1}^{NC} CG_i$ respectively. As mentioned before the approximated robust optimization problem is solved in Step 1. The only difference between the approximated robust optimization problem and the deterministic optimization problem is their constraints. In the approximated robust optimization problem the modified Taylor's series approximation of the deterministic optimization problem constraint is used as a constraint. It is assumed that gradient calculation computational cost (used for calculating modified Taylor's series) per uncertain input is 2 function calls. Consequently for all of the uncertain inputs it becomes $2 \times NU$ function calls. Therefore if the deterministic optimization problem requires "DO" function calls the approximated robust optimization problem requires $2 \times NU \times DO$. In Step 2 the global

optimization is used for each constraint function. Therefore the computational cost is approximated by a summation of CG's. This formulation is applied to two numerical test examples in Section 3.7 for demonstration.

In the next section a faster robust optimization method, compared to GARO, will be described. This method is aimed at problems in which objective (only if the objective robustness is considered) and constraint functions are both quasi-concave with respect to uncertain inputs.

3.4 Quasi-Concave Gradient Assisted Robust Optimization (QC-GARO) Algorithm

As it will be shown in this section, if QC-GARO numerically converges to a solution the robustness of the solution is guaranteed for problems with quasi-concave objective and constraint functions. In this section, this method is first demonstrated for a two-variable case in which the uncertainty is only in the design variables. Subsequently, this method will be extended to a case in which there are multiple uncertain design variables and/or parameters.

The general structure of QC-GARO is the same as GARO (Figure 3.4) with the exception of Step 2. Here, in Step 2 instead of executing a global optimization method, a gradient-based algorithm with a "gradient cutting mechanism" is employed.

The gradient cut $T(\mathbf{x}_k^*)$ (Malakooti, 1988, Maddulapalli et al., 2007) is defined as the half space bounded by the plane ($p_n(\mathbf{x}_k^*)$) that passes through point $\mathbf{x}_k^*$ and is normal to gradient vector at point $\mathbf{x}_k^*$ (i.e., $\nabla g(\mathbf{x}_k^*)$) . The gradient vector at point $\mathbf{x}_k^*$ ($\nabla g(\mathbf{x}_k^*)$

) points in an outward direction with respect to gradient cut $T(\mathbf{x}_k^*)$. The gradient cut does not include plane ($p_n(\mathbf{x}_k^*)$). Mathematically a gradient cut $T(\mathbf{x}_k^*)$ at the point $\mathbf{x}_k^*$ can be stated as:

$$T(\mathbf{x}_k^*)=\{\mathbf{x}|(\mathbf{x}-\mathbf{x}_k^*).\nabla g(\mathbf{x}_k^*)<0\} \tag{3.30}$$

It was shown by Bazaraa et al., (1993) and Sundaram, (1996) that for all points in the gradient cut $T(\mathbf{x}_k^*), \mathbf{x} \in T(\mathbf{x}_k^*)$, the value of the quasi-concave function $g(\mathbf{x})$ is less than $g(\mathbf{x}_k^*)$. Mathematically:

$$\forall \mathbf{x} \in T(\mathbf{x}_k^*),\ g(\mathbf{x}) < g(\mathbf{x}_k^*) \tag{3.31}$$

In the QC-GARO method the gradient cutting mechanism benefits from the quasi-concavity of the constraint functions with respect to the uncertain design variables and parameters. The role of the cutting mechanism is to eliminate a part of the uncertainty region while checking the robustness of a constraint at a candidate point using a gradient-based optimization (maximization) method. The gradient cut is generated each time the gradient-based optimization method calculates the gradient.

Figure 3.6 shows the graphical cutting mechanism for a two-variable feasible domain with only one constraint. This is a two-variable case, and the interval uncertainty around a specific point is rectangular (in the multi-variable case it will be a hyper rectangle).

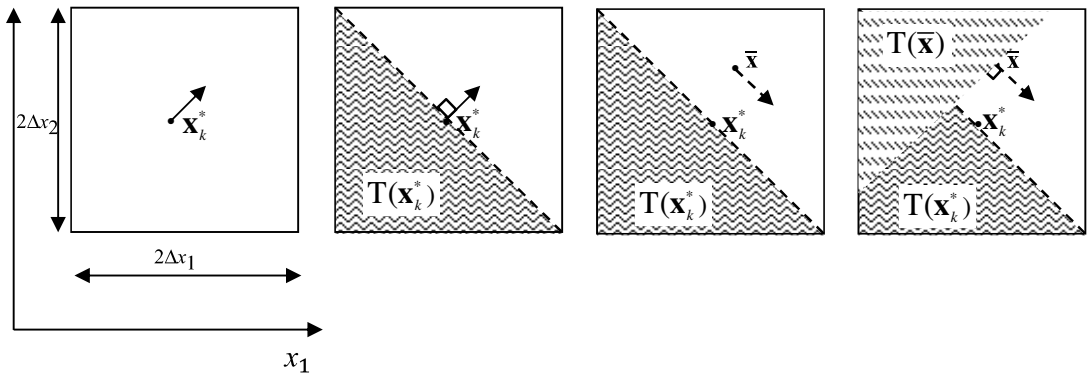

(a) **(b)** **(c)** **(d)**

Figure 3.6: Graphical representation of the cutting mechanism: (a) uncertainty interval with the gradient of constraint function at a point $\mathbf{x}_k^*$.; (b) the shaded region is the gradient cut region;(c) the next point in which the gradient of constraint function is calculated in gradient-based maximization; (d) the shaded regions are the gradient cut regions

In Figure 3.6(a), the arrow shows the gradient of the constraint function at point $\mathbf{x}_k^*$, which is the result of Step 1 (see Figure 3.1). The dashed line in Figure 3.6(b) is the line ($p_n(\mathbf{x}_k^*)$) normal to the gradient vector at the point $\mathbf{x}_k^*$. In Figure 3.6(b), the gradient cut at point $\mathbf{x}_k^*$ ($T(\mathbf{x}_k^*)$) is shown by a shaded triangle.

Based on equation (3.30) it can be concluded that in Figure 3.6(b) the maximum of the constraint function does not exist in the shaded triangle (set $T(\mathbf{x}_k^*)$). Therefore, this region can be cut from the search region for finding the maximum of the constraint function in the uncertainty region around $\mathbf{x}_k^*$.

Figure 3.6(c) depicts the next point at which the gradient is calculated during the maximization algorithm. Denote this point as $\bar{\mathbf{x}}$. The gradient vector at this point is shown as a dashed arrow. Similarly, the constraint function maximum does not exist in the upper shaded area in Figure 3.6(d).

It should be noted that each time the gradient is calculated, a gradient cut is generated. However, the cuts are implemented after performing the gradient-based maximization procedure. After implementing the cuts, if there remains an unexplored part in the uncertainty region, another gradient-based maximization will be executed with the added cuts and with a starting point inside of the unexplored region. This process is continued until the entire uncertainty region around the point $\mathbf{x}_k^*$ is examined.

In general, when there are uncertain variables and parameters, the cutting plane and the uncertainty region will be multi-dimensional. The principles of the cutting mechanism can be demonstrated for the general case by replacing $\mathbf{x}_k^*$ with $\mathbf{z}_k^*$ in equations (3.30) and (3.31). In such cases where there are multiple constraint functions, the maximization process should be performed for each of the constraints separately.

The computational complexity of this algorithm is calculated by equation (3.32).

$$number\ of\ \ function\ calls = \left(2 \times DO \times NU + \sum_{1}^{NC} CGB_i \right) \times k \tag{3.32}$$

CGB: Constraint Gradient-Based Optimization Number of Function Calls

DO: Deterministic Optimization number of Function Calls

NU Number of Uncertain Variables and Parameters

It should be noted that, the CGB is smaller than CG (equation (3.29)). Due to the fact that CGB uses gradient-base maximization whereas CG uses a Hybrid Genetic algorithm.

For demonstration purposes equation (3.32) will be applied to two numerical test examples in Section 3.7.

As it will be shown in Section 3.5, the computational cost of QC-GARO is significantly lower than GARO. Meanwhile, QC-GARO might lead to a non-robust answer when applied to problems with non-quasi-concave functions. Therefore, for solving general robust optimization problems, the following strategy, referred to as the combined method, is proposed. In the combined method QC-GARO is applied first. Subsequently, the robustness of the QC-GARO result is examined. If the result is robust a robust optimum is achieved. Otherwise the GARO method should be employed with a QC-GARO optimum point and its corresponding $\boldsymbol{\alpha}$ as the initial condition. It should be noted that the QC-GARO optimum point is only needed if local search optimization methods are used in Step 1 of GARO.

3.5 Test Problems and Results

In this section, the GARO and QC-GARO algorithms are used to solve 17 test problems with various levels of difficulty. This problem set includes 11 numerical test problems, 5 engineering problems and 1 problem that involves a black-box simulation. To compare the performance of GARO and QC-GARO with previous methods, the solutions for 4 test problems are compared with the reported results of Siddiqui et al., (2011) and 1 test problem with the reported results of Gunawan and Azarm (2004b). Moreover all of the 17 test problems were compared with the method of Li et al., (2006) whose robust optimization computer code was available. It should be noted that the Li et al., (2006) method is a multi-objective robust optimization method, and comparing it with single objective methods may not be a fair

comparison. The results of Li et al., (2006) method are generated by the author of this dissertation. Therefore there may not be a perfect representation of Li et al., (2006) method capabilities.

Two numerical, 2 engineering and 1 black-box simulation problems will be discussed in detail and compared with previous methods in Sections 3.7.1-3.7.3 respectively. The test problems in Sections 3.7.1 and 3.7.2 are taken from (Siddiqui et al., (2011) and Gunawan and Azarm, (2004b). This is done in order to compare GARO and QC-GARO results with Siddiqui et al., (2011) and Gunawan and Azarm, (2004b) reported results without dealing with the implementation issues of those methods. The remaining 12 test problems are summarized in Section 3.7.4 while their problem formulation and detailed results are given in the Appendix B. The comparison of the methods is summarized in Section 3.7.5. Gradient-based optimization algorithms were used to solve Step 1 of both QC-GARO and GARO except for the "Welded-Beam v3" test problem in which genetic algorithm was used as a demonstration case. It should be noted that the test problems were run at least 10 times to capture the stochasticity of the hybrid genetic algorithm. The population size of 25 per uncertain variable is used. The tournament selection (Matlab 2010a) was chosen as the selection function. Fmincon (Matlab 2010a) was selected as the hybrid function. The rest of the settings are set as the default of Matlab 2010a (Matlab 2010a) genetic algorithm setting of global optimization toolbox.

3.5.1 Numerical Test Problems

The two numerical test problems discussed in this section are robust optimization versions of the problems 100 and 106 of Hock and Schittkowski, (1980). It should be

noted that Hock and Schittkowski, (1980) test problems are deterministic optimization test problems. Siddiqui et al., (2011) developed two robust optimization problems based on problems 100 and 106 of Hock and Schittkowski, (1980) and referred to them as Hock 100 and Hock 106 respectively. Here the same terminology is used for these two test problems. Hock 100 is a nonlinear robust optimization problem. Hock 106 is a nonlinear robust optimization problem with quasi-convex (with respect to uncertain input) objective and constraint. The robust optimization results of GARO, QC-GARO and methods of Li et al., (2006) and Siddiqui et al., (2011) are shown in Table 3.2 and Table 3.3 for Hock 100 and Hock 106 respectively. Although a hybrid genetic algorithm was used in GARO, no discrepancy was observed in GARO results of Hock 100 and Hock 106 except for the number of function calls. Moreover, the standard deviation of the number of function calls was less than 5%. This is due to the fact that hybrid genetic algorithm is only used for checking the robustness; however, the Step 1 optimization was performed using gradient based optimization method. The results confirm this explanation since only the number of function calls has discrepancy.

The estimated number of function calls for both GARO (equation 3.29) and QC-GARO (equation 3.32) algorithms are also given in both tables. The estimated number of function calls is significantly higher than the actual number of function calls. The reason is that to calculate the estimated number of function calls, it is assumed that the number of iterations is equal to 20, which is greater than the observed number of iterations.

Before comparing the computational cost of different methods, it should be noted that

the reported number of function calls has the same basis. Siddiqui et al., (2011) reported numbers of function calls are based on GAMS (GAMS, 2010) software function call counter. Based on the Siddiqui, (2011) the GAMS (GAMS, 2010) software function call results are at least one order of magnitude lower than the Matlab 2010a (Matlab 2010a) number of function calls. Both this dissertation and Siddiqui et al., (2011) solved the same deterministic problem with the same starting point as given in Hock and Schittkowski, (1980). Therefore in order to make the comparison, the numbers of function calls are scaled based on the deterministic optimization number of function calls. Regarding the robust case, Siddiqui et al., (2011) approach had the least reported number of function calls. However, in the case of the general robust optimization problems, the robustness of the results obtained by algorithms without a built-in verification scheme should be checked. This is due to the fact that there is no guarantee of arriving at a robust solution for the algorithms without a built-in verification scheme when applied to general problems. Therefore, to make a fair comparison the computational cost of robustness checking should be added to the computational cost of methods without a built-in verification scheme. Hence, here the total number of function calls (reported computational cost plus the robustness checking computational cost) is employed as a comparison base. Siddiqui et al., (2011) method and QC-GARO have the fewest total number of function calls for Hock 100 and Hock 106 respectively.

The results of Siddiqui et al., (2011) were not robust solution for both problems and had a violation. Hock 106 constraint functions were quasi-concave with respect to uncertain variables; consequently, robustness checking was not required for QC-

GARO results. Siddiqui et al., (2011) claim that their approach has the potential to arrive at a robust solution (reducing the violation) by increasing the number of checking points, which will increase the number of function calls. Based on the results of Table 3.2 and 3.3, the method of Siddiqui et al., (2011) should be executed at least one more time with more checking points in order to arrive at a robust optimum point within their tolerance (0.00001).

Li et al., (2006) method had the highest computational cost, which is at least five orders of magnitude higher than GARO. Both GARO and method of Li et al., (2006) have a built-in robustness verification scheme. Hence their results do not require robustness verification.

Table 3.2: Hock 100 results

Information	Det	Det Siddiqui et al., (2011)	GARO	QC-GARO	Li et al., (2006)	Siddiqui et al., (2011)
x_1	2.3305	2.3304	2.190	1.979	1.627	2.235
x_2	1.9514	1.9514	1.855	1.879	2.233	1.855
x_3	-0.4775	-0.4775	-0.468	-0.659	0.258	-0.475
x_4	4.3657	4.3657	4.362	4.360	2.821	4.3535
x_5	-0.6245	-0.6245	-0.625	-0.6250	-0.002	-0.6255
x_6	1.0381	1.0381	1.032	1.135	1.334	1.036
x_7	1.5942	1.5942	1.601	1.464	1.579	1.597
$f(x)$	680.630	680.630	692.723	693.492	732.080	692.385
function calls	129	7	2.568×10^5	2,177	2.524×10^8	19
Scaled function calls	129	129	2.568×10^5	2,177	2.524×10^8	350
Robustness checking	N/A	N/A	N/A	49,974	N/A	49974
Total function calls	N/A	N/A	2.568×10^5	52,151	2.524×10^8	50324
Robust?	No	No	Yes	Yes	Yes	No*
ENFC	N/A	N/A	1.015×10^6	1.692×10^4	N/A	N/A

*Denote **z**=[x_1, x_2, x_3, x_4, x_5, x_6, x_7,p] and **G**=[g_1,g_2,g_3,g_4]. The Siddiqui et al., (2011) reported a solution at which **G**=[-9.2782, -253.5548, -147.4902, -0.9516] is not robust and has a violation. The non-robustness of the solution is due to the fact that

constraint g_1 is violated at **z**=[2.3350, 1.9550, -0.4750, 4.3535, -0.6255, 1.0360, 1.5970, 126.9000] with g_1=0.0373, and constraint g_4 is violated at **z**=[2.3350, 1.7550, -0.4750, 4.3535,-0.6255, 1.0360, 1.5970, 127.0108] with g_4=0.6594.

Table 3.3. Results of the Hock 106

Information	Det	Det Siddiqui et al., (2011)	GARO	QC-GARO	Siddiqui et al., (2011)	Li et al., (2006)
x_1	579.307	579.32	390.790	390.790	388.73	---
x_2	1360.171	1359.94	1553.176	1553.176	1540.21	---
x_3	5109.770	5110.07	5275.291	5275.291	5290.11	---
x_4	182.018	182.02	151.070	151.070	150.89	---
x_5	295.609	295.60	288.992	288.992	288.40	---
x_6	217.982	217.98	208.930	208.930	209.11	---
x_7	286.409	286.42	262.077	262.077	262.49	---
x_8	395.609	395.60	388.992	388.992	388.40	---
f(x)	7049.248	7049.33	7219.257	7219.257	7219.06	---
function call	90	5	1.036×10^5	3897	17	$>2\times10^9$
Scaled function calls	90	90	1.036×10^5	3897	306	$>2\times10^9$
Robustness checking	N/A	N/A	N/A	N/A	25020	N/A
Total function calls	N/A	N/A	1.036×10^5	3897	25326	$>2\times10^9$
Robust?	No	No	Yes	Yes	No*	---
ENFC			5.148×10^5	1.640×10^4		

* Denote **z**=[x_1, x_2, x_3, x_4, x_5, x_6, x_7, x_8, p] and **G**=[g_1,g_2,g_3,g_4,g_5,g_6]. The Siddiqui et al., (2011) reported robust optimum at which, **G**=[-0.1000, 0, 0, -6.1194, 0.0640, -11.0000], has violations for constraint g_4 and g_5 in the uncertainty range around the reported robust optimum. The maximum violation for constraint g_4 happens at **z**= [388.63,1540.11,5290.01,150.89,288.40,209.11,262.49,388.40,0.90] with g_4=4.79, and for constraint g_5 at **z**= [388.63,1540.11,5290.01,150.89,288.40,209.11,262.49,388.40,1.10] with g_5=11.22.

3.5.2 Engineering Test Problems

In this section the performance of GARO and QC-GARO algorithms is compared to the methods of Li et al., (2006), Siddiqui et al., (2011) and Gunawan and Azarm, (2004b) by using two representative engineering test problems. The first test problem is the well-known welded-beam design problem, and the second one is the heat-exchanger design problem.

Welded-Beam Design Problem Version 1

The well-known welded-beam problem was originally introduced in Ragsdell and Phillips (1976). The robust version of this problem is available in Gunawan and Azarm, (2004b), and it is different from the robust welded-beam problems that will be introduced in Section 3.5.3.

Both the deterministic and robust optimization results of GARO, QC-GARO, Siddiqui et al., (2011) and Gunawan and Azarm, (2004b) are shown in Table 3.4. The deterministic result of this dissertation is the same as Siddiqui et al., (2011) though the number of function calls is significantly higher due to use of GAMS (GAMS, 2010) solver by Siddiqui et al., (2011). Thus, numbers of function calls of Siddiqui et al., (2011) are scaled as mentioned in Section 3.5.1.

Once again, the total number of function calls is used to compare the methods. Gunawan and Azarm, (2004b), both deterministic and robust solutions, are inferior to the solutions of this dissertation and to that of Siddiqui et al., (2011). With respect to the robust case, both the methods of Siddiqui et al., (2011) and Gunawan and Azarm, (2004b) report non-robust solutions while the results of GARO and QC-GARO are robust. The computational cost difference among Siddiqui et al., (2011) and Gunawan and Azarm, (2004b) and QC-GARO is negligible, and their computational costs are in the same order of magnitude as GARO. Gunawan and Azarm, (2004b) has the fewest number of function calls. If it is assumed that the Siddiqui et al., (2011) method can arrive at the robust solution by one more robust optimization execution with more checking points, its computational cost will increase at least by a factor of 2 which is greater than the computational cost of GARO.

Table 3.4: The welded-beam design problem version 1

	Det	Det Siddiqui et al., (2011)	Det Gunawan and Azarm, (2004)	GARO	QC-GARO	Siddiqui et al., (2011)	Gunawan and Azarm, (2004)
h	0.244	0.244	0.241	0.2415	0.2415	0.2392	0.246
l	6.219	6.219	6.158	5.6694	5.6694	5.6753	5.461
t	8.291	8.291	8.5	9.1681	9.1681	9.1225	9.138
b	0.244	0.244	0.243	0.2415	0.2415	0.2392	0.248
f_{cost}	2.381	2.381	2.39	2.4597	2.4597	2.4238	2.486
function calls	76	8	N/A	31599	535	38	250
Scaled function calls	76	76	N/A	31599	535	361	250
Robustness checking	N/A	N/A	N/A	N/A	15672	15663	15654
Total function calls	N/A	N/A	N/A	31618	16207	16024	15904
Robust?	No	No	No	Yes	Yes	No*	No*

*Denote $\mathbf{z}=[h, l, t, b, F, L, \tau_d, \sigma_d]$ and $\mathbf{G}=[g_1,g_2,g_3,g_4,g_5,g_6]$. The Siddiqui et al., (2011) reported a solution at which **G**=[-0.0001, -0.1560, -0.9516, -0.0003, 0, -0.4774] is not robust. This non-robustness is due to the fact that constraint g_1 and g_4 are violated in the uncertainty range around the reported robust optimum. The maximum violation happens at **z**=[0.2392,5.6753,9.1225,0.2392,6000,14.250,13600,30000] for both constraints with g_1=0.01 and g_4=0.03. The Gunawan and Azarm, (2004b) reported robust optimum at which **G**=[-0.0018, -0.1887, -0.9536, -0.1039, -0.0081, -0.4919] is not robust due to a violation of g_1 in the uncertainty region around their reported robust optimum. The maximum violation happens at **z**=[0.246, 5.461, 9.138, 0.248, 6000, 14.250, 13600, 30000] with g_1=0.01.

Heat-Exchanger Design Problem

This problem was originally introduced in Magrab et al., (2004). The robust optimization problem formulation is available in Siddiqui et al., (2011). The robust optimization results of GARO, QC-GARO, Siddiqui et al., (2011) and Li et al., (2006) methods are shown in Table 3.5. Here to make a fair comparison, the total number of function calls is used. As it can be seen from Table 3.5 the Siddiqui et al., (2011), QC-GARO and GARO methods total computational costs were in the same order of magnitude. Meanwhile, the Li et al., (2006) method total computational cost

was higher at least by three orders of magnitude. Siddiqui et al., (2011) reported result had a minor robustness violation while having the fewest number of function calls; the method described in Li et al., (2006) did not converge in less than 2×10^9 function calls. However, if it had been converged it would probably have converged to a robust solution due to its built-in verification scheme.

Table 3.5: Heat-exchanger results

Information	GARO	QC-GARO	Li et al., (2006)	Siddiqui et al., (2011)
ms	14.092	14.656	---	14.000
mt	9	9	---	9
Ds	0.37	0.37	---	0.39
PT	0.0321	0.0473	---	0.0311
di	0.0149	0.0157	---	0.0149
Q	906.09	906.09	---	906.09
function calls	5.025×10^5	9146	$>2\times10^9$	984
Robustness checking	N/A	165860	N/A	164740
Total function calls	9.934×10^5	175006	$>2\times10^9$	165724
Robust?	Yes	Yes	---	No*

*Denote **z**=[$ms,mt,Ds,PT,di,Tc_1,Th_1,k_{Tube},Load$]**.** The Siddiqui et al., (2011) reported robust optimum has a minor robustness violation. The minor non-robustness is due to the violation of constraint g_5 at **z**=[14,9,0.380,0.0211,0.0159,18 65,60,600] with g_5=0.0048.

It should be mentioned that except for the number of function calls no discrepancy was observed in the results of GARO algorithm for both welded-beam v1 and heat-exchanger optimization problems. The observed discrepancy of the number of function calls for the GARO algorithm was less than 5%.

3.5.3 Power Plant Design Problem

The following robust optimization problem is a HYSYS (HYSYS 7.1) simulation of a 100 MW gas turbine combined cycle power plant. The goal of this optimization is to

design a plant that provide 100 MW of power in various ambient temperatures and after reasonable component efficiency degradation due to the operation and aging of the power plant. The HYSYS model is shown in Figure 3.7. The design variables and their maximum uncertainties are shown in Table 3.6. Also the parameters that have uncertainty are shown in Table 3.6 with their nominal value and maximum uncertainty. The objective is minimizing the power plant fuel consumption, which is assumed to be pure methane.

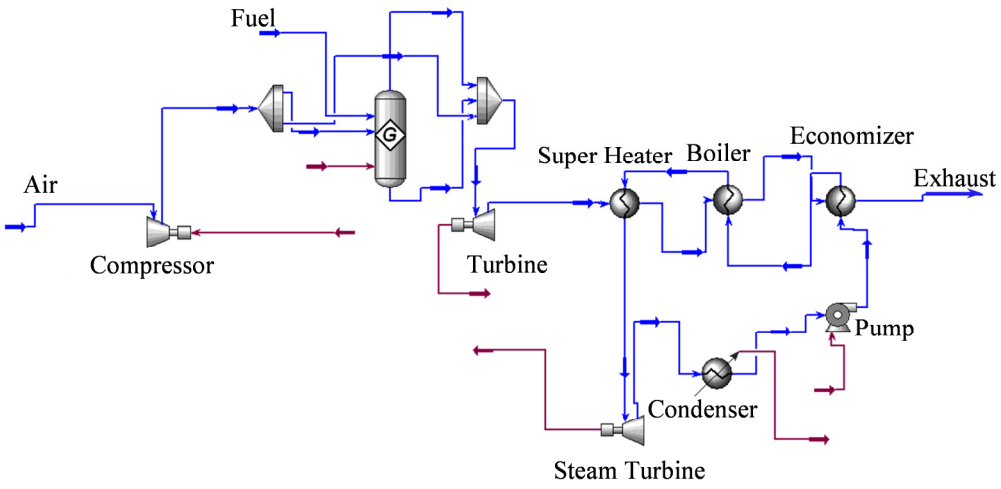

Figure 3.7: HYSYS model of gas turbine combined cycle

Table 3.6: Power plant design variable and parameters and their corresponding maximum uncertainty

V	Information	$\Delta\tilde{x}$	P	Information	p($\Delta\tilde{p}$)	P	Information	p($\Delta\tilde{p}$)
x_1	Steam Mass Flow Rate [kg/s]	1	p_1	Gas Turbine Compressor Efficiency	86 (1)	p_6	Economizer Pressure Drop [kPa]	10 (5)
x_2	Boiler Pressure [kPa]	200	p_2	Gas Turbine Turbine Efficiency	86.275 (1.275)	p_7	Pump Efficiency	88 (2)
x_3	Super Heater Temperature [°C]	5	p_3	Steam Turbine Efficiency	89 (1.5)	p_8	Condenser Temperature [°C]	45 (5)
x_4	Air Volume Flow Rate [m^3/s]	0	p_4	Super Heater Pressure Drop [kPa]	10 (5)	p_9	Ambient Air Temperature [°C]	30 (15)
x_5	Fuel Mass Flow Rate [kg/s]	0	p_5	Boiler Pressure Drop [kPa]	10 (5)			

There are seven constraints in this problem. The constraints are as follows:

g_1=10-SHPT ≤ 0

g_2=10-BPT ≤ 0

g_3=10-EPT ≤ 0

g_4=180-ET ≤ 0

g_5=0.9-SQ ≤ 0

g_6=FT-1124 ≤ 0

g_7=100000-TP ≤ 0

where

SHPT: Super Heater Pinch Temperature [°C]

BPT: Boiler Pinch Temperature [°C]

EPT: Economizer Pinch Temperature [°C]

ET: Exhaust Temperature [°C]

SQ: Steam Quality

FT: Firing Temperature [°C]

TP: Total Power [kW]

Table 3.7 shows the robust optimization results of the power plant problem. These results demonstrate that QC-GARO could be applied to some black-box problems. In this test problem the QC-GARO number of function calls is the largest in comparison to the other test problems. This difference is due to fact that, first, the algorithm has performed several iterations in order to accurately approximate seven constraints; second, checking the robustness of the candidate solution required a relatively high number of function calls due to large uncertainties in the problem input. The Li et al., (2006) method could not converge to a solution within 2 weeks, therefore, the optimization was stopped. QC-GARO could converge in 47 minutes, and GARO in less than 11 hours.

Table 3.7: Power plant design problem results

Information	GARO	QC-GARO	Li et al., (2006)
x_1	35.063	35.063	---
x_2	1699.9	1699.9	---
x_3	489.963	489.962	---
x_4	0.503	0.503	---
x_5	6.919	6.919	---
$f(x)$	6.919	6.919	---
function calls	417,644	32,385	Computationally prohibitive

3.5.4 Other Test Problems

The results of the remaining 12 test problems are shown in Table 3.6. The problems are sorted based on increasing complexity level. There are 9 numerical test problems and 3 engineering test problems. The details of these test problems are given in the Appendix B. Test problems "Self 1-4" are designed by the author of this dissertation. "Sch." problems are taken from Schittkowski (1987) where the three digits show the problem number, and "v" stands for different robust problem versions. The difference between different versions are in the uncertainty range and in the number of uncertain variables and parameters. It should be noted that the two welded-beam robust optimization problems are more complex versions [all variables and parameters (only for version 3) are considered as uncertain] of the robust optimization problem given in Gunawan and Azarm, (2004b), which was discussed earlier.

As mentioned earlier, the welded-beam v3 was solved using genetic algorithm as the GARO Step 1 optimizer. All the other test problems could also be solved using genetic algorithm or any global search methods. However the computational cost will be higher by at least one order of magnitude. The power tool example is taken from Hamel, (2010) and converted to a robust problem by the author. As it is shown in Table 3.8, the GARO method could solve all 12 test problems with a significantly lower computational cost than the Li et al., (2006) algorithm. Since the rest of test problems except problem "Self 1" were not quasi-concave, QC-GARO was not successful in solving some of them. However, its computational cost was at least one order of magnitude and four orders of magnitude lower in comparison to the GARO and the Li et al., (2006) algorithms respectively.

Table 3.8: Results of the different test problems

Method				GARO		QC-GARO		Li et al., (2006)	
Problem	V	U(V+P)	C	FV	FC	FV	FC	FV	FC
Self 1	1	1+0	2	1.2031	2.31×10^{4}	1.2031	2.50×10^{2}	1.2	5.5×10^{6}
Self 2	2	0+6	3	0.035	3.77×10^{4}	0.035	3.00×10^{2}	0.0376	5.5×10^{8}
Self 3	2	0+7	4	0.2356	5.03×10^{4}	0.2356	4.09×10^{2}	0.2356	5.8×10^{8}
Self 4	2	2+1	4	0.3074	4.21×10^{4}	0.3074	1.92×10^{2}	0.3261	2.4×10^{8}
Sch 372 v1	9	8+0	12	952458	1.43×10^{5}	952458	1.52×10^{3}	---	$>2\times10^{9}$
Sch 380 v1	12	12+0	3	176.086	4.41×10^{5}	182.076	9.15×10^{3}	---	$>2x10^{9}$
Sch 369	8	8+0	6	5379.318	3.08×10^{6}	Failed	Failed	6497.104	1.2×10^{9}
Sch 380 v2	12	12+30	3	298.494	8.14×10^{5}	Failed	Failed	---	$>2\times10^{9}$
Sch 372 v2	9	9+0	12	1.80×10^{6}	4.90×10^{5}	Failed	Failed	---	$>2\times10^{9}$
Welded-Beam v2	4	4+0	6	4.931	5.09×10^{5}	4.9394	1.05×10^{3}	5.4371	8.1×10^{8}
Welded-Beam v3	4	4+4	6	5.553	2.59×10^{6}	Failed	Failed	---	$>2\times10^{9}$
Power Tool	18	6+0	22	313.690	4.25×10^{5}	Failed	Failed	---	$>2\times10^{9}$

3.5.5 Summary of Results

The results for test problems demonstrate the performance of GARO and its faster version QC-GARO. GARO and QC-GARO can be combined and used as a single method as it was discussed earlier in Section 3.4. Therefore, the QC-GARO and GARO computational cost should be considered as the lower and upper bound of the combined method computational cost respectively. The superiority of the combined method in comparison to method of the Li et al., (2006) and Gunawan and Azarm, (2004b) is obvious based on the results presented in Section 3.5.1-3.5.4. Clearly, the

Li et al., (2006) method has limited applicability due to its high computational cost. The method of Gunawan and Azarm, (2004b) tends to eliminate some of the solutions due to its back-mapping mechanism. Therefore, their reported result was inferior to the other methods.

Based on the results, Siddiqui et al., (2011) method computational cost was the lowest. However, since Siddiqui et al., (2011) method does not have a built-in robustness checking scheme, the robustness of its results should be checked when it is applied to general problems. Meanwhile, due to the use of global search methods in checking the robustness of the answers, a significant amount of computation is required. Based on the results, if the robustness checking computational cost is considered, Siddiqui et al., (2011) method computational cost will be in the same order of magnitude as the combined method.

3.6 Limitations of GARO and QC-GARO

The numerical convergence of both GARO and QC-GARO depends on the convergence of the deterministic algorithm that is used in their Step 1. Although GARO has a built-in numerical verification scheme, due to the limitations of the deterministic global optimization methods there is no guarantee for robustness of its solution when it is applied to a general problem. Therefore the robustness of the GARO solution mainly depends on the accuracy of the global optimization method that is used in its Step 2. If QC-GARO numerically converges to a solution the robustness of the solution is only guaranteed for problems in which the constraint functions are quasi-concave with respect to uncertain variables and parameters. Moreover as mentioned before, QC-GARO does not have built-in numerical

verification scheme. Therefore the robustness of its results should be checked when it is applied to a general problem. Multi-objective genetic algorithm cannot be used as the optimization method of both QC-GARO and GARO. This issue is discussed in further details in Section 5.3.1.

3.7 Conclusion

In this chapter two efficient robust optimization algorithms are presented for solving robust optimization problems with input (both variable and parameters) interval uncertainty. The first method, called "GARO", is applicable to general engineering problems and leads to a numerically verified robust solution. The second method, called "QC-GARO", can only arrive at a guaranteed robust solution for problems with quasi-concave constraints with respect to uncertain inputs. Nevertheless QC-GARO can be applied to general problems. This flexibility is due to the fact that the quasi concavity of the constraint with respect to uncertain variables is only required at the candidate optimum points in order to arrive at the robust optimum. It may be more efficient to combine QC-GARO and GARO together since the computational cost of the combined methods is greater than QC-GARO and less than GARO. Seventeen different test problems were used to demonstrate the performance superiority of QC-GARO and GARO in comparison to 3 previous methods. The problems include 11 numerical, 5 engineering and 1 black-box simulation.

In the next chapter the GARO algorithm will be used to design a refrigerant mixture that is relatively insensitive to the feed gas mixture composition for an APCI LNG plant. Due to the fact that development of the refrigerant mixture involves back box simulations and QC-GARO does not have a built-in numerical verification scheme,

QC-GARO is not used to design a robust refrigerant in the next chapter.

Chapter 4: Developing a Robust Refrigerant Mixture for APCI LNG Plants

4.1 Introduction

In this chapter, Research Task 3 is discussed in detail. As mentioned in Chapter 1, one of the challenges in designing a mobile LNG plant is developing a refrigerant mixture composition whose performance is relatively insensitive to the natural gas mixture variation. Developing and optimizing refrigerant mixtures for natural gas liquefaction cycle have been considered in several previous studies, as discussed next.

Paradowski et al., (2004), Venkatarathnam, (2008), Alabdulkarem et al., (2011) and Wang et al., (2012) optimized APCI liquefaction cycle energy consumption. Taleshbahrami et al., (2010) enhanced APCI liquefaction cycle energy consumption by optimizing the MCR cycle refrigerant composition. Lee et al., (2002), Aspelund et al., (2010), Shirazi and Mowla, (2012) and Xu et al., (2012) optimized refrigerant mixture composition of single mixed refrigerant natural gas liquefaction cycles. Vaidyaraman and Maranas (2002) minimize the power consumption of a cascade mixed refrigerant cycle by optimizing refrigerant mixture composition and other cycle variables. Nogal et al., (2008) developed a thermodynamic model for mixed refrigerant cycles and optimized their refrigerant composition. Jensen and Sigurd (2006) optimized mixed fluid cascade natural gas liquefaction cycle. However, none of the previous studies considered the uncertainty in the feed gas compositions in developing and optimizing refrigerant mixtures for natural gas liquefaction plants.

In this chapter the GARO algorithm will be used to develop a MCR cycle refrigerant mixture that is relatively insensitive to the uncertainty of the natural gas mixture for the APCI LNG plant. A relatively insensitive refrigerant refers to a refrigerant that for variations (uncertainty) of the natural gas mixture it satisfies the following design constraints:

i. The refrigerant temperature remains at least 3°C colder than the natural gas mixture in the MCR cycle evaporators
ii. The refrigerant entering the MCR cycle compressors is super-heated (i.e., does not contain liquid droplets)

The rest of this chapter is organized as follows. In Section 4.2 the APCI cycle model development is discussed. Optimization methodology, results and discussion are discussed in Sections 4.3 and 4.4 respectively followed by conclusions in Section 4.5.

4.2 Model Development

In this section a new model for the APCI natural liquefaction cycle will be developed. The modeling equations of different cycle components are the same as those in Chapter 2. The HYSYS simulation software (HYSYS 7.1) is selected for modeling due to ease of connectivity between HYSYS software and Matlab (Matlab 2010a) in which GARO is implemented. The fractionation plant is not considered since its operation is independent of the MCR cycle. Due to the fact that optimization is not performed on the propane cycle of the APCI liquefaction cycle the propane cycle will not be modeled in detail. Instead each cooling stage of the propane cycle is modeled separately. To model each cooling stage of the propane cycle, it is assumed that the

cooling is provided by a separate propane cycle that has only one evaporator with a fixed evaporating temperature. The schematic diagrams of the propane cycles associated with the cooling stages are shown in Figure 4.1-4.5. The evaporating temperature of these propane cycles are the same as their corresponding cooling stage (details regarding the propane cycle cooling stages were provided in Chapter 2). The simulated COPs of the propane cycles associated with cooling stages are listed in Table 4.1. To simulate propane cycle power consumption, the COPs of the propone cycles associated with each cooling stage are used. The MCR cycle assumptions are the same as APCI base cycle MCR cycle of the Chapter 2. The schematic diagram of the new model of the APCI liquefaction cycle and its corresponding HYSYS model are shown in Figure 4.6 and 4.7 respectively.

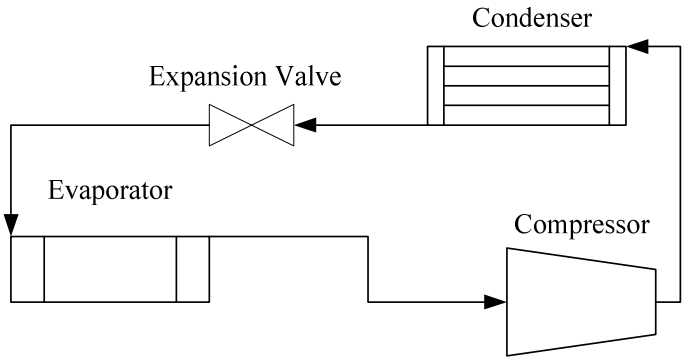

Figure 4.1 Propane cycle associated with the first stage of the APCI propane cycle

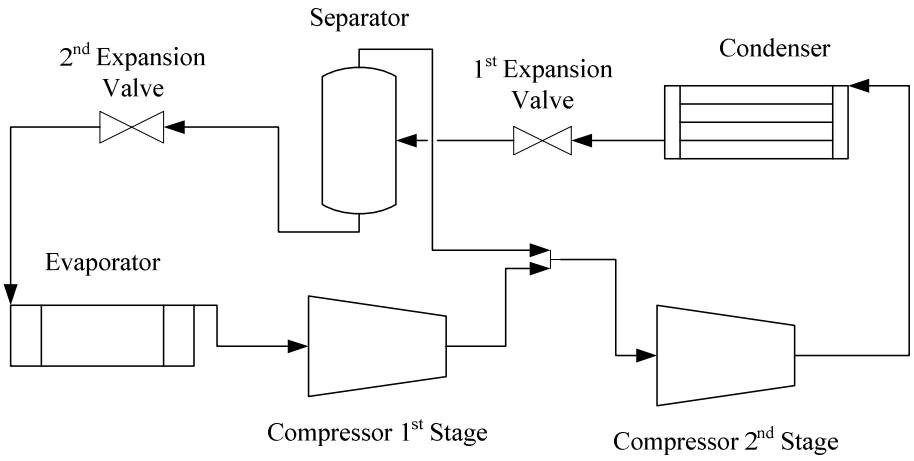

Figure 4.2 Propane cycle associated with the second stage of the APCI propane cycle

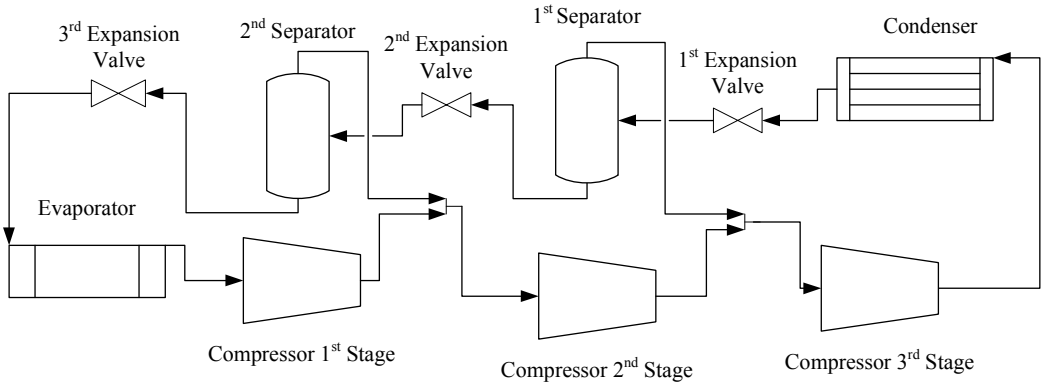

Figure 4.3 Propane cycle associated with the third stage of the APCI propane cycle

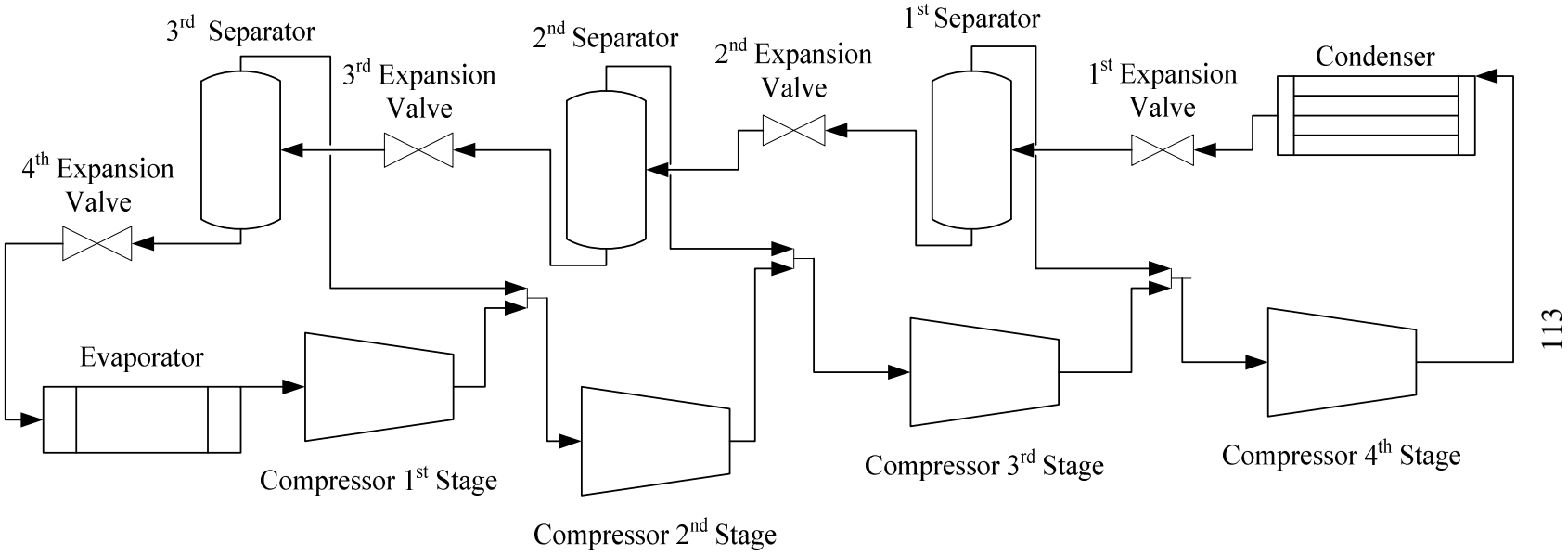

Figure 4.4. Propane cycle associated with the fourth stage of the APCI propane cycle

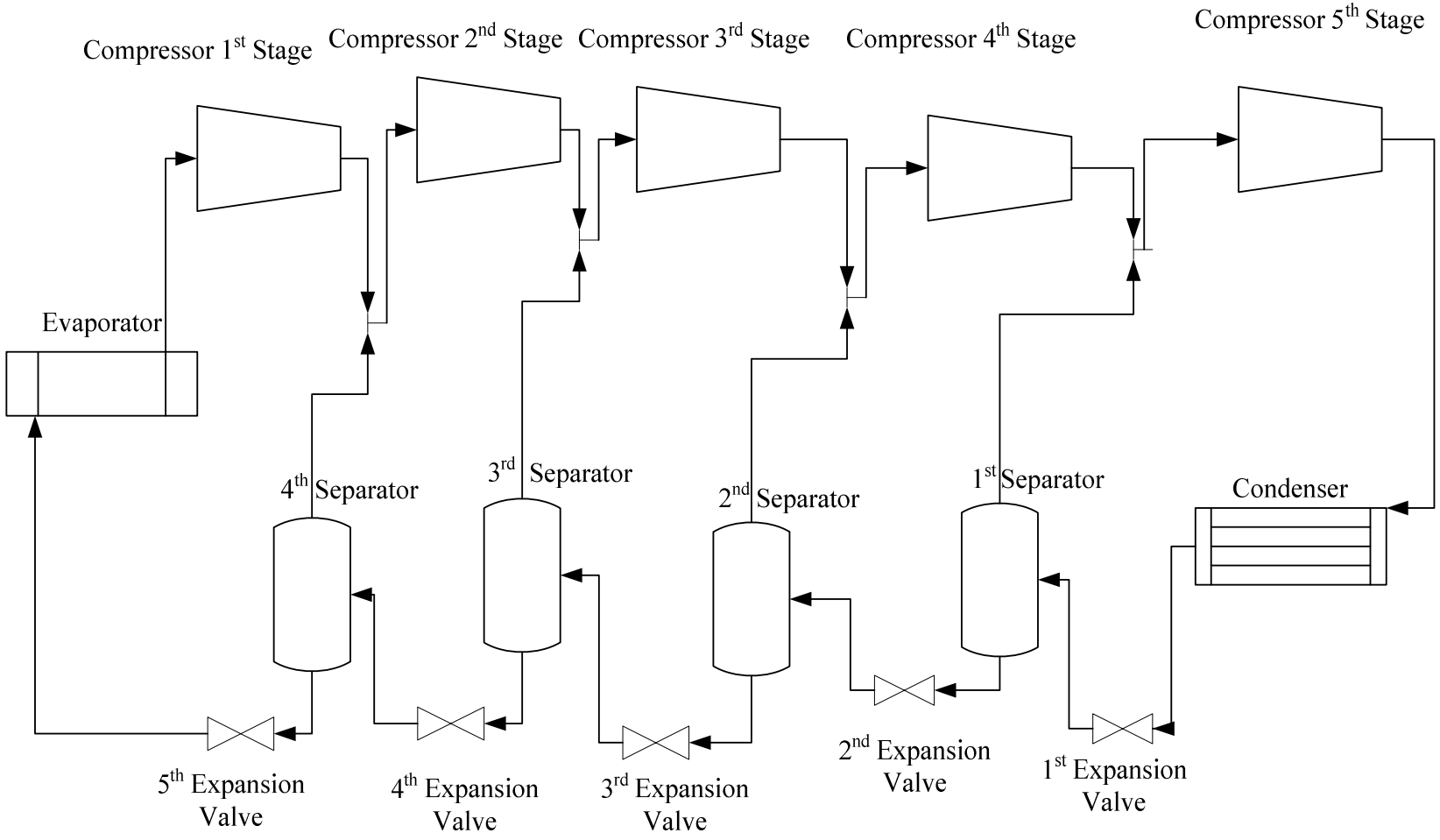

Figure 4.5 Propane cycle associated with the fifth stage of the APCI propane cycle

Table 4.1 The simulated COPs of the propane cycles associated with cooling stages of APCI propane cycle

	Evaporator Temperature °C	Condenser Temperature °C	COP
1st Stage	22	43	9.8829
2nd Stage	9	43	5.9611
3rd Stage	-5	43	4.0547
4th Stage	-19	43	2.9897
5th Stage	-35	43	2.2272

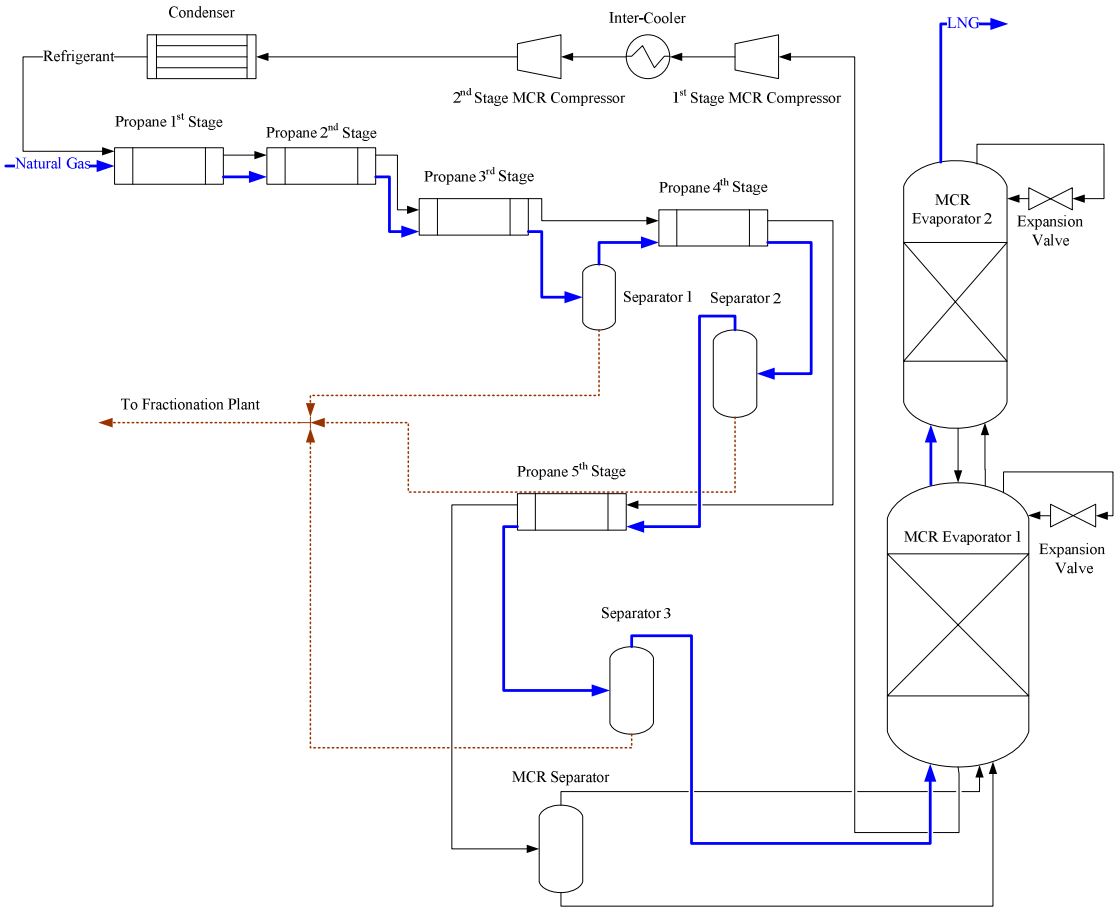

Figure 4.6. The schematic diagram of the new model of the APCI liquefaction cycle.

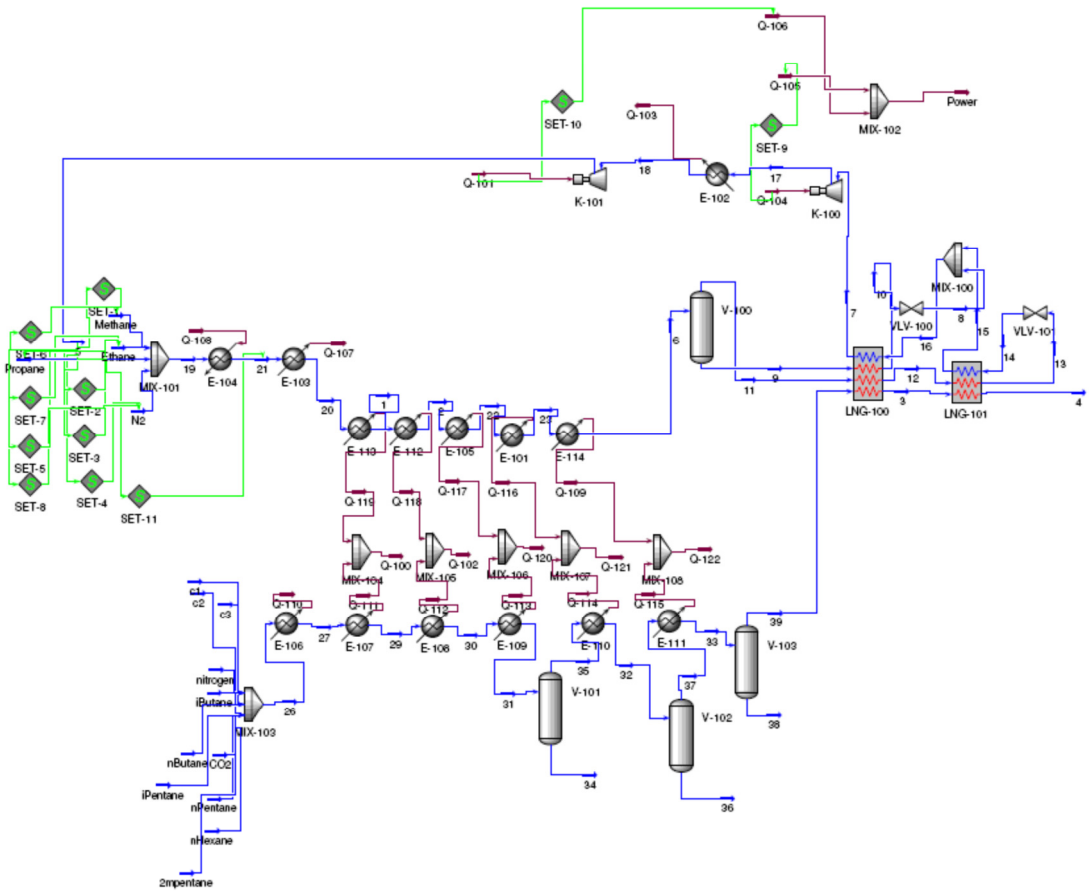

Figure 4.7 The HYSYS model of the new APCI liquefaction cycle model.

4.3 Optimization Model

The optimization model is shown by equation (4.1). Here the design variables are refrigerant component mass flow rates (Nitrogen, Methane, Ethane and Propane), the discharge pressures of the MCR compressor stages and the pressure of the MCR evaporators. The uncertain design parameters are mass fractions of the natural gas components. The pentane and heavier hydro carbons in the natural gas are condensed and sent to the fractionation unit before entering the MCR cycle heat exchangers. Therefore any uncertainty in their mass fraction does not affect the performance of the MCR cycle. Consequently the pentane and heavier hydrocarbons mass fraction

uncertainties are not considered. The remaining gas components after the sweetening are Nitrogen, Methane, Ethane, Propane, Iso-Butane and n-Butane. The uncertainty in the natural gas mixture is modeled by varying mass fractions of Nitrogen, Ethane, Propane, Iso-Butane and n-Butane as shown in equation (4.1). To solve the optimization problem of equation (4.1), GARO (recall Chapter 3) is used. The hybrid genetic algorithm (Matlab 2010a) is used as the optimizer for Step 1 and Step 3 of GARO. The settings of the hybrid genetic algorithms are the same as the settings mentioned in Section 3.5.

$$\min_{\mathbf{dv}} \; Power_{Total}(\mathbf{dv}, \mathbf{p}+\Delta\mathbf{p}) = Power_{1^{st}\ Stage\ MCR\ Comp.} + Power_{2^{nd}\ Stage\ MCR\ Comp.} + \frac{Q_{Propane\ Eva.1^{st}}}{COP_{Propane1^{st}\ Stage}} + \frac{Q_{Propane\ Eva.2^{nd}}}{COP_{Propane2^{nd}\ Stage}} + \frac{Q_{Propane\ Eva.3^{rd}}}{COP_{Propane3^{rd}\ Stage}} + \frac{Q_{Propane\ Eva.4^{sth}}}{COP_{Propane4^{th}\ Stage}} + \frac{Q_{Propane\ Eva.5^{th}}}{COP_{Propane5^{th}\ Stage}} \tag{4.1}$$

S.t.

$$\max_{\Delta\mathbf{p}} g_1(\mathbf{dv}, \mathbf{p}+\Delta\mathbf{p}) : 3\ ^{\circ}\text{C-}\Delta T_{p,MCR\ Eva.\#1} \le 0$$

$$\max_{\Delta\mathbf{p}} g_2(\mathbf{dv}, \mathbf{p}+\Delta\mathbf{p}) : 3\ ^{\circ}\text{C-}\Delta T_{p,MCR\ Eva.\#2} \le 0$$

$$\max_{\Delta\mathbf{p}} g_3(\mathbf{dv}, \mathbf{p}+\Delta\mathbf{p}) : 1\text{-}x_{Inlet,1^{st}\ Stage\ MCR\ Comp.} \le 0$$

$$\max_{\Delta\mathbf{p}} g_4(\mathbf{dv}, \mathbf{p}+\Delta\mathbf{p}) : 1\text{-}x_{Inlet,2^{nd}\ Stage\ MCR\ Comp.} \le 0$$

$$\mathbf{dv} = [\dot{m}_{N_2}, \dot{m}_{CH_4}, \dot{m}_{C_2H_6}, \dot{m}_{C_3H_8}, P_{Outlet,1^{st}\ Stage\ MCR\ Comp}, P_{Outlet,2^{nd}\ Stage\ MCR\ Comp}, P_{MCR\ Eva.\#2}]$$

$$\mathbf{p} = [\omega_{C_2H_6}, \omega_{C_3H_8}, \omega_{N_2}, \omega_{i\text{-}C_4H_{10}}, \omega_{n\text{-}C_4H_{10}}] = [0.1157, 0.0792, 0.0014, 0.0298, 0.0298]$$

$$[9, 30, 90, 5, 900, 2900, 90] \le \mathbf{dv} \le [50, 110, 180, 70, 3000, 6000, 900]$$

$$\Delta\mathbf{p} \in [-\Delta\tilde{\mathbf{p}}, \Delta\tilde{\mathbf{p}}]$$

$$\Delta\tilde{\mathbf{p}} = [0.0553, 0.04, 0.0007, 0.015, 0.015]$$

4.4 Results

The results of the optimization are shown in Table 4.2 in which a comparison is made

with other refrigerants from the literature. It should be noted that the other refrigerant mixture pressure values and total refrigerant mass flow rate are optimized for the nominal natural gas composition. However the mass fractions of the refrigerant components are held constant. The power values listed in Table 4.2 corresponds to the total power consumption for a liquefaction plant (i.e., including propane cycle power consumption) for the nominal natural gas mixture. To evaluate the robustness of the refrigerants, the uncertainty set of natural gas mixtures is divided to 10 different subsets. Each subset is represented by a natural gas mixture. The natural gas mixtures corresponding to the subsets are listed in Table 4.3. The total power consumption of the liquefaction cycle using different refrigerant mixture for different natural gas compositions are shown in Table 4.4. It should be noted that in Table 4.4 for the natural gas mixtures for which the refrigerant violates one of the constraints the violated constraints are listed instead of the power value. As shown in Table 4.4 only the robust refrigerant satisfied the constraints for all natural gas mixtures while other refrigerants are not feasible for at least five different natural gas mixtures. Although the refrigerant that was developed by using robust optimization technique is insensitive to the variation of the natural gas it has the highest power demand. Venkatarathnam, (2008) refrifrigerant and refrigerant #1 of Alabdulkarem et al., (2011) have the least amount of power consumption for the nominal gas mixture. However, these two refrigerant mixtures are the most sensitive refrigerants to the variation of natural gas mixture. The fact that the most efficient refrigerants for the nominal feed gas mixture are the most sensitive one to feed gas mixture can be explain by studying the temperature difference between natural gas mixture and the

refrigerant (approach temperature) in different sections of the MCR evaporators. The two most efficient refrigerants have the minimum approach temperature in different sections of the MCR evaporators. Therefore if the average boiling temperature of the natural gas reduces due to the variation in its mixture the approach temperature may become zero (i.e., no possible heat transfer). However the robust refrigerant has the maximum approach temperature in comparison to the other refrigerants in different sections of the MCR evaporator. The other refrigerant mixture characteristic that affects both the performance and the robustness of the refrigerant is its degree of super heat before entering the compressor. Increasing the degree of super heat of a refrigerant will lead increase in power consumption. A refrigerant degree of super heat is reduced by increasing the average boiling temperature of the natural gas. Therefore the refrigerant flow at the inlet of the MCR compressor might become two phase by variation of the natural gas mixture. The robust refrigerant has the highest degree of the super heat while entering the compressor in comparison to the other refrigerants. It should be noted that increasing the degree of the superheat of the refrigerant entering the compressor will increase the compressor power. To summarize two factors contribute in higher power demand of the robust refrigerant in comparison to the other refrigerants which are higher approach temperature at different sections of MCR evaporator and higher degree of super heating at the inlet of the MCR compressor. These two factors arise from the fact that the robust refrigerant has the lowest average boiling temperature. Having the lowest average boiling temperature is due to the lower mass fraction of propane in the robust refrigerant mixture in comparison to the other refrigerant mixtures.

Table 4.2.The robust refrigerant design values and refrigerant mixtures from other literatures

Refrigerant	Power (MW)	$\dot{m}_{N_2}$ (kg/s)	$\dot{m}_{CH_4}$ (kg/s)	$\dot{m}_{C_2H_6}$ (kg/s)	$\dot{m}_{C_3H_8}$ (kg/s)	$P_{Outlet,1^{st}\ Stage}$ (kpa)	$P_{Outlet,2^{nd}}$ (kpa)	$P_{MCR\ Eva.\#2}$ (kpa)
Robust	138.841	31.239	80.227	170	10	1292	4877	368
Mortazavi et al., (2012)	113.328	28.052	64.280	157.306	39.262	2300	4000	420
Alabdulkarem et al., (2011) #1	103.652	26.872	57.042	138.837	38.909	2346	4137	451
Alabdulkarem et al., (2011) #2	121.552	20.421	70.008	147.809	41.122	2259	3967	333
Venkatarathnam, (2008)	105.398	17.035	58.249	78.105	81.582	2900	4665	302
Paradowski et al., (2004)	122.170	11.814	65.391	107.057	57.838	2284	4446	239

Table 4.3.The natural mixtures corresponding to the natural gas uncertainty subsets

Gas mixture	$\omega_{C_2H_6}$	$\omega_{C_3H_8}$	ω_{N_2}	$\omega_{i\text{-}C_4H_{10}}$	$\omega_{n\text{-}C_4H_{10}}$
1	0.0553	0.04	0.0007	0.015	0.015
2	0.0698	0.0499	0.0009	0.0187	0.0187
3	0.0842	0.0598	0.001	0.0224	0.0224
4	0.0987	0.0697	0.0012	0.0262	0.0262
5	0.1132	0.0796	0.0014	0.0299	0.0299
6 (Nominal)	0.1157	0.0792	0.0014	0.0298	0.0298
7	0.1276	0.0895	0.0016	0.0336	0.0336
8	0.1421	0.0994	0.0017	0.0374	0.0374
9	0.1565	0.1093	0.0019	0.0411	0.0411
10	0.171	0.1192	0.0021	0.0448	0.0448

Table 4.4.The power demand of different refrigerant mixtures for different natural gas mixtures

	Liquefaction Cycle Power Demand (MW)									
Natural Gas Mixture	1	2	3	4	5	6	7	8	9	10
Robust	140.7	140.3	139.9	139.4	138.9	138.8	138.2	137.5	136.6	135.7
Mortazavi et al., (2012)	g1	115.5	114.9	114.2	113.3	113.3	g3	g3	g3	g3
Alabdulkarem et al., (2011) #1	g1,g2	g1,g2	g1	g1	103.7	103.7	102.8	g3	g3	g3
Alabdulkarem et al., (2011) #2	g2	g2	g2	g2	121.6	121.6	120.5	g3	g3	g3
Venkatarathnam, (2008)	g1	g1	g1	g1	g1	105.4	g3	g3	g3	g3
Paradowski et al., (2004)	g2	g2	g2	g2	122.2	122.2	120.9	119.4	g3	g3

4.5 Conclusion

To develop a MCR cycle refrigerant mixture that is insensitive to the natural gas composition variation (i.e., robust refrigerant), a HYSYS model of APCI liquefaction cycle with a simplified propane cycle was generated. GARO algorithm was used for development of the refrigerant. The performance of the robustly optimum refrigerant mixture was compared to five different refrigerants mixtures from the literature. To illustrate the performance superiority of the developed robust refrigerant to the other refrigerants, the uncertainty set of natural gas mixture was divided to 10 different subsets. Each subset was represented by a natural gas mixture. The developed robust refrigerant was the only refrigerant that satisfied all the liquefaction cycle design constraints while the other refrigerants were infeasible at least for 5 different natural gas mixtures. However the power demand of other refrigerants is lower than the robust refrigerant. Moreover the refrigerants with the least power demand are the most sensitive to the natural gas composition variation.

In the next chapter, concluding remarks, main contributions and some future research directions will be discussed.

Chapter 5: Conclusions

This chapter provides a summary of the three research tasks that are accomplished in the dissertation. The research tasks are: (i) LNG plant enhancements and optimization, (ii) development of two new robust optimization methods, and (iii) an application of robust optimization for selection of the refrigerant mixture for APCI LNG plants.

The rest of this chapter is organized as follows: In Section 5.1, a summary and highlights of the results in the three research tasks are provided. In Section 5.2, the main contributions of the dissertation are listed followed by, in Section 5.3, some proposed future studies as an extension to this work.

5.1 Concluding Remarks

5.1.1 LNG Plant Enhancement and Optimization

In Chapter 2, two new APCI liquefaction cycle enhancement options and 10 new driver cycle enhancement options were proposed, studied and compared with the other enhancement options.

It was shown that the best APCI liquefaction cycle enhancement option was the one in which all the expansion valves of LNG expansion process and MCR cycle expansion valves are replaced with two-phase expanders and the expansion valves of the propane cycle are replaced with liquid turbines. This liquefaction enhancement option could improve the liquefaction cycle energy efficiency and production capacity by about 7.07% and 1.24% respectively.

For enhancing the driver cycles, 10 new LNG plant driver cycle configurations were proposed, studied, optimized and compared with five conventional driver cycle configurations. The comparison of the proposed driver cycles and the conventional driver cycle was done for different steam turbine efficiencies and minimum exhaust temperatures. The most efficient driver cycle was a triple gas turbine combined cycle with a double pressure steam cycle with reheat and a single effect absorption chiller with the thermal efficiency of 54% .The obtained thermal efficiency was 38% which was 5% higher than the thermal efficiency of the base driver cycle which was the best considered conventional driver cycle respectively.

5.1.2 Development of Robust Optimization Algorithms

In Chapter 3, two robust optimization algorithms were devised for solving robust optimization problems with interval uncertainty. The first method, called "Gradient Assisted Robust Optimization" (GARO), has a built-in numerical robustness verification scheme. GARO is applicable to general engineering problems with large uncertainty. The second method, called "Quasi-Concave Gradient Assisted Robust Optimization" (QC-GARO), can only arrive at a robust solution for problems with quasi-concave constraints with respect to uncertain inputs. However, QC-GARO can be applied to general problems due to the fact that to arrive at a robust optimum the quasi-concavity of the constraint with respect to uncertain variables is only required at the candidate optimum points. It is possible to combine QC-GARO and GARO. The computational cost of the combined QC-GARO and GARO methods is greater than QC-GARO and less than GARO. Seventeen different test problems were used to demonstrate the performance superiority of QC-GARO and GARO in comparison to

three previous methods. The problems include eleven numerical, five engineering and one black-box simulation. The GARO algorithm was also used to develop an feed gas refrigerant mixture for APCI LNG plants that was relatively insensitive to variation of natural gas mixture..

5.1.3 Developing a Robust Refrigerant Mixture for APCI LNG Plants

In Chapter 4, a simplified HYSYS model of APCI liquefaction cycle was generated to develop a MCR cycle refrigerant mixture that is relatively insensitive to the natural gas composition variation (i.e., robust refrigerant). GARO algorithm was used as the robust optimization algorithm for development of the refrigerant mixture. The performance of robust refrigerant was compared to five different refrigerants mixtures from the literature. Based on the simulation results only the developed refrigerant could satisfy the robustness constraints while the other refrigerant became infeasible by variation of the natural gas mixture. On the contrary other refrigerant had a lower power demand for the nominal natural gas mixture in comparison to the developed robust refrigerant.

5.2 Main Contributions

5.2.1 Investigating the Effect of Replacing Valves with the Expanders on the Performance of APCI LNG Plants

Several options to enhance the liquefaction cycle energy efficiency by recovering expansion losses were considered. Compared to the previous studies, the current study has the following novelties: i) It considered the expansion loss recovery in the performance assessment of the entire APCI liquefaction cycle (i.e., propone and MCR

cycles, fractionation and LNG expansion). ii) Two new expansion recovery options were proposed, studied and compared to other expansion recovery options.

5.2.2 Developing New Driver Cycle Configurations for APCI LNG Plants

Several new triple gas turbine steam cycle and absorption chiller combined cycle configurations which have not been considered before for LNG plants are introduced. Compared to previous studies on the performance enhancement of APCI driver cycles the current study have the following distinct characteristics: i) ten new driver cycle configurations are proposed, studied, optimized and compared with five conventional driver cycles. It should be noted that there has not been even a single study for APCI LNG plants in which the performances of the selected conventional driver cycles are compared with each other. ii) This study was based on the full scale modeling of the both liquefaction and driver cycles while there has been no previous study containing full scale modeling of both driver cycle and liquefaction cycle. iii) The effect of exhaust temperature and gas turbine efficiency on performance of the liquefaction driver cycles were considered while there has been no previous study for LNG plants that has considered these two parameters.

5.2.3 Developing Gradient Assisted Robust Optimization (GARO) Algorithm

A novel robust optimization method called GARO is presented for solving constrained single-objective robust optimization problems with interval uncertainty. Compared to some previous methods, the GARO method has the following distinct characteristics: i) The GARO method is applicable to general robust-design

optimization problems and can obtain a numerically-verified robust solution, and ii) GARO has a sequential structure rather than a double loop one. GARO sequential structure contributes to its lower computational cost in comparison to methods with double loop structure.

5.2.4 Developing Quasi-Concave Gradient Assisted Robust Optimization (QC-GARO) Algorithm

A new robust optimization method, QC-GARO, was developed for solving constrained single-objective robust optimization problems with interval uncertainty. Compared to some previous methods, QC-GARO has the following distinct characteristics: i) QC-GARO can obtain a robust solution for problems with quasi-concave functions with respect to uncertain inputs; ii) QC-GARO has a sequential structure rather than a double loop one. Although QC-GARO can be applied to general robust optimization problems the robustness of its solution should be checked.

5.2.5 Developing a Robust Refrigerant for APCI LNG Plants

A new model for developing a robust optimum refrigerant mixture for APCI LNG plants was introduced. This study has the following distinct characteristics: i) There has been no previous work considering the effect of natural gas uncertainty on the performance of liquefaction cycle. ii) A new liquefaction model was developed that was aimed for optimizing the MCR cycle refrigerant mixture. The main novelty of this model is that it predicts the power demand of the propane cycle without dealing with the unnecessary details of the propane cycle. Therefore the liquefaction cycle

model converges faster which leads to reduce optimization time.

5.3 Some Future Research Directions

5.3.1 Multi-Objective GARO and QC-GARO

GARO and Quasi-GARO are geared for single-objective optimization problems. However there are many engineering problems that involve more than one objective function. GARO and Quasi-GARO algorithms could be easily extended to multi objective problems by using multi-objective methods such as an ε-constraint approach (Arora 2004). Meanwhile if the current version of GARO and QC-GARO are coupled with methods like Multi-Objective Genetic Algorithm (MOGA) that compute several Pareto points in each iteration, it may be difficult to obtain a robust Pareto frontier. This is due to the fact that to couple MOGA with GARO (QC-GARO), the number of α parameters needed for each constraint should be equal to the number of points on the Pareto frontier. However, the main challenge here is how to calculate the α parameters efficiently without making the algorithm computationally intractable.

6.3.2 Extending the Modified Taylor Series Approximation Techniques to Solve Optimization Problems with More Than Two Levels

The structure of some engineering optimization problems consist of multiple optimization levels, such as some chemical engineering problems which may have up to five different levels (Rooney and Biegler 2003). The modified Taylor series approximation concept that was used to convert a two level robust optimization problem to a sequential optimization problem could be extended to optimization

problems with multiple levels and convert them to a sequential optimization problem. However for each additional optimization level a new parameter similar to α parameter in GARO algorithm is needed for each constraint (i.e., if the problem has m constraint and n levels at least $m \times n$ parameters needed).

5.3.3 Enhancing the AP-X Liquefaction Cycle by the Enhancement Options Introduced In This Dissertation

The enhancement options introduced in this dissertation could be used to enhance other natural gas liquefaction cycles. However the best candidate is AP-X (Chang et al., 2011) liquefaction cycle which is a modified version of APCI liquefaction cycle designed for large capacity stationary plants. The main difference between AP-X cycle and APCI cycle is that AP-X has additional nitrogen cooled cycle after the MCR cycle. Therefore most of the enhancement options are applicable to the AP-X cycle.

5.3.4 Implement the Robust Optimization Techniques to Design a Mobile Natural Gas Liquefaction Plant

Designing a mobile LNG plant is a multi-disciplinary problem. However, in this dissertation only the refrigerant mixture development aspect was addressed. The mobile LNG plant should be installed on a marine vessel which is subject to the sea waves. One of the main challenges in developing mobile LNG plants is designing a liquefaction cycle and also LNG storage that are insensitive to the vessel motion caused by sea waves. Since sea waves directions are random (i.e., uncertain), the robust optimization techniques would be a good tool for designing such a plant.

Therefore, some possible extensions include: i) Designing a mobile LNG storage that is subject to the sea waves by considering the bulk movement of LNG in the storage. ii) Designing the liquefaction cycle components while considering the vessel movement induced by the sea waves.

Appendices

Appendix A Further Details of the APCI Liquefaction Cycle ASPEN Model (Taken from Mortazavi et al., 2012)

In this section further details of the APCI liquefaction cycle ASPEN model components and streams are provided. This model was discussed in Section 2.4. The modeling parameters are shown in Tables A.1 through A6. The following abbreviations are used in the tables.

NG	Natural Gas
RMFR	Refrigerant Mass Flow Rate
RIP	Refrigerant Inlet Pressure
MCR	mixed component refrigerant
PD	Pressure Drop
DSH	Degree of Super Heating
RIT	Refrigerant Inlet Temperature
OT	Outlet Temperature

Table A.1. Modeling assumptions of the propane evaporators #1 to #5.

Evaporator No.	#1	#2	#3	#4	#5
RMFR [kg/s]	36.554	31.051	54.51	83.457	68.083
RIP [kPa]	882	618	406	253	138
NG PD [kPa]	20	20	20	20	20
MCR PD [kPa]	20	20	20	20	20
Propane PD [kPa]	10	0	0	0	0
Propane DSH [°C]	10	10	10	10	10
NG OT [°C]	25	12	-2	-16	-30
MCR OT [°C]	25	12	-2	-16	-30

Table A.2. Modeling assumptions of the propane evaporators #6 to #8.

Evaporator #6		Evaporator #7		Evaporator #8	
RMFR [kg/s]	0.793	RMFR [kg/s]	0.991	RMFR [kg/s]	9.054
RIP [kPa]	406	RIP [kPa]	253	RIP [kPa]	138
Propane PD [kPa]	10	Propane PD [kPa]	10	Propane PD [kPa]	10
Propane Outlet Temperature [°C]	-6	Propane (refrigerant) Outlet Temperature [°C]	-6	Propane Outlet Temperature [°C]	-29
C4 Outlet Temperature [°C]	-2	C3 Outlet Temperature [°C]	-16	C2 Outlet Temperature [°C]	-32

Table A.3. Modeling assumptions of the propane compressor stages #1 to #4 and the propane condenser.

Propane Compressor Stage No.	Propane Compressor Stage #1	Propane Compressor Stage #2	Propane Compressor Stage #3	Propane Compressor Stage #4	Propane Condenser	
RMFR [kg/s]	84.408	184.295	265.32	445	Oulet Temperature [°C]	43
RIP [kPa]	118	200	340	580	PD [kPa]	60
RIT [°C]	-27	-9	9	25.2		

Table A.4. Modeling assumptions of the MCR evaporator #1.

MCR Evaporator #1			
RIP [kPa]	420	NG PD [kPa]	400
RIT [°C]	-121	MCR Liquid Stream PD [kPa]	400
Refrigerant PD	50	MCR Gaseous Stream PD [kPa]	400
RMFR [kg/s]	270	C2 PD [kPa]	400
NG Inlet Temperature [°C]	-30	NG Mass Flow Rate [kg/s]	96.858
MCR Liquid Stream Inlet Temperature [°C]	-30	MCR Liquid Stream Mass Flow Rate [kg/s]	165.818
MCR Gaseous Stream Inlet Temperature [°C]	-30	MCR Gaseous Stream Mass Flow Rate [kg/s]	104.182
C2 Inlet Temperature [°C]	-32	C2 Mass Flow Rate [kg/s]	3.251
NG Inlet Pressure [kPa]	4440	NG Outlet Temperature [°C]	-116
MCR Liquid Stream Inlet Pressure [kPa]	3850	MCR Liquid Stream Outlet Temperature [°C]	-116
MCR Gaseous Stream Inlet Pressure [kPa]	3850	MCR Gaseous Stream Outlet Temperature [°C]	-116
C2 Inlet Pressure [kPa]	3300	C2 Outlet Temperature [°C]	-116

Table A.5. Modeling assumptions of the MCR evaporator #2.

MCR Evaporator #2			
RIP [kPa]	420	NG Mass Flow Rate [kg/s]	96.858
RIT [°C]	-165	MCR Mass Flow Rate [kg/s]	104.182
Refrigerant PD	0	C2 Mass Flow Rate [kg/s]	3.251
RMFR [kg/s]	104.182	NG PD [kPa]	400
NG Inlet Temperature [°C]	-116	MCR PD [kPa]	400
MCR Inlet Temperature [°C]	-116	C2 Inlet PD [kPa]	400
C2 Inlet Temperature [°C]	-116	NG Outlet Temperature [°C]	-160
NG Inlet Pressure [kPa]	4040	MCR Outlet Temperature [°C]	-160
MCR Inlet Pressure [kPa]	3450	C2 Outlet Temperature [°C]	-160
C2 Inlet Pressure [kPa]	2900		

Table A.6. Modeling assumptions of the MCR compressor stages #1 and #2 and MCR condenser.

MCR Compressor Stage No.	Stage #1	Stage #2	MCR Condenser	
RMFR [kg/s]	270	270	Oulet Temperature [°C]	40
MCR Inlet Pressure [kPa]	370	2260	PD [kPa]	20
MCR Inlet Temperature [°C]	-35	40		
MCR Outlet Temperature [°C]	80	81		
MCR Outlet Pressure [kPa]	2300	4000		

Appendix B Additional Details of the Chapter 3 Test Problems

The robust optimization formulation and results of the test problems Self 1-4 are shown Table B.1. The robust optimization formulation and results of test problems Sch 369 (Schittkowski 1987) and Sch 372 (Schittkowski 1987) v1 and v2 are shown Table B.2. The robust optimization formulation and results of Sch 380 v1and v2, welded beam design problem v2 and V3 and power tool design problem are shown in Tables B.3 – B.5 respectively.

Self 1:

min x

Subject to:

x^2-1≥0

x≥-1

$\Delta\tilde{x}$=1.1

Self 2:

min $f(x)=(x_1-4)^4+(x_2-4)^4$

Subject to:

$g_1=c_1x_1+c_2x_2\leq 8$

$g_2=c_3x_1+c_4x_2\leq 5$

$g_3=c_5x_1+c_6x_2\leq 10$

Where

c=[1,1,-2,1,-1,-3], $\Delta\tilde{\mathbf{c}}_j$ =0.1 for j =1,…, 6 and $\Delta\tilde{\mathbf{x}}$ =[0,0].

Self 3:

min f(x)=$(x_1-4)^4+(x_2-4)^4$

Subject to:

$g_1=c_1x_1+c_2x_2\leq 8$

$g_2=c_3x_1+c_4x_2\leq 5$

$g_3=c_5x_1+c_6x_2\leq 10$

$g_4=c_7x_1^4+c_8x_2\leq -4$

Where

c=[1,1,-2,1,-1,-3,2,-64], $\Delta\tilde{\mathbf{c}}_j$ =0.1 for j =1,…, 8 and $\Delta\tilde{\mathbf{x}}$ =[0,0].

Self 4:

The formulation is the same as Self 3 however the uncertainty ranges are different.

$\Delta\tilde{\mathbf{c}}$=[0,0,0,0,0,0,0.1,0] and $\Delta\tilde{\mathbf{x}}$ =[0.1,0.1]

Table B.1: Results of Self 1-4

	Self 1		Self 2		Self 3		Self 4	
	GARO	QC-GARO	GARO	QC-GARO	GARO	QC-GARO	GARO	QC-GARO
f(x)	1.2031	1.2031	0.035	0.035	0.2356	0.2356	0.3074	0.3074

x1	1.2031	1.2031	3.6364	3.6364	3.3033	3.3033	3.2753	3.2755
x2	---	---	3.6364	3.6364	3.9694	3.9694	4.4215	4.4223

Sch 369:

This problem is a modified version of problem 369 of Schittkowski (1987).

$$\min_x \tilde{x}_1 + \tilde{x}_2 + \tilde{x}_3 + \tilde{x}_4\tilde{x}_6 + \tilde{x}_5^{\,2} + \tilde{x}_7\tilde{x}_8$$

Subject to:

$$g_1 = c_{10}\tilde{x}_4 + c_{11}\tilde{x}_6 + \frac{\cos(\tilde{x}_2)}{\tilde{x}_3} - 1 \le 0$$

$$g_2 = c_{12}\tilde{x}_5 + c_{13}\tilde{x}_7 + c_{14}\tilde{x}_4 - 1 \le 0$$

$$g_3 = c_{15}\tilde{x}_8 + c_{16}\tilde{x}_5 + \frac{\tilde{x}_7\tilde{x}_5}{\tilde{x}_3} - 1 \le 0$$

$$g_4 = \frac{c_1\tilde{x}_4}{\tilde{x}_1\tilde{x}_6} + \frac{c_2}{\tilde{x}_6} + \frac{c_3}{\tilde{x}_1\tilde{x}_6} - 1 \le 0$$

$$g_5 = \frac{c_4\tilde{x}_5}{\tilde{x}_2\tilde{x}_7} + \frac{c_5\tilde{x}_4}{\tilde{x}_7} + \frac{c_6\tilde{x}_4}{\tilde{x}_2\tilde{x}_7} - 1 \le 0$$

$$g_6 = \frac{c_7}{\tilde{x}_3\tilde{x}_8} + \frac{c_8\tilde{x}_5}{\tilde{x}_8} + \frac{c_9\tilde{x}_5}{\tilde{x}_3\tilde{x}_8} - 1 \le 0$$

Where

c=[833.33252,100,-83333.333,1250,1,-1250,125000,1,-2500,0.0025, 0.0025, 0.0025, 0.0025,- 0.0025,0.01,-0.01]

$\mathbf{x}_l$=[100,1000,1000,10,10,10,10,10]

$\mathbf{x}_u$=[10000,10000,10000,1000,1000,1000,1000,1000]

$\Delta\tilde{\mathbf{x}}$=[50,100,100,5,5,5,5,5], $\Delta\tilde{\mathbf{c}}_\mathbf{j}$ =0 for j =1,…, 16.

Sch 372 v1:

This problem is a modified version of problem 372 of Schittkowski (1987).

Only design variable have uncertainty and their uncertainty values are:

$$\min \sum_{i=4}^{9} \tilde{x}_i^2$$

Subject to:

$g_1=127-\tilde{x}_1-\tilde{x}_2 \exp(-5\tilde{x}_3) -\tilde{x}_4\leq 0$

$g_2=151-\tilde{x}_1-\tilde{x}_2 \exp\left(-3\tilde{x}_3\right) -\tilde{x}_5\leq 0$

$g_3=379-\tilde{x}_1-\tilde{x}_2 \exp(-\tilde{x}_3) -\tilde{x}_6\leq 0$

$g_4=421-\tilde{x}_1-\tilde{x}_2 \exp(\tilde{x}_3) -\tilde{x}_7\leq 0$

$g_5=460-\tilde{x}_1-\tilde{x}_2 \exp(3\tilde{x}_3) -\tilde{x}_8\leq 0$

$g_6=426-\tilde{x}_1-\tilde{x}_2 \exp(5\tilde{x}_3) -\tilde{x}_9\leq 0$

$g_7=-127+\tilde{x}_1+\tilde{x}_2 \exp(-5\tilde{x}_3) -\tilde{x}_4\leq 0$

$g_8=-151+\tilde{x}_1+\tilde{x}_2 \exp\left(-3\tilde{x}_3\right) -\tilde{x}_5\leq 0$

$g_9=-379+\tilde{x}_1+\tilde{x}_2 \exp(-\tilde{x}_3) -\tilde{x}_6\leq 0$

$g_{10}=-421+\tilde{x}_1+\tilde{x}_2 \exp(\tilde{x}_3) -\tilde{x}_7\leq 0$

$g_{11}=-460+\tilde{x}_1+\tilde{x}_2 \exp(3\tilde{x}_3) -\tilde{x}_8\leq 0$

$g_{12}=-426+\tilde{x}_1+\tilde{x}_2 \exp(5\tilde{x}_3) -\tilde{x}_9\leq 0$

$\Delta\tilde{\mathbf{x}}$ =[100,1,0, 100,100,100,100,100,100]

Sch 372 v2:

Only design variable have uncertainty and their uncertainty values are:

$\Delta\tilde{\mathbf{x}}$ =[100,1,1, 100,100,100,100,100,100]

Table B.2: Results of Sch 369, Sch 372 v1and Sch 372 v2

	Sch 369	Sch 372 v1	Sch 372 v2	
Information	GARO	GARO	QC-GARO	GARO
x_1	100	453.6917	453.6917	323.761
x_2	1000	-104.1912	-104.1912	0.509
x_3	2603.421	-0.2227	-0.2227	0.038
x_4	14.534	513.9317	513.9317	640.570
x_5	10.141	494.5176	494.5176	555.979
x_6	10.004	380.4241	380.4241	365.460
x_7	25.284	330.7404	330.7404	417.918
x_8	56.464	311.0062	311.0062	570.913
x_9	---	304.8736	304.8736	668.290
$f(x)$	5379.318	952458	952458	1800211.133

Sch 380 v1:

This problem is a modified version of problem 380 of Schittkowski (1987).

$$\text{Min } 10^5(\tilde{x}_1^{-0.00133172}\tilde{x}_2^{-0.002270927}\tilde{x}_3^{-0.00248546}\tilde{x}_4^{-4.67}\tilde{x}_5^{-4.671973}$$

$$\tilde{x}_6^{-0.00814}\tilde{x}_7^{-0.008092}\tilde{x}_8^{-0.005}\tilde{x}_9^{-0.000909}\tilde{x}_{10}^{-0.00088}\tilde{x}_{11}^{-0.00119})$$

Subject to:

$$g_1=c_1\tilde{x}_1+c_2\tilde{x}_2+c_3\tilde{x}_3+c_4\tilde{x}_4\tilde{x}_5-1\leq 0$$

$$g_2=c_5\tilde{x}_1+c_6\tilde{x}_2+c_7\tilde{x}_3+\frac{c_8}{10^4}\tilde{x}_4\tilde{x}_{12}+\frac{c_9}{10^4}\frac{\tilde{x}_5}{\tilde{x}_{12}}+\frac{c_{10}\tilde{x}_6}{\tilde{x}_{12}}+c_{11}\tilde{x}_7\tilde{x}_{12}$$

$$+c_{12}\tilde{x}_4\tilde{x}_5+\frac{c_{13}\tilde{x}_2\tilde{x}_5}{x_{12}}+\frac{c_{14}}{10^{18}}\tilde{x}_2\tilde{x}_4\tilde{x}_5+c_{15}\tilde{x}_2\tilde{x}_5/(\tilde{x}_4\tilde{x}_{12}^2)+c_{16}\tilde{x}_{10}/\tilde{x}_{12}-1\leq 0$$

$$g_3=c_{17}\tilde{x}_1+c_{18}\tilde{x}_2+c_{19}\tilde{x}_3+\frac{c_{20}}{10^4}\tilde{x}_4+\frac{c_{21}}{10^4}\tilde{x}_5+c_{22}\tilde{x}_6+c_{23}\tilde{x}_8+c_{24}\tilde{x}_4\tilde{x}_5+c_{25}\tilde{x}_2\tilde{x}_5$$

$$+\frac{c_{26}}{10^{18}}\tilde{x}_2\tilde{x}_4\tilde{x}_5+\frac{c_{27}}{10^4}\tilde{x}_2\tilde{x}_5/\tilde{x}_4+c_{28}\tilde{x}_9+c_{29}\tilde{x}_1\tilde{x}_9+c_{30}\tilde{x}_{11}-1\leq 0$$

The uncertainty values are:

$\Delta\tilde{\mathbf{x}}$ =[1,1,1,1,1,1,1,1,1,1,1,1], $\Delta\tilde{\mathbf{c}}_j$ =0 for j =1,…, 30.

Sch 380 v2:

The uncertainty values are:

$\Delta\tilde{\mathbf{x}}$ =[1,1,1,1,1,1,1,1,1,1,1,1], $\Delta\tilde{\mathbf{c}}$=[0.005,0.002,0.009,0.0006,10^{-7}, 10^{-6}, 10^{-7}, 10^{-7}, 10^{-5}, 10^{-3}, 10^{-5},0.01,1.6×10^{-5}, 10^{-6},1.9×10^{-7}, 10^{-4}, 10^{-7}, 10^{-6}, 10^{-7}, 10^{-6}, 10^{-6}, 10^{-4}, 10^{-4},0.01,1.6×10^{-6}, 10^{-6},1.9×10^{-5}, 10^{-6},1×10^{-5}, 10^{-5}]

Table B.3: Results of Sch 380 v1 and Sch 380 v2

	Sch 380 v1		Sch 380 v2
Information	GARO	QC-GARO	GARO
x_1	0.2813	0.1000	0.29248
x_2	0.2027	0.4297	0.103113
x_3	0.1184	2.1617	0.1
x_4	0.1113	1.5082	2.338918
x_5	0.1000	2.5582	1.49815
x_6	1.7675	2.2136	0.345101
x_7	2.2470	0.1018	0.1
x_8	1.2785	12.4223	0.20835
x_9	11.5588	2.3809	1.049959
x_{10}	1.8271	1.5091	22.45512
x_{11}	63.5239	8.8870	7.817512
x_{12}	3.4346	34.1035	12.58863
$f(x)$	155.9511	182.0759	298.4942

Heat-Exchanger Design Problem (Mortazavi et al., 2012):

The goal in this problem is to maximize the heat transfer (Q) between the cold and hot fluids inside a shell and tube heat exchanger. The schematic of the shell and tube heat exchanger is shown in Figure 4. The problem formulation is summarized here. Further details regarding the heat exchanger modeling and robust optimization problem formulation can be found in Magrab et al., (2004) and Siddiqui et al., (2011) respectively.

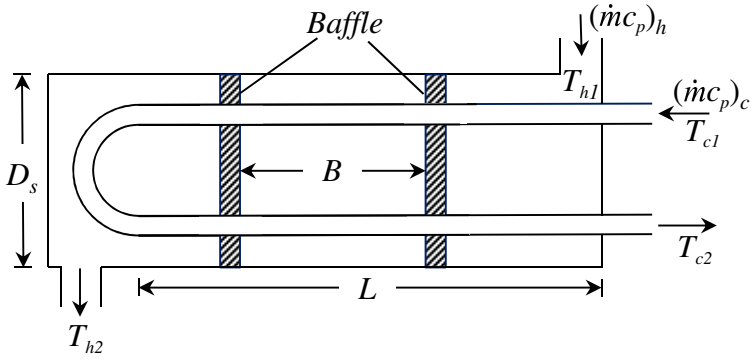

Figure B.1: Schematic of a heat exchanger (Taken From Mortazavi et al., 2012):

max Q,		$Q=UAF\Delta T_m = (\dot{m}_t c_p)_h(T_{h1}-T_{h2})$	
Subject to:			
$g_1=f_s\dot{m}_s^2(N_b+1)D_s/(2A_s^2\rho D_e\varphi_s)-35000\leq 0$		$g_2= C_0 f\, \dot{m}_t^3/(UF\Delta T_m)-50000\leq 0$	
$g_3= T_{h1} -(\dot{m}c_p)_t(T_{c2} - T_{c1})/(\dot{m}c_p)_s-60\leq 0$		$g_4=\pi d_i^2 N_T/4-A_s\leq 0$, $g_5=d_o-P_T \leq 0$	
$L \leq 40$, $7 \leq m_t \leq 10$, $13 \leq m_s \leq 16$		$0.001 \leq D_s \leq 2$, $0.002 \leq P_T \leq 0.1$, $0.0001 \leq d_i \leq 0.1$	
$\mathbf{z}=[\dot{m}_s,\dot{m}_t, D_s,P_T,d_i,T_{c1},T_{h1},k_{Tube}]$		$\Delta\tilde{\mathbf{z}}=[1,1,0.01,0.01,0.01,1,1,1]$	
Q	Heat-transfer rate (W)	U	Average overall heat transfer coefficient based on A (W/(m^2 K))
A	Total heat transfer area (m^2)	F	LMTD correction factor
ΔT_m	LMTD (K)	$\dot{m}_t$	Tube-side mass flow rate (kg/s)
T_{h2}	Outlet temperature of hot fluid (K)	c_p	Specific heat of water *(J/kg K)*
f_s	Friction factor shell side	T_{h1}	Inlet temperature of hot fluid (K)
N_b	Number of Baffles (Integer = B/L)	$\dot{m}_s$	Shell-side mass flow rate (kg/s)
L	Tube length (m)	B	Baffle spacing (m)
A_s	Cross-flow area at or near shell centerline (m^2)	D_s	Shell inside diameter (m)
D_e	Equivalent diameter of shell (m)	ρ	Density (kg/m^3)
φ_s	Viscosity correction factor	f	Tube flow friction factor
T_{c2}	Outlet temperature of cold fluid (K)	T_{c1}	Inlet temperature of cold fluid (K)
d_i	Tube inside diameter (m)	N_T	Number of Tubes
d_o	Tube outside diameter (m)	P_T	Pitch size (m)
K_{tube} Thermal conductivity of tubes (W/(mK))			

Welded-Beam v2 and v3 (Mortazavi et al., 2012):

This problem was originally introduced in Ragsdell and Phillips (1976). The problem formulation is summarized as:

$$\min f_{\cos t} = (1+c_3)h^2 l + c_4 tb(L+l)$$

Subject to:

$$g_1 = \frac{\tau}{\tau_d} - 1 \le 0,\ g_2 = \frac{\sigma}{\sigma_d} - 1 \le 0,\ g_3 = \frac{\delta}{0.25} - 1 \le 0,\ g_4 = \frac{F}{P_C} - 1 \le 0,\ g_5 = \frac{h}{b} - 1 \le 0,\ g_6 = \frac{0.125}{h} - 1 \le 0$$

h	Thickness of the weld	τ_d	Allowable normal stress of the beam (30,000 psi)
l	Length of the weld	σ	Maximum normal stress in the beam (psi)
t	Thickness of the beam	σ_d	Allowable normal stress of the beam (30,000 psi)
b	Width of the beam	δ	Deflection at the beam end (inch)
c_3	Cost of weld material ($0.1047/inch^3)	F	Force acting on the tip of the beam (6000 lbf)
c_4	Cost of beam material ($0.0481/inch^3)	P_c	Allowable buckling load (lbf)
τ	Maximum shear stress in weld (psi)	L	Length of unwelded beam (14 inch)

In version 2 only the design variables have uncertainty while in version 3 all of the design variables and parameters have uncertainty. Denote $\mathbf{x} = [h, l, t, b]$, in version 2 the uncertainties of variables are as $\Delta\tilde{\mathbf{x}}$=[0.05,0.05,0.05,0.05]. In version 3 the uncertainties of variables are the same as those in version 2. Denote $\mathbf{p} = [F, L, \tau_d, \sigma_d]$, the uncertainties of parameters in version 3 are as $\Delta\tilde{\mathbf{p}}$=[500,0.2,1000,1000]. The GARO and QC-GARO results are shown in Table B.4.

Table B.4: Welded beam v2 and v3 results

	Version 1		Version 2
	GARO	QC-GARO	GARO
h	0.3143	0.3144	0.3470
l	9.9849	9.9999	10
t	6.4676	6.4630	6.6682
b	0.5148	0.5157	0.5486
f_{cost}	4.9310	4.9394	5.5535
function calls	5.094×10^{5}	1.048×10^{3}	2.593×10^{6}

Power Tool Problem (Williams 2007, Mortazavi et al., 2012):

This problem is taken from Williams (2007) and converted to a robust problem by the authors of this paper. Here the objective is to maximize the ratio of the power to the mass of a cordless hand-held angle grinder. The grinder consists of three main components, which are motor, bevel gear and battery. The problem formulation is summarized below. In the formulation, for compactness, the dependent variables are shown as a function of design variable and parameters:

$$\min \frac{P_{out}(\mathbf{z})}{M_t(\mathbf{z})}$$

Subject to:

System Level Constraints		
$g_1 = M_t(\mathbf{z}) - 15 \le 0$	$g_2 = N(\mathbf{z}) / r - 10000 \le 0$	
Battery Constraints		
$g_3 = \frac{\rho_{Ni} t_{Ni}}{9.172\times10^7} - \frac{\rho_{Sep} t_{Sep}}{1.802\times10^7} \le 0$	$g_4 = \frac{\rho_{Ni} t_{Ni}}{9.172\times10^7} - \frac{0.25\rho_{Cd} t_{Cd}}{1.124\times10^8} \le 0$	$g_5 = h_{cell} - h_{cell\max} \le 0$
$g_6 = r_{cell}(\mathbf{z}) - r_{cell\max} \le 0$	$g_7 = I_{\min} - I \le 0$	$g_8 = I - I_{\max} \le 0$
$g_9 = M_{cell}(\mathbf{z}) - M_{cell\max} \le 0$		
Motor Constraints		
$g_{10} = \frac{L}{l_r(\mathbf{z})} - 5 \le 0$	$g_{11} = \frac{\phi(\mathbf{z})}{A_a(\mathbf{z})} - 1.5 \le 0$	$g_{12} = \frac{\phi(\mathbf{z})}{2A_s(\mathbf{z})} - 1.5 \le 0$
$g_{13} = \frac{\phi(\mathbf{z})}{A_g(\mathbf{z})} - 1.5 \le 0$	$g_{14} = \frac{N_c I}{\pi l_r(\mathbf{z})} - 10000 \le 0$	$g_{15} = \frac{N_c I}{\pi(l_r(\mathbf{z}) + t_s)} - 10000 \le 0$
$g_{16} = \pi N l_r(\mathbf{z}) - 3858 \le 0$	$g_{17} = T_{\max}(\mathbf{z}) - T_{steel} \le 0$	$g_{18} = N_{motor}(\mathbf{z}) - 40000 \le 0$
$g_{19} = D_{shaft} - r_{Stator} \le 0$		
Bevel Gear Constraints		
$g_{20} = \sigma_b(\mathbf{z}) - 1.45\times10^8 \le 0$	$g_{21} = \sigma_c(\mathbf{z}) - 7.2\times10^8 \le 0$	$g_{22} = D_{shaft} - D_p \le 0$
P_{out} : Grinder Power (w)	M_t :Grinder Mass (kg)	N : Revolutions Per Minute
r : Gear Ratio	ρ_{Ni} : Density of Ni (kg/m^3)	t_{Ni} :Ni Reactant Sheet Thickness
ρ_{Sep} : Density Of Separator (kg/m^3)	t_{Sep} : Separator Sheet Thickness (μ_m)	ρ_{Cd} : Density Of Cadmium (kg/m^3)
t_{Cd} : Cadmium Reactant Sheet Thickness (μ_m)	h_{cell} : Battery Cell Height	$h_{cell\max}$: Max Battery Cell Height
r_{cell} : Battery Cell Radius (mm)	$r_{cell\max}$: Max Battery Cell Radius (mm)	$I_{\min}$: Min Current (A)
I : Current (A)	$I_{\max}$: Max Current (A)	$M_{cell}(\mathbf{z})$:Battery Cell Mass (kg)
$M_{cell\max}$: Maximum Battery Cell Mass (kg)	L : Stack length L (m)	$l_r(\mathbf{z})$:Armature Diameter (m)
$\phi(\mathbf{z})$:Flux (Tesla)	$A_a(\mathbf{z})$:Armature Cross Section (m^2)	$A_s(\mathbf{z})$:Stator Cross Section

$A_g(\mathbf{z})$:Gap Cross Section (m^2)

N_c :Armature Turns

t_s :Stator Thickness (m)

$T_{\max}$:Max Shear Stress (Pa)

T_{steel} :Steel Shear Stress (Pa)

N_{motor} : Motor RPM

D_{shaft} :Motor-Gear Shaft Diameter (m)

r_{Stator} :Stator Outer Radius (m)

σ_b :Bending Stress

σ_c :Contact Stress (Pa)

D_p :Pinion Pitch Diameter (m)

It is assumed that only 6 of the design variables have uncertainty and design parameters do not have uncertainty. Grinder RPMs in loaded state (100), battery cell height in millimeters (0.5), stator outer radius in millimeters (0.5), stator thickness in millimeters (0.5), gap length in millimeters (0.1) and stack length in millimeters (0.5) are uncertain design variables, and the numbers inside the parentheses represent the uncertainty range from a nominal value. The GARO results are shown in Table B.4.

Table B.5: Power tool design results

Information	GARO	Information	GARO
x_1	30	x_{10}	10
x_2	48354.145	x_{11}	0.01
x_3	32.604	x_{12}	0.0168
x_4	5	x_{13}	0.0005
x_5	1	x_{14}	0.02
x_6	1.247	x_{15}	0.005
x_7	1	x_{16}	0.005
x_8	1	x_{17}	0.2
x_9	115.083	x_{18}	0.009
f(x)	313.690	*function calls*	425026

References

1. Alabdulkarem, A., Mortazavi, A., Hwang, Y. and Radermacher, R., and Rodgers, P., 2011, "Optimization of Propane Pre-cooled Mixed Refrigerant LNG Plant", *Applied Thermal Engineering*, 31, pp. 1091-1098.
2. Arora, J. S., 2004, "Introduction to Optimum Design", Elsevier, San Diego, CA, USA.
3. Aspelund, A., Gundersen, T., Myklebust, J., Nowak, M.P., Tomasgard, A., 2010, "An Optimization-Simulation Model for a Simple LNG Process", *Computers & Chemical Engineering*,34, pp. 1606-1617.
4. Aspen Plus, Version 7.1, 2009, Aspen Technology Inc., Burlington, MA, U.S.A.
5. Balling R. J., Free J. C., and Parkinson A. R., 1986, "Consideration of Worst-Case Manufacturing Tolerances in Design Optimization," *Journal of Mechanisms, Transmission, and Automation and Design*, 108, pp. 438–441.
6. Barclay M., 2005, "Selecting Offshore LNG processes", LNG Journal, 34e6.
7. Bazaraa M., Sherali H., Shetty C., 1993, "Nonlinear Programming: Theory and Algorithms", 2nd ed. Wiley, New York, NY, pp. 438–448.
8. Ben-Tal A., Nemirovski A., 2002, "Robust Optimization-Methodology and Applications", *Mathematical Programing*, 92:453–48.
9. Bertsimas D., Sim M., 2006, "Tractable Approximations to Robust Conic Optimization Problems", *Mathematical Programming*, 107:5–3.
10. Bertsimas D., Nohadani O., 2010, "Robust Optimization with Simulated Annealing", *Journal of Global Optimization*, 48, pp. 323-334.
11. Bertsimas D., Nohadani O., Teo K. M., 2010, "Nonconvex Robust Optimization

for Problems with Constraints", *INFORMS Journal on Computing*, 22, pp. 44-58.

12. Beyer H.-georg, Sendhoff B., 2007, "Robust Optimization – A Comprehensive Survey", *Journal of Mechanical Design*, 196, pp. 3190-3218.
13. Boston, J., Mathias, P., 1980, "Phase Equilibria in a Third-Generation Process Simulator", Proceedings of the 2nd International Conference on Phase Equilibria and Fluid Properties in the Chemical Process Industries, West Berlin, pp. 823-849.
14. Bumagin, G., Borodin D., 2007, "Natural Gas Liquefier Based on an EGD-Generator-Expander", *Chemical and Petroleum Engineering*", 43, pp.17-20.
15. Cook L., 2005, "The Role of LNG in a Global Gas Market", Oil & Money Conference, London.
16. Chang, H., Chung, M., J., Lee, S., Choe, K., H., 2011, "An efficient multi-stage Brayton–JT cycle for liquefaction of natural gas", *Cryogenics*, 51, pp. 278-286.
17. Chen W., Wiecek M. M., Zhang J., 1999, "Quality Utility-A Compromise Programming Approach to Robust Design", *Journal of Mechanical Design*, 121, pp. 179-187.
18. Choi K. K., Tu J., Park Y. H., 2001, "Extensions of Design Potential Concept for Reliability-Based Design Optimization to Nonsmooth and Extreme Cases", *Structural Multidisciplinary Optimization*, 22, pp. 335-350.
19. Del Nogal, F., Kim, J., Perry, S., Smith, R., 2008, "Optimal design of mixed-refrigerant cycles"**,** *Industrial and Engineering Chemistry Research*, 47, pp. 8724-8740.
20. Del Nogal, F. L., Kim, J.-K. , Perry, S. Smith, R., 2011a, "Synthesis of

Mechanical Driver and Power Generation Configurations, Part 1: Optimization Framework", *American Institute of Chemical Engineers Journal*, 56, pp. 2356-2376.

21. Del Nogal, F. L., Kim, J.-K. , Perry, S. Smith, R., 2011b, "Synthesis of Mechanical Driver and Power Generation Configurations, Part 2: LNG Applications", *American Institute of Chemical Engineers Journal*, 56,pp. 2377-2389.
22. Di Napoli, R. N., 1980, "Gas Turbine Prove Effective as Drivers for LNG Plants", *Oil and Gas Journal*, 78, pp. 47-52.
23. Du X., Chen W., 2000, "Towards a Better Understanding of Modeling Feasibility Robustness in Engineering Design", *Journal of Mechanical Design*, 122, pp. 385–394.
24. Faruque Hasan, M. M., Shamsuzzaman Razib, Md., Karimi, I.A., 2009, "Optimization of Compressor Networks in LNG Operations", *Computer Aided Chemical Engineering*, 27, pp. 1767-1772.
25. Finn A., Johnson G., Tomlinson T., 1999, "Developments in Natural gas Liquefaction", *Hydrocarbon Processing*, 78, pp. 47-59.
26. Foss M. M., 2007, "Introduction To LNG", Center For Energy Economics, Available at : http://www.beg.utexas.edu/energyecon/lng/documents/CEE_INTRODUCTION_TO_LNG_FINAL.pdf, Last access 11/21/2011.
27. Gancarova M., Todd M.J., 2011, "A Robust Robust Optimization Result", *Operations Research Letters*, In Press.

28. GE Energy, 2007, “Gas Turbine Performances Data”.

29. Gunawan S., Azarm S., 2004a, “On a Combined Multi-Objective and Feasibility Robustness Method for Design Optimization”, CD-ROM Proceed- ings of the tenth AIAA/ISSMO MDO, Albany, NY, September.

30. Gunawan S., Azarm S. 2004b, “Non-gradient Based Parameter Sensitivity Estimation for Single Objective Robust Design Optimization”, *Journal of Mechanical Design*, 126,pp. 395-40.

31. Gunawan S., 2004, “Parameter Sensitivity Measures for Single Objective, Multi-Objective and Feasibility Robust Design Optimization”, Ph.D. dissertation, University of Maryland, College Park, May.

32. Gunawan S., Azarm S., 2005a, “Multi-Objective Robust Optimization Using A Sensitivity Region Concept”, *Structural and Multidisciplinary Optimization*, 29, pp. 50-60.

33. Gunawan S., Azarm S., 2005b, “A Feasibility Robust Optimization Method using a Sensitivity Region Concept”, *Journal of Mechanical Design*, 127, pp. 858–868.

34. Hamel J.M., 2010, “Sensitivity Analysis Based Approaches For Mitigating The Effects of Reducible Interval Input Uncertainty On Single- and Multi-Disciplinary Systems Using Multi-Objective Optimization”, PhD Thesis, University of Maryland, College Park, MD, USA.

35. Herold, K., Radermacher, R. Klein, S. A., 1996, “Absorption Chillers and Heat Pumps”, CRC Press.

36. Hock W., Schittkowski K.,1980, “Test Examples for Nonlinear Programming Codes”, Springer, New York, NY, USA.

37. Hubbard B., 2004, "A Fresh Approach to LNG", *Hydrocarbon Engineering*, 9, pp. 29-32.
38. Hu, W., Li, M., Azarm, S. Almansoori, A., 2011, "Multi-Objective Robust Optimization under Interval Uncertainty Using Online Approximation and Constraint Cuts", *Journal of Mechanical Design*, 133, 061002-1-9.
39. HYSYS 7.1 manual [online]. Available from: http://chemelab.ucsd.edu/aspendocs/v7/HYSIS/AspenHYSYSV7_1-Usr.pdf. [Accessed: 05 May 2012].
40. International Energy Outlook 2010, "Natural Gas", EIA, Available at: http://www.eia.gov/oiaf/ieo/nat_gas.html, Last access 05/27/2011.
41. International Energy Outlook 2011, EIA, Report Number: DOE/EIA-0484(2011).
42. Jensen J., Sigurd S., 2006, "Optimal Operation of a Mixed Fluid Cascade LNG Plant", 6th European Symposium on Computer Aided Process Engineering and 9th International Symposium on Process Systems Engineering.
43. Jung D. H., Lee B. C., 2002, "Development of a Simple and Efficient Method for Robust Optimization", *International Journal of Numerical Methods Engineering*, 23, pp. 2201-2215.
44. Kalinowski, P., Hwang, Y., Radermacher, R., Al-Hashimi, S. Rodgers, P., 2009, "Application of Waste Heat Powered Absorption Refrigeration System to the LNG Recovery Process", *International Journal of Refrigeration*, 32, pp. 687-694.
45. Kanoglu, M., 2001, "Cryogenic Turbine Efficiencies", *Exergy International Journal*, 1, pp. 202-208.
46. Kim N.-kyung, Kim D.-hun, Kim D.-wook, Kim H.-geun, Lowther D. A.,

Sykulski J. K., 2010, “Robust Optimization Utilizing the Second-Order Design Sensitivity Information”, *IEEE Transactions on Magnetics*, 46, pp. 3117-3120.

47. Lee, G. C., Smith, R. Zhu, X. X., 2002, “Optimal Synthesis of Mixed refrigerant Systems for Low Temperature Processes”, *Industrial and Engineering Chemistry Research*, 41, pp. 5016-5028.
48. Lee K., Park G., 2001, “Robust Optimization Considering Tolerances of Design Variables”, *Computer and Structure*, 79, pp. 77-86.
49. Li M., Azarm S., Boyars A., 2006, “A New Deterministic Approach Using Sensitivity Region Measures for Multi-Objective Robust and Feasibility Robust Design Optimization”, *Journal of Mechanical Design*, 128, pp. 874.
50. Li M., Gabriel S., Shim Y., Azarm S., 2011, “Interval Uncertainty-Based Robust Optimization for Convex and Non-convex Quadratic Programs with Applications in Network Infrastructure Planning”, *Networks and Spatial Economics*, 11,pp. 159-191.
51. Maddulapalli, K., S. Azarm A. Boyars, 2007, “Sensitivity Analysis for Product Design Selection with an Implicit Value Function”, *European Journal of Operational Research*, 180, pp.1245-1259.
52. Magrab E., Azarm S., Balachandran B., Duncan J., Herold K., Walsh G., 2004, “An engineer’s guide to Matlab”, Prentice Hall, New York.
53. Malakooti B., 1988, “A Decision Support System and a Heuristic Interactive Approach for Solving Discrete Multiple Criteria Problems”, *IEEE Transactions on Systems, Man, and Cybernetics*, 18, pp. 273-284.
54. Matlab 2010a manual [online].Available from: www.mathworks.com/help.

[Accessed: 05 May 2012].

55. Messac A., Yahaya A. I., 2002, "Multiobjective Robust Design Using Physical Programming", *Structural Multidisciplinary Optimization*, 23, pp. 357-371.
56. Mokarizadeh Haghighi Shirazi M., Mowla D., 2010, "Energy Optimization for Liquefaction Process of Natural Gas in Peak Shaving Plant", *Energy*, 35, pp. 2878-2885.
57. Mortazavi, A., Azarm, S., Gabriel, S., 2012, "Adaptive Gradient Assisted Robust DESIGN Optimization under Interval Uncertainty", *Engineering Optimization*, In Press.
58. Mortazavi, A., Somers, C., Alabdulkarem, A., Hwang, Y., Radermacher, R., 2010, "Enhancement of APCI Cycle Efficiency with Absorption Chillers", *Energy*, 35, pp. 3877-3882.
59. Mortazavi, A., Somers, C., Hwang, Y., Radermacher, R., Al-Hashimi, S., Rodgers, P., 2012, "Performance Enhancement of Propane Pre-cooled Mixed Refrigerant LNG Plant", *Applied Energy*, 93 pp. 125-131.
60. Nogal F. D., Kim J.-K., Perry S., Smith R., 2008, "Optimal Design of Mixed Refrigerant Cycles", *Industrial & Engineering Chemistry Research*, 47, pp. 8724-8740.
61. Olander, D. R., 2008, "General Thermodaynamics", CRC Press, Boca Raton, FL, USA.
62. Ordonez, C. A., 2000, "Liquid Nitrogen Fueled, Closed Brayton Cycle Cryogenic Heat Engine", *Energy Conversion & Management*, 41, pp.331-341.
63. Paradowski, H., Bamba, M., Bladanet, C., 2004, "Propane Precooling Cycles for

Increased LNG Train Capacity", 14th International Conference and Exhibition on Liquefied Natural Gas, pp. 107-124.

64. Parkinson A., Sorensen C., Pourhassan N. A., 1993, "General Approach to Robust Optimal Design", *Journal of Mechanical Design*, 115, pp. 74-80.
65. Patel B., 2005, "Gas Monetisation: A Techno-Economic Comparison of Gas-To-Liquid and LNG", 7th World Congress of Chemical Engineering Glasgow.
66. Ragsdell K., M, Phillips D., T, 1976, "Optimal design of a class of welded structures using geometric programming", *Journal of Engineering for Industry*, 98, pp. 1021-1025.
67. Ray T., 2002, "Constrained Robust Optimal Design using a Multi-objective Evolutionary Algorithm", in Congress on Evolutionary Computation (CEC'2002), IEEE Service Center, Piscataway, NJ, 1, pp. 419-424.
68. Renaudin, G., 1995, "Improvement of Natural Gas Liquefaction Processes by Using Liquid Turbines", Proceedings of the Eleventh International Conference on Liquefied Natural Gas, Institute of Gas Technology, Chicago.
69. Rodgers, P., Mortazavi, A., Eveloy, V., Al-Hashimi, S., Hwang, Y. ,Radermacher, R., "Enhancement of LNG Plant Propane Cycle through Waste Heat Powered Absorption Cooling", *Applied Thermal Engineering*, In Press.
70. Rooney, W., C., Biegler, L., T., 2003, "Optimal Process Design with Model Parameter Uncertainty and Process Variability", *American Institute of Chemical Engineers Journal,* 49, pp. 438-449.
71. Schittkowski K., 1987, "More Test Examples for Nonlinear Programming Codes", Springer, New York, NY, USA.

72. Shen R., Zhang S., 2008, "Robust Portfolio Selection Based On a Multi-Stage Scenario Tree", *European Journal of Operational Research* , 191, pp. 864-887.

73. Siddiqui S., Azarm S., Gabriel S., 2011, "A Modified Benders Decomposition Method for Efficient Robust Optimization under Interval Uncertainty", *Structural and Multidisciplinary Optimization*, 43, pp.1-17.

74. Somers, C., 2009, "Simulation of Absorption Cycles for Integration Into Refining Processes", Master's Thesis, University of Maryland, College Park, MD, USA.

75. Somers, C., Mortazavi, A., Hwang, Y., Radermacher, R., Al-Hashimi, S. , Rodgers, P., "Modeling Water/Lithium Bromide Absorption Chillers in ASPEN Plus", *Applied Energy*, 88, pp. 4197-4205.

76. Soyster A., (1973), "Convex Programming with Set-Inclusive Constraints and Applications to Inexact Linear Programming", *Operation Research*, 21, pp. 1154-1157.

77. Sundaram, R.,K., 1996, "A First Course in Optimization Theory", Cambridge University Press, U.K.

78. Sundaresan S., Ishii K., Houser D., 1992, "Design Optimization for Robustness Using Performance Simulation Programs", *Engineering Optimization*, 20, pp. 163-178.

79. Sunderasan S., Ishii, K., Houser D. R., 1993, "A Robust Optimization Procedure with Variation on Design Variables and Constraints", *Advances in Design Automation*, 65, pp. 379-386.

80. Su J., Renaud J. E., 1997, "Automatic Differentiation in Robust Optimization", *American Institute of Aeronautics and Astronautics Journal*, 35, pp. 1072-1079.

81. Taguchi, G., 1978, "Performance Analysis Design", *International Journal of Production Research*, 16, pp. 521-530.

82. Taleshbahrami H., Saffari H., 2010, "Optimization of the C3MR Cycle with Genetic Algorithm", Transactions of the Canadian Society for Mechanical Engineering, 34, pp. 433-448.

83. Tangen G., Mønvik M. J., 2009, "Scenarios for remote gas production", *Applied Energy*, 86, pp. 2681-2689.

84. Teo K.M., 2007, "Nonconvex Robust Optimization, PhD Dissertation", Massachusetts Institute of Technology, Cambridge, MA.

85. Tu J., Choi K. K., Park Y. H., 1999, "A New Study on Reliability-Based Design Optimization", *Journal of Mechanical Design*, 121, pp. 557-564.

86. Vaidyaraman, S., Maranas, C. D., 2002, "Synthesis of Mixed Refrigerant Cascade Cycles", *Chemical Engineering Communications*, 189, pp. 1057-1078.

87. Venkatarathnam G., 2008, Cryogenic Mixed Refrigerant Processes, Springer-Verlag New York, LLC.

88. Wang M., Zhang J., Xu Q., 2012, "Optimal Design and Operation of a C3MR Refrigeration System for Natural Gas Liquefaction", *Computers & Chemical Engineering*, 39, pp. 84-95.

89. Xu X., Liu J., Jiang C., Cao L., 2012, "The Correlation between Mixed Refrigerant Composition and Ambient Conditions in the PRICO LNG process", Available Online in *Applied Energy*.

90. Yang S., Ong Y. S., Jin Y., 2007", Evolutionary Computation in Dynamic and Uncertain Environments", Springer.

91. Youn B. D., Choi K. K., Park Y. H., 2003, "Hybrid Analysis Method for Reliability-Based Design Optimization", *Journal of Mechanical Design*, 125, pp. 221- 232.

92. Yu J. C., Ishii K., 1998, "Design for Robustness Based on Manufacturing Variation Patterns", *Journal of Mechanical Design*, 120, pp. 196-202.

93. Zhu J., Ting K. L., 2001, "Performance Distribution Analysis and Robust Design", *Journal of Mechanical Design*, 123, pp. 11-17.